A FINITE ELEMENT MODEL FOR THE PREDICTION OF THERMAL STRESSES IN MASS CONCRETE

By

ADRIAN M. LAWRENCE

A DISSERTATION PRESENTED TO THE GRADUATE SCHOOL
OF THE UNIVERSITY OF FLORIDA IN PARTIAL FULFILLMENT
OF THE REQUIREMENTS FOR THE DEGREE OF
DOCTOR OF PHILOSOPHY

UNIVERSITY OF FLORIDA

2009

To my family

ACKNOWLEDGMENTS

I would first like to express my deepest gratitude to Dr. Mang Tia for his help and guidance during the course of my study at The University of Florida. I would also like to thank the members of my supervisory committee: Dr. Reynaldo Roque, Dr. Fazil Najafi, Dr. John Lybas of the civil and coastal engineering department, and Dr. Larry Muszynski of the school of building construction, for their insightful suggestions that aided in determining the main focus of this study. Special gratitude is extended to Dr. Jonathan F. Earle for his encouragement and timely advice. Thanks also to my partner in this research and fellow doctoral student Christopher Ferraro, who led and conducted the research on the physical input parameters needed for the finite element model. I would also like to acknowledge and thank the Florida Department of Transportation for funding this research. I would especially like to thank Mr. Michael Bergin and Mr. Charles Ishee of the FDOT Materials Laboratory, Gainesville, for their invaluable support and contributions to this study. Sincere thanks to Mr. Richard DeLorenzo, Mr. Joseph Fitzgerald, Mr. Craig Roberts, Mr. Toby Dillow, and all the staff in the laboratory for their help in the physical experiments on the material properties of the concrete used in this study. Thanks to the students who also helped in this study: Carrie Ulm, Boris Haranki, and Patrick Bekoe. Finally, I would like to thank my family. My wife Andrea, daughter Gabrielle, parents Dr. Vincent and Beverley Lawrence, my sister Marilyn, and brothers Neil and Gregory for their support and motivation throughout my years of study.

TABLE OF CONTENTS

page

LIST OF TABLES

LIST OF FIGURES

Abstract of Dissertation Presented to the Graduate School
of the University of Florida in Partial Fulfillment of the
Requirements for the Degree of Doctor of Philosophy

A FINITE ELEMENT MODEL FOR THE PREDICTION OF THERMAL STRESSES IN MASS CONCRETE

By

Adrian Lawrence

December 2009

Chair: Mang Tia
Major: Civil Engineering

This dissertation presents the development of a finite element model for the prediction of the distribution of temperatures within a hydrating massive concrete element. The temperature distribution produced by the finite element thermal analysis of the model is used in the finite element structural analysis to quantify the maximum allowable thermal gradient before cracking will initiate in the concrete.

Temperature differences within the concrete occur when the heat being generated by the concrete is dissipated to the surrounding environment causing the temperature at the surface of the concrete to be lower than the temperature at the interior of the concrete. At the same time the heat generated is a function of the temperature and time history of the concrete. Therefore, individual locations in the concrete will experience different levels of heat. The temperature difference between the concrete at the center of the element and the concrete in the outer region will create stresses. If the induced tensile stresses are larger than the early age tensile strength of the concrete, cracking will occur.

The requirements for the control of heat generation and maximum allowable temperature difference in mass concrete vary on a state by state basis. Currently, there is no agreement on

what should be the maximum allowable temperature differential between the center of a mass concrete element and its surface. How the various states arrive at their respective values is not clear. The development of an effective model for analysis of mass concrete behavior will enable the establishment of rational requirements for mass concrete to reduce cracking.

To verify the results obtained in the finite element model, four different mixes of concrete, typical of use in mass concrete applications in Florida, were produced, and each mix used to make two large-scale 3.5ft x 3.5 ft x 3.5 ft (1.07 m x 1.07 m x 1.07 m) concrete blocks. In each mix, one block was insulated on all six sides to simulate a fully adiabatic process, while the other block was insulated on five of the faces with the top face left open and exposed to environmental conditions. Measurements of the temperature and strain at predetermined locations within the blocks were recorded until the equilibrium temperature was achieved.

Using the developed model, a parametric analysis was performed to evaluate the effects of cement heat generation, concrete thermal properties, dimension of concrete structure, insulation of structure, convection of heat, etc. on the temperature distribution and induced stresses in mass concrete structures. Recommendations on methods for evaluating the potential performance of mass concrete structures are presented.

CHAPTER 1
INTRODUCTION

Background

Whenever fresh concrete is used in the construction of large homogeneous structures such as foundations and dams, consideration is always given to the amount of heat that will be generated and the resulting volume change. Volume changes occur due to temperature changes in the structure which initially increase as the concrete hydrates and decrease as the reaction is exhausted. Temperature difference per unit distance between one point and another in a structure is called a thermal gradient. Temperature gradients are produced when the heat being generated in the concrete is dissipated to the surrounding environment causing the temperature at the surface of the concrete to be lower than the temperature at the interior of the concrete. This temperature drop at the surface results in the contraction of the concrete. With the interior of the concrete being more mature than the surface, it acts as a restraint against the contraction, creating tensile stresses in the surface. Since the concrete is still in its early age, its full tensile strength is not developed, and if the tensile stresses are larger than the early age tensile strength, cracking will occur.

The behavior of concrete at early age is influenced by the heat generated, which, by extension, dictates the temperature distribution during hydration. The temperature profile of a concrete element is further affected by the specific heat capacity, thermal diffusivity, and emissivity of the concrete. At the same time, the rate of development of mechanical strength of concretes at early age increases with increasing temperature and hence can be expressed as a function of temperature and time.

Past research leading to the creation of numerical models for the prediction of temperature distribution in mass concrete has mainly focused on using generic heat generation

functions for the calculation of adiabatic temperature rise. The use of actual measured heat of hydration results from calorimetry testing of the concrete paste has been mostly neglected. At the same time, attempts at modeling hydrating mass concrete (Radovanic (2004)) have treated the heat generated by the reacting cement as being uniform throughout the concrete mass, whereas, in reality, the heat generation is a function of the temperature and time history of the concrete at individual locations in the concrete mass. Different locations in a mass concrete element have different time-temperature conditions.

This research is aimed at formulating a finite element model, taking into consideration the non-homogeneity of heat generation within concrete, to accurately predict the distribution of temperature in a hydrating concrete mass, the resulting thermal gradients and associated thermal stresses and strains. Knowledge of these phenomena will allow for a reasonably accurate prediction of the location and potential for cracking of concrete.

The thermal stresses that occur during the hardening of mass concrete are extremely complex and difficult to assess. This is due to several factors, chief among which is the complex distribution of temperature changes throughout the volume of the mass concrete.

As depicted in Figure 1-1, the central region of the mass concrete at early age experiences high but uniform temperatures while the temperature in the outer region decreases as we move closer to the surface. Since the maturity of concrete and strength are functions of temperature, the central region of the mass concrete structure will be more mature and stronger than the outer region.

As the concrete hydrates faster in the middle, large thermal gradients are produced, and strength and maturity decreases moving outwards towards the surface. Since the concrete in the outer region of mass concrete is being cooled by the atmospheric environment, contraction will

occur. Restraint against this contraction will cause tensile stresses and strains to develop, creating the possibility that cracks will occur at or close to the surface of the concrete. These cracks will initiate when the tensile stresses exceed the low tensile strength at the surface as depicted in Figure 1-2. The magnitude of the tensile stresses are dependent on the thermal differential in the mass concrete, the coefficient of thermal expansion, modulus of elasticity, creep or relaxation of the concrete, and the degree of restraint in the concrete. If cracking does occur, it will ultimately affect the ability of the concrete to withstand its design load, and allow the infiltration of deleterious materials which undermine durability.

Mass Concrete

Research has shown that the inner core of massive concrete elements experience compressive stresses as it tries to expand but is restricted by the slower hydrating and hence less mature outer region. Conversely, moving out towards the surface, the outer region of the hydrating concrete element acts in tension as it is being pushed against by the expanding inner core. Figure 1-3 shows a graph of temperature balance computed from temperature differences distributed across a typical mass concrete lock wall (U.S. Army Corps of Engineers 1997). Tension is induced along the surface, while the central interior portion experiences compressive stresses. Since concrete is strong in compression but weak in tension, this suggests that cracking will initiate close to the surface and towards the edges and corners of a structure.

Thermal Gradients

Temperature differences per unit distance along a particular path in a structure are called thermal gradients. These gradients result from the surface of a mass concrete element being cooled by the ambient environment while the internal concrete temperature remains high due to the exothermic reaction of hydration. This causes the surface concrete to be restrained by the interior concrete. This may result in the cracking of the surface concrete. For this reason, many

state Departments of Transportation incorporate into their specifications a limit on the maximum allowable temperature differential between the exterior and interior portions of mass concrete elements during curing.

The magnitude of the thermal gradients experienced by concrete depends on the initial placing temperature, the thermal properties (specific heat, thermal conductivity), environmental temperature, wind speed, and precipitation.

Research Needs

The high amount of heat that develops during the hydration of massive concrete structures produces very high temperatures throughout the structure. The variation in the rate of heat production at different locations within the concrete results in temperature gradients that have the potential to cause microcracking as some sections cool down towards ambient temperature while others are still being heated. Though the effects thermal gradients have on concrete is well known, there is no agreement on what the maximum allowable temperature differential between the center of a mass concrete element and its surface should be.

Some researchers have modeled the thermal behavior of hydrating mass concrete with some degree of success. However, none have studied the effects of the variation in hydration rates on the distribution of temperatures, the thermal gradients, and resulting stresses. This research focuses on the development of a finite element analysis model that takes into consideration these factors.

Objective of Study

The goal of the research is to develop a finite element model of mass concrete, which is based on the input of measured thermal and mechanical characteristics, and which can predict the temperature distribution during hydration and the thermal stresses that result from the thermal gradients within the structure. Previous attempts at predicting the temperature

distribution in mass concrete by way of finite element models has mainly focused on using generic heat generation functions for the calculation of adiabatic temperature rise. The heat generated by hydrating mass concrete has also been widely modeled as being uniform throughout the concrete mass, whereas in reality the heat generation is a function of the temperature and time history of individual locations in the concrete mass. The developed finite element model will take into consideration the time-temperature conditions of individual locations within a hydrating mass concrete structure. A stress analysis utilizing changing strength properties of the concrete will also be conducted and the results compared with the experimentally measured strain data as a means of validation.

Research Hypothesis

The hydration reaction between cement and water in a mass concrete structure does not occur uniformly. It is driven in part by the temperature conditions under which the reaction is taking place. Since the temperature within a mass concrete element is not homogeneous, the heat generation will also not be homogeneous. To properly model the behavior of mass concrete at an early age, the temperature-time condition at individual points within the concrete needs to be considered.

Research Approach

The modeling of the large scale concrete blocks is done with the aid of the commercially available TNO DIANA software. The analysis is done in two parts, first a thermal analysis, in which the thermal properties are modeled, the hydration process simulated, and the resulting temperature distribution obtained. The second part of the analysis is a stress analysis in which the physical properties such as elastic modulus and coefficient of thermal expansion are used along with the temperature histories obtained in the thermal analysis to calculate the stresses and strains produced by the thermal gradients. The cracking potential is then assessed.

As a means of validation, four different mixes of concrete, typical of use in mass concrete applications in Florida, were produced, and each mix used to make two 3.5ft x 3.5 ft x 3.5 ft (1.07m x 1.07m x 1.07m) concrete blocks. For each mix, one block was insulated on all six sides to simulate a fully adiabatic process, while the other block was insulated on five of the faces with the top face left open and exposed to environmental conditions. Measurements of the temperature and strain at predetermined locations within the blocks were recorded until the equilibrium temperature was achieved.

At the time of casting the blocks, concrete taken from the same mix were used to perform the evaluation of small-scale samples which are then stored at 73°F ± 2°F and 100% relative humidity until the time of testing for the mechanical properties at ages of 1 day, 2 days, 3 days, 7days, 14 days, and 28days. Tests for the thermal properties, heat of hydration, specific heat capacity, and thermal diffusivity were also done at these ages.

Finally, a parametric analysis was conducted to determine what effects the size of the concrete structure, amount of insulation used, specific heat capacity and diffusivity, would have on the temperature distribution, induced stresses and the cracking risk.

Significance of Research

The requirements for the control of heat generation and temperature distribution in mass concrete vary on a state by state basis. Currently there is no agreement on what should be the maximum allowable temperature differential between the center of a mass concrete element and its surface.

The states of Florida, Iowa, Virginia, and West Virginia Departments of Transportation's specification requirements currently include a requirement that the temperature differential in

elements designated as mass concrete be controlled to a maximum of 35 degrees Fahrenheit (20 degrees Celcius).

Colorado's specification states that the temperature differential between the midpoint and a point 2 inches inside the exposed face of all mass concrete elements shall not exceed 45 degrees Fahrenheit as measured between temperature sensors. It further states that the maximum peak curing temperature of all mass concrete elements shall not exceed 165 degrees Fahrenheit.

The state of Delaware's specification calls for a range of maximum differential temperatures based on the number of hours after casting of the concrete as follows:

First 48 hours	40° F
Next 2 to 7 days	50° F
Next 8 to 14 days	60° F

North Dakota's Department of Transportation specifies that measures and procedures should be taken to maintain, monitor and control the temperature differential of 50 degrees Fahrenheit or less between the interior and exterior of the mass concrete element.

Considering the inconsistencies in the maximum allowable temperature differential in mass concrete structures, how the various states arrive at their respective values is not clear. Therefore, the determination of a maximum temperature gradient limit based on the analysis of a finite element model that accurately predicts the behavior of a hydrating mass concrete element would constitute a substantial contribution to this area of engineering.

Outline of Dissertation

Chapter 2 is a review of the literature citing specifications currently in use and other attempts at modeling the behavior of mass concrete. Chapters 3 and 4 discuss the finite element model input parameters, material model, element type and boundary conditions used in the thermal and stress analyses respectively.

Chapter 5 discusses the mix proportions of the concrete used in the experimental blocks as well as the types and location of the monitoring instruments used.

Chapter 6 describes the test procedures carried out on concrete specimens sampled directly from the concrete used in the construction of the experimental blocks.

Chapters 7 and 8 present and discuss the results obtained from the finite element analyses, with comparisons of the analytical results of the temperature distribution and stress state with those measured in the experimental blocks.

Chapter 9 presents a parametric study of mass concrete elements of varying sizes and levels of insulation in order to determine the limiting temperature gradient to prevent thermal cracking. Chapter 10 provides discussion, conclusions and recommendations for future research efforts.

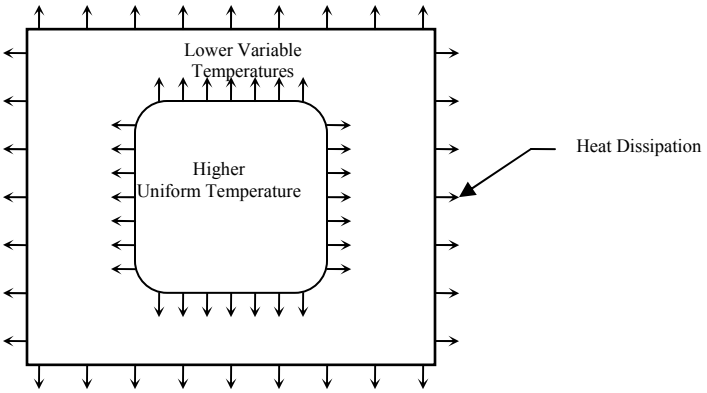

Figure 1-1. Typical temperature characteristics of a mass concrete element

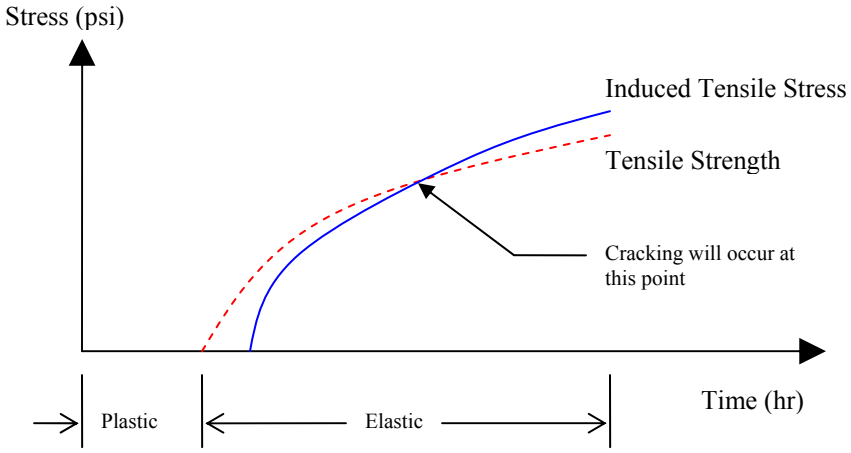

Figure 1-2. Stress vs. time plot showing time of crack initiation

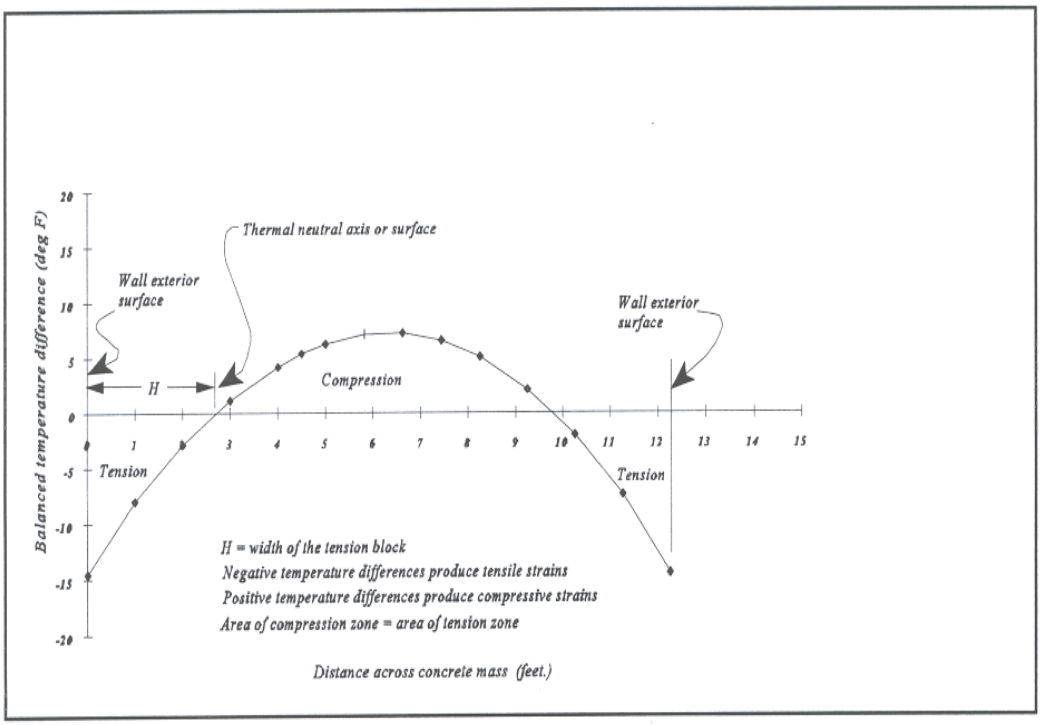

Figure 1-3. Temperature balance computed from temperature difference distribution for surface gradient analysis of lock wall (U.S. Army Corps of Engineers 1997)

CHAPTER 2
LITERATURE REVIEW

Introduction

Mass concrete is defined by the American Concrete Institute (ACI) as "any volume of concrete with dimensions large enough to require that measures be taken to cope with generation of heat from hydration from cement and attendant volume change to minimize cracking" (ACI 207.1-R96). Increasingly, this definition refers to a larger spectrum of structures, but most importantly applies to concrete dams and large concrete foundations, the failure of which can have disastrous consequences to human life and property. For this reason the study and understanding of mass concrete has been of interest to engineers for the last 70 years.

Methods of controlling mass concrete temperatures range from simple to complex, and from inexpensive to costly. Some of the methods commonly used are: low-heat generating concrete mixes that contain pozzolans; precooling of concrete; post cooling of concrete with cooling pipes; insulation or insulated formwork; and aggregates with low-thermal-expansion aggregates.

Past studies on mass concrete have focused on methods to control the heat generated during cement hydration, modeling adiabatic temperature rise, and predicting thermally induced internal stresses. The studies vary in the environmental conditions in which the mass concrete is poured, purpose of the mass concrete structure, duration, and placement of thermocouples and strain gages. Three such field studies are presented here.

Supplementary Cementitious Materials

The temperature rise in the centers of large concrete sections is approximately proportional to the cement content used in the mix design of the concrete. This

temperature rise is affected by the rate at which heat is developed due to the hydration of the cement. The rate and quantity of heat generated is further affected by the fineness and chemical composition of the Portland cement. Cements with high Tricalcium Aluminate (C_3A) content tend to hydrate rapidly producing high adiabatic temperature rises.

The most direct way of reducing the temperature rise in concrete is by lowering the cement content in the concrete mix design. However this cannot always be done due to strength and durability restrictions, hence the use of supplementary cementitious materials such as Fly Ash (FA) and Ground Granulated Blast-Furnace Slag (GGBF) is an effective way of reducing the temperature in the concrete without compromising the strength and durability. This reduction in the temperature rise is due to the slower rate of hydration reaction that occurs in concretes with these materials. Figure 2-1 shows the effect of increasing the percent content of these supplementary cementitious materials on the heat of hydration

There is however a negative to replacing a percentage of Portland cement with fly ash and or blast-furnace slag in concrete. It has been observed that for a given strength, blended cement concretes tend to be less ductile, resulting in a higher elastic modulus, lower creep, and a reduced strain capacity (Bamforth 1984). It is important therefore to ensure that the percentage of replacement will result in temperatures low enough to compensate for the loss of ductility.

Long Spruce Dam Rehabilitation Project

The Long Spruce Dam in northern Manitoba, Canada, was found to have a crack that runs from the downstream side to the upstream side of the structure. In order to perform an effective rehabilitation procedure, an in-depth analysis to understand the stresses involved in the failure of the crack was undertaken. A Two-Dimensional Finite

Element Analysis with the aid the commercial software ANSYS was conducted to achieve this goal.

Two theoretical models, namely a transient thermal model and a transient stress model were developed to predict the early stage behavior of the concrete used in the construction of the dam. The finite element analysis sought to investigate whether the residual thermal stresses caused by the heat of hydration of the massive concrete pour were responsible for the apparent loss of strength in the construction joints. The early thermal behavior of a 0.6m x 0.6m laboratory concrete specimen and a dam structure model consisting of an upper and lower block cast 102 hours apart were modeled and observed. The thermal qualities of interest were the temperature field, thermal flux and thermal gradient.

The thermal properties of the concrete in the laboratory specimen model were assumed to be independent of time and temperature during hydration. The thermal conductivity was assigned a constant value of 4.1 KJ/m-hr-$^{\circ}$C, and the specific heat 1971 KJ/m^3 -$^{\circ}$C, obtained from literature. The ambient temperature in the laboratory analysis was also kept constant at 23 $^{\circ}$C to represent a controlled environment.

For the dam structure model, the thermal properties were slightly different to reflect the use of larger aggregate. The initial temperature of the concrete was set at 10 $^{\circ}$C because of the use of ice water to pre-cool the large blocks. The boundary condition of convection is imposed on all sides except the bottom where a prescribed temperature is described. For the stress analysis, the bottom surface is constrained in all directions, representing the contact friction of the block resting on the floor.

The analysis for the laboratory specimen model was conducted in six hour load steps. The beginning of thermal process in the dam structure model was analyzed every six hours, and then increased to every 12 hours, then finally every 24 hours.

The adiabatic temperature rise resulting from the heat of hydration was calculated using the expression developed and presented by Tanabe, T., Kawasumi, M., and Yamashita, Y., in Seminar Proceedings for Finite Element Analysis of Reinforced Structured, Tokyo, Japan (1985), and published by the American Society of Civil Engineers (ASCE) in 1986:

$$T(t) = K(1- e^{-\alpha t})$$

Where,

T = temperature (°C)
t = time (days)
K = constant based on casting temperature (°C)
α = constant based on casting temperature

The values for K and α are obtained from the plots in Figure 2-2.

The total amount of heat generated was then calculated by the following equation:

$$Q(t) = C_p \rho_T(t) = KC_p \rho(1- e^{-\alpha t})$$

Where,

C_p = specific heat capacity of the concrete J/g-°C
ρ_T = density of the concrete g/m^3
t = time (days)
K = constant based on casting temperature (°C)
α = constant based on casting temperature

And the rate of heat generation calculated as:

$$R(t) = KC_p \rho \alpha e^{-\alpha t}$$

Where,

C_p = specific heat capacity of the concrete J/g-°C
ρ_T = density of the concrete g/m^3
t = time (days)
K = constant based on casting temperature (°C)
α = constant based on casting temperature

The highest temperature was found to occur in the middle section of the specimen and decreased as it got closer to the sides of the model. This confirms the theory that the outer section of the concrete loses heat more quickly than the middle because of its greater exposure to the atmospheric conditions.

Radovanic (2004) found that the 0.6m x 0.6m laboratory specimen was too small to realistically predict the behavior of massive concrete structures. This led to the enlargement of the FE model by the two, five and ten orders of magnitude. The size that came closest to a realistic characterization of the behavior of the Long Spruce Dam was the 6m x 6m model. However the maximum temperature for this size model was much higher than the dam specimen. The reason given by Radovanic (2004) was that the dam specimen was cast in September, when the outside temperature was much lower than the initial temperature used for the laboratory specimen. Radovanic (2004) concluded that assumptions made in the calculation of the heat generation rates, material properties and boundary conditions were reasonable and that the finite element algorithm was accurate enough to predict the early age thermal behavior of the laboratory concrete specimen and dam.

A finite element stress analysis of the laboratory specimen and the dam were conducted. As a worse case scenario, the maximum stress occurring in the models were considered as the residual stress. The process of hardening was implemented by

calculating the development of the modulus of elasticity of the concrete with time based on the ACI charts. Radovanic (2004) concluded that the results of the analysis showed that the stresses produced by the thermal gradients were significant enough to cause cracking in the early age concrete.

Reinforced Concrete Wall on Basemat Concrete Slab Project

As part of a field study (Machida; Uehara, 1987), a wall structure consisting of reinforced concrete measuring 1.0m thick, varying height of 3.9 – 4.73m, and 15.0m long was cast on a 1.5m thick basemat concrete slab. The wall was instrumented with thermocouples, effective stress meters, mold type strain gages, and non-stress strain gages, to capture the temperatures, strain and stress responses at different locations within the wall, as shown in Figure 2-3. The measurement time interval used for this instrumentation setup was 1 hour in the first three days, 3 hours until the seventh day, and 6 hours until the thirtieth day, last day of the experiment.

The concrete stress and strain condition immediately after placing was unstable, with recordings becoming stable after 6 hours. The tensile strength was measured using the cleavage test, and the elastic modulus taken as the secant modulus of one-third the collapse strength. The stress-strain relation of one of the non-stress gages was used to calculate the coefficient of thermal expansion which was then assumed to be a constant value throughout the experiment.

A finite element model of half of the concrete wall, basemat slab, and the soil beneath was created to evaluate and forecast cracking in the concrete wall. This was achieved by conducting a heat transfer analysis of the cement's heat of hydration, and the phenomena of heat conduction and convection, followed by a thermal stress analysis for the mechanical characteristics.

Although the atmospheric temperature of the actual structure varied day by day, a fixed temperature of 22 °C was assumed for this analysis. The heat generation rate for the concrete used in the wall was calculated by differentiating with respect to time the equation for adiabatic temperature rise developed by Tanabe et al.

$q = 1/24\ KC_p\rho\alpha e^{-\alpha t/24}$ (kcal/m^{3}h)

Where,

C_p = specific heat capacity of the concrete cal/g-°C
ρ_T = density of the concrete g/m^3
t = time (hours)
K = constant based on casting temperature (°C)
α = constant based on casting temperature

A comparison of the thermal analysis results with the experimental results revealed that the maximum measured temperature occurred along the mid-length of the wall and was 2.1 °C higher than the maximum analytical temperature which also occurred along the mid-length of the wall model. After the peak temperature was obtained, the analytical temperature decrease was larger than the experimental, but after 12 days the temperature of the structure equaled the ambient temperature. The difference in the estimation of temperature decrease was attributed to the difference in the assumed heat convectivity in the model and the actual convection, and the variance in atmospheric temperature of the experimental wall instead of the assumed constant temperature in the model.

The stress analysis model was similar to the one used in the thermal analysis. It was assumed that no sliding took place between the basemat and the subsoil. The degrees of freedom were constrained in the direction perpendicular to the structural symmetry plane and perpendicular to the subsoil's outside surface plane. The compressive and

tensile strengths and elastic modulus of the wall were calculated using empirical formulas that related their development with the temperature of the hydrating concrete. Constant values for the Poisson's ratio and coefficient of thermal expansion were also assumed.

The results showed that the maximum expansion in the structure was recorded after 24 hours. The maximum compressive stress occurred in the mid-length one day after concrete placement in both the experiment and finite element analysis. The compressive stress became a tension stress in the middle and bottom of the wall as the concrete aged.

The experiment showed that the upper mid-length of the structure experienced a small compression peak at 18 hours which then became a tensile stress, peaking after about 2 days becoming a compressive stress again peaking at 8 days after placement. On the other hand, the finite element analysis results showed no clear compressive stress peak, but a tensile peak at 60 hours, after which it began to decrease but remained in the tensile stress region. Again, the difference in the measured and analytical results for the mid-length point close to the surface was attributed to the real atmospheric conditions of the structure being different than the assumed constant values assigned in the finite element model.

The James Bay Concrete Monolith Project

The James Bay concrete monolith project (Ayotte et al., 1997), a joint effort between the Societe d'Energie de la Baie James (SEBJ) and the Ecole Polytechnique de Montreal, focused on developing a methodology, based on finite elements, that could be used to predict the heat generated and resulting thermal stresses in mass concrete. The project included both an experimental component and a modeling component.

Three concrete monoliths were built directly on bedrock in the St. James Bay Territory in Northern Quebec Canada, on the site of a major hydroelectric project. The

dimensions of the monoliths were 2 meters wide, 10 meters long, and 2 to 3 meters high, with the height depending on the bedrock profile. Each monolith was instrumented with 26 T-type (Copper-Constantan alloy) thermocouples to monitor temperature distribution with time, and 8 pairs of mechanical strain targets on the skin reinforcement to measure the induced strain (See Figure 2-4). To observe the performance of the concrete when subjected to severe freeze thaw cycles, the monoliths were cast in February inside large individual heated shelters in which the temperature was maintained at 30 to 32 $^{\circ}$C during the construction phase.

Two and three dimensional modeling of the concrete thermal behavior was conducted using the finite element software ADINA-T while the mechanical response, stresses and strains, were obtained using ADINA. To accommodate simultaneous changes of temperature and mechanical property, a modeling technique which employed a step-by-step incremental approach of calculating the thermally induced strains was developed to bypass the link between ADINA-T and ADINA.

The cement type used was Portland cement Type 20M which was specially made for Hydro-Quebec, so a generic function for the heat of hydration as a function of time was obtained by interpolating between the known functions of Type 20 and Type 50 cements, which was then calibrated by comparing the calculated temperatures with the temperatures measured by the thermocouples. The values for other concrete thermal properties, which included specific heat, the thermal conductivity and convection coefficient, were obtained from various literature sources. Radiation was not considered because the monoliths were built inside shelters which blocked the heat radiation. Convection boundary conditions were used to model the heat loss to the ambient air,

while rock elements were added below the concrete elements for the heat dissipation through the rock foundation.

The structural model for the monolith was identical to the three-dimensional model used in the thermal analysis. Displacements were restricted in the directions of the planes of symmetry, and in all directions at the bottom of the rock elements. The mechanical properties, which included elastic modulus, compressive and tensile strength, were modeled as varying with time, while the coefficient of thermal expansion was given a constant value of 10 $\mu\varepsilon/^{\circ}C$. To include creep and relaxation, an effective reduced elastic modulus that accounts for the reduction in stresses was adopted. The computation of the incremental stresses was done by modifying the ADINA file containing the temperatures from the thermal analysis by calculating the incremental temperature

$\Delta T_i = T_i - T_{i-1}$

Then computing the incremental stresses in which the current Young's Modulus E_i at each step is used

$\Delta\sigma = E_i \Delta\varepsilon = E_i \alpha(\Delta T_i - 0)$

Then finally the total stresses were obtained using the previous time step (σ_{i-1})

$\sigma_i = \sigma_{i-1} + \Delta\sigma_i$

Ayotte et al. (1997) found that the calculated temperature at the center of the monolith model followed almost perfectly the temperatures measured experimentally. However there was a gap between the temperatures calculated at a point near the top of the monolith and those experimentally measured. In the structural analysis, they found that the largest strains were located at the top of the monolith where there was the least restraint, while the strains at the base were very small due to the restraint of the

foundation. It was also observed that the stress variation on the top surface of the monolith was in tension while compressive stresses were computed on the vertical faces due to the insulating effect of the formwork which limited the temperature difference between this surface and the core.

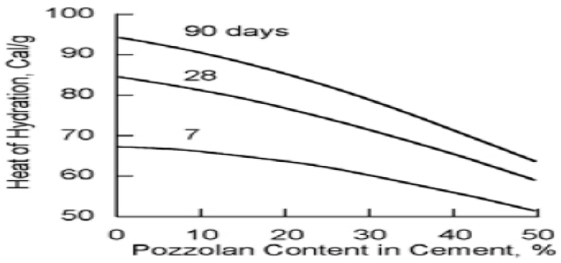

Figure 2-1. Effect of substituting an Italian natural pozzolan on the heat of hydration of Portland cement. (Massazza and Costa, 1979)

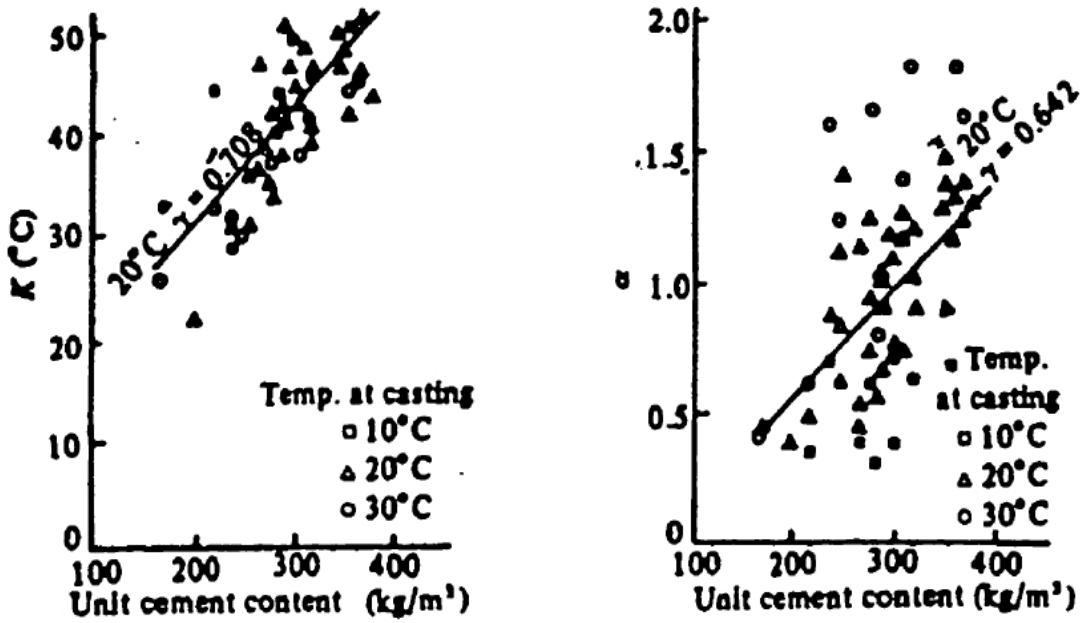

Figure 2-2. K and α Values of adiabatic temperature rise (Radovanic, 1998)

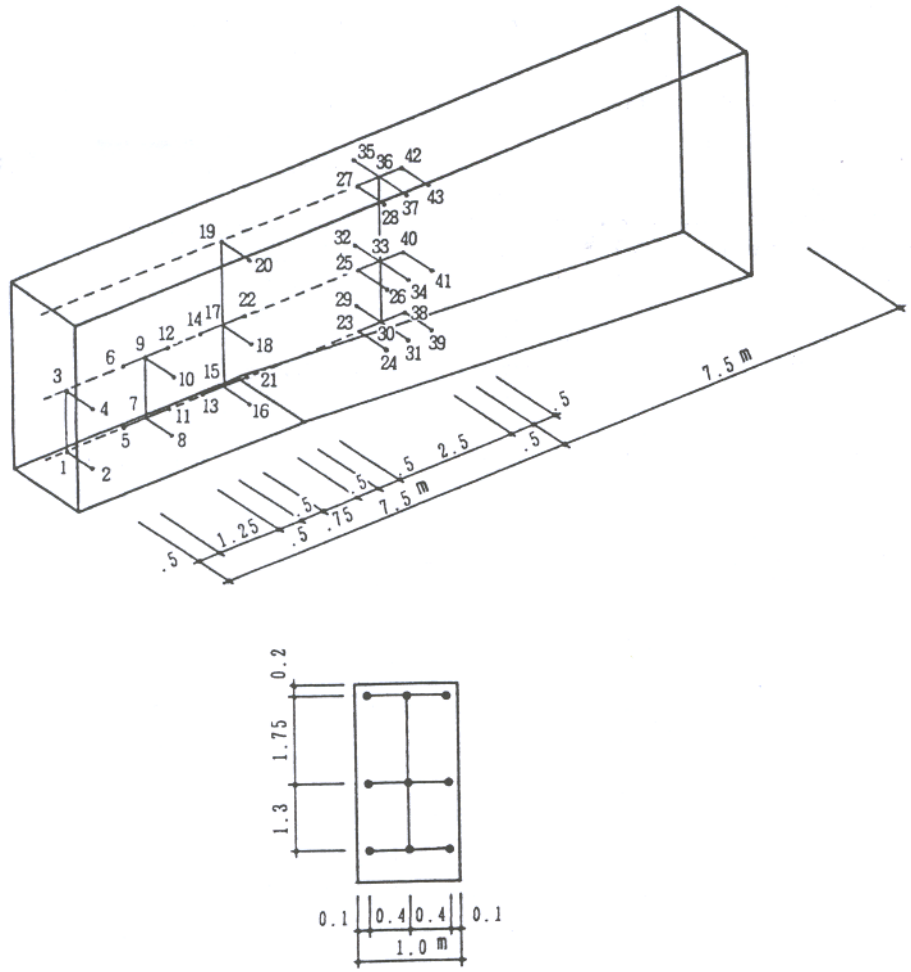

Figure 2-3. Locations for temperature and stress measurements in a reinforced concrete wall (Machida and Uehara, 1987)

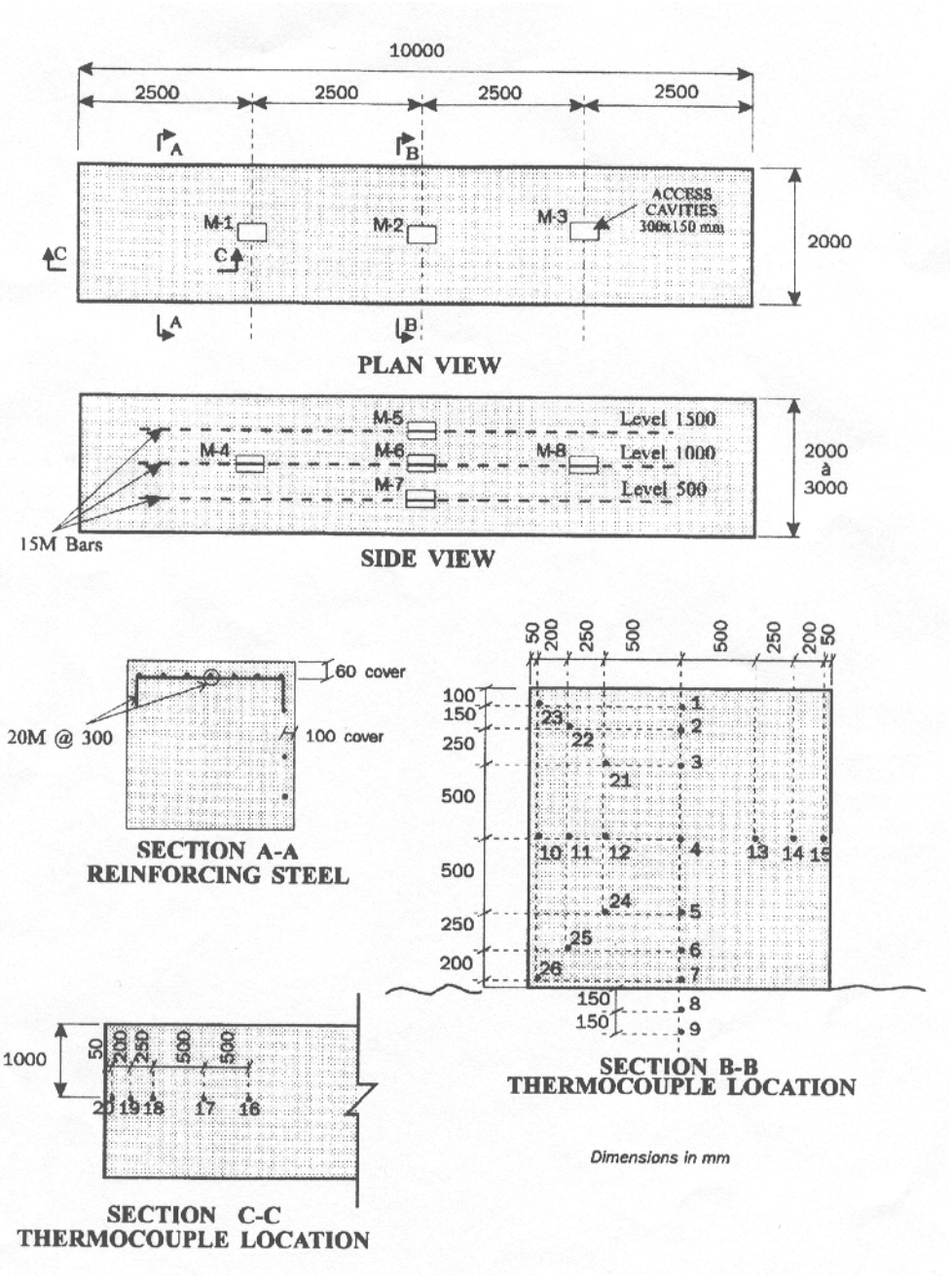

Figure 2-4. Thermocouple and strain gage locations in the James Bay concrete monolith (Ayotte, Massicotte, Houde, and Gocevski, 1997)

CHAPTER 3
FINITE ELEMENT THERMAL MODEL

Introduction

The modeling of the early age thermal behavior of concrete was conducted with the aid of the commercially available TNO DIANA software package. This software package was chosen because it offers a wide range of material models for the analysis of non-linear concrete material behavior including the behavior of young hardening concrete. It can make the assessment of the temperature development due to the cement hydration and the computation of the associated stress development within the concrete mass. Main modeling features utilized are:

- Equivalent age calculation
- Temperature and time dependent material properties
- Crack index calculation to assess risk of cracking

The finite element analysis utilized DIANA's 'staggered flow-stress analysis' feature, in which the thermal analysis is combined with a subsequent structural analysis. The model comprises two domains: one for the thermal flow analysis and one for the structural analysis. These domains overlap for a considerable part of the analysis and so reside in a domain called the 'flow-stress domain'.

Formwork used in the construction of massive concrete structures including plywood and polystyrene foam was explicitly modeled. Since we were only interested in their effects on the transfer of the thermal energy generated by the concrete, these materials were modeled with flow elements, and thus are only active in the thermal analysis. The concrete however is active in both the thermal analysis and structural analysis and therefore lies in the flow-stress domain. For this reason, the concrete is modeled with a quadratically interpolated structural element that is converted during the thermal analysis to a linearly interpolated flow element.

Element Selection

As stated above, the concrete in this analysis is active in the flow-stress domain and therefore is modeled with a structural element. For this, we selected the structural element CHX60, a three dimensional twenty-node brick element that is converted to the three dimensional eight-node HX8HT isoparametric brick element for the thermal analysis. Both types of elements, shown in Figure 3-1, have coinciding corner nodes. However, because the structural CHX60 element is quadratically interpolated and element HX8HT is a linearly interpolated element, the mid-nodes of the CHX60 are disregarded in the thermal analysis. The basic theory and required material properties needed for the structural analysis with element CHX60 will be discussed in further detail in Chapter 4.

Element HX8HT is effective in simulating the phenomenon of convection-diffusion, and is especially useful for the analysis of heat transfer problems. It utilizes linear interpolation and Gauss integration with a 2 x 2 x 2 integration scheme. Heat transfer is modeled by assigning the thermal conductivity and heat capacity of the concrete, where the conductivity can be modeled as isotropic, orthotropic or anisotropic, while the heat capacity is always isotropic. Both the conductivity and capacitance may be constant or depend on temperature, or time or both. For the model described in this paper, both the conductivity and heat capacity were modeled as constant.

Additional properties used to model the internal heat generation of the concrete are the Arrhenius constant (activation energy divided by the universal gas constant), and the heat generation function, which can either be a table that provides a direct description of the heat production rate with respect to the degree of hydration as shown in Table 3-1, or a table that describes the adiabatic temperature rise, in degrees Celsius (°C), with respect to time shown in Table 3-2.

The plywood and polystyrene were directly modeled with element HX8HT, using each of its conductivity and heat capacity to describe the way the heat would be transferred between the concrete, plywood and polystyrene.

The boundary convection was modeled using the BQ4HT element, shown in Figure 3-2, which is a four-node isoparametric quadrilateral element specially used to describe boundaries in three-dimensional thermal analyses. It uses linear interpolation and Gauss integration in its computational scheme. The four nodes in this element were modeled to coincide with the corner nodes of the surface of the brick elements they lie on.

Input Parameters

Heat of Hydration

To properly model the behavior of hydrating concrete, knowledge of the heat produced during the hydration reaction as well as both the material properties of the concrete itself and the environmental conditions in which it is placed are needed.

As previously stated the heat produced during hydration is a function of the temperature history of the concrete. The momentary heat production rate is defined as

$$qv(r,T) = \alpha \cdot q_r(r) \cdot q_T(T) \qquad (3\text{-}1)$$

Where:

r = the degree of reaction
T = the temperature °C
α = the maximum value of the heat production rate (J/m^3-hr)
q_r = the degree of reaction dependent heat production (J/m^3-hr)
q_T = the temperature dependent heat production (J/m^3-hr)

and,

$$q_T(T) = e^{\frac{\frac{E_a}{R}(r,T)}{T+273}} \qquad (3\text{-}2)$$

In which,

E_a = the activation energy of the concrete J/mol

R = the universal gas constant, 8.3144 J/mol-°C

The heat production rate which is dependent on degree of reaction, q_r, can also be determined by DIANA using preprocessing. The temperature history produced under adiabatic hydration conditions is used as the input in this case. DIANA derives the heat production q(t) from

$$q(t) = c(T,r)\frac{\partial T}{\partial t} \tag{3-3}$$

Where

$c(T,r)$ = the capacitance dependent on temperature and degree of reaction

DIANA then approximates the degree of reaction and the temperature dependent heat production

$$r_m = \frac{Q_m}{Q_n} \tag{3-4}$$

$$Q_m \approx \sum_{i=1}^{m} c(T_i^*, r_i^*)\Delta T_i \tag{3-5}$$

Where,

n = specified time points

m = 1,…,n

and,

$$\Delta T = T_i - T_{i-1} \tag{3-6}$$

$$r_i^* = \frac{r_{i-1} + r_i}{2} \tag{3-7}$$

$$T_i^* = \frac{T_{i-1} + T_i}{2} \tag{3-8}$$

Finally, DIANA approximates $\frac{\partial T}{\partial t}$ numerically at m = 1,…,n points and uses equations (3-1) and (3-2) to calculate the corresponding degree of reaction dependent heat production rate $q_{r,m}$

$$q_m = c_m \frac{\partial T}{\partial t} \approx c\frac{T_{m+1} - T_{m-1}}{t_{m+1} - t_{m-1}} \tag{3-9}$$

$$\alpha q_{r,m} = \frac{q_m}{q_{T,m}} \tag{3-10}$$

The preprocessing method was utilized in this research. This method was chosen because the adiabatic temperature rise with respect to time, which is the output obtained from the semi-adiabatic calorimetry test (shown in Figure 3-3), could be conveniently input into DIANA directly.

Power data obtained from isothermal calorimetry testing on cementitious mixtures, shown in Figure 3-4, can be integrated with respect to time to obtain the energy rise,

$$Q = \int_{t=0}^{t} P\, dt \tag{3-11}$$

which is then approximated to the energy rise of the hydrating concrete that is being represented by the mixture by multiplying by the percent cementitious content. The cementitious content of concretes mixtures that will be used to validate the model are presented in Table 3-3. Finally, the adiabatic temperature rise, presented in Figure 3-5, is calculated from the energy using the relationship described by the first law of thermodynamics and expressed in Equation 3-12. This method was used to maintain consistency in the type of input used to describe the concrete hydration.

$$\Delta Q = m \cdot C_p \cdot \Delta T \qquad \text{or} \qquad \Delta T = \frac{\Delta Q}{m \cdot C_p} \tag{3-12}$$

Where:

ΔQ = energy rise (J)
m = mass of concrete (g)
C_p = specific heat capacity (J/g-°C)
ΔT = the change in temperature or temperature rise (°C)

Conductivity and Heat Capacity

Heat energy transferred by way of conduction is caused by the physical interaction between adjacent molecules that have different temperatures. Experimental observations have shown that in the one dimensional plane, the rate of heat transfer through a finite area can be

expressed by what is known as the Fourier law of conduction, expressed by Equation (3-13), and illustrated in Figure 3-6.

$$q_x = -kA_x \frac{\partial T}{\partial x} \tag{3-13}$$

where,

q_x = Heat Flow, J
k = the thermal conductivity, J/m-hr-°C
A = The surface area, m^2
T = Temperature, -°C
x = coordinate, m

The thermal conductivity of a solid is its ability or the ease with which it transmits heat. The minus sign denotes a negative temperature gradient reflecting the fact that the heat flows in the direction of decreasing temperature.

Expanded to the three-dimensional case, as shown in Figure 3-7, the Fourier equation for heat transfer becomes

$$q^n = -k \nabla T = -k \left(i \frac{\partial T}{\partial x} + j \frac{\partial T}{\partial y} + k \frac{\partial T}{\partial z} \right) \tag{3-14}$$

Where,

x, y, z = the axes of the coordinate system
i, j, k = the vectors directions in the coordinate system

Consider the case of a heat-conducting solid such as mass concrete which also has an internal source of heat generation. If q^* is used to denote the rate at which heat is being internally generated per unit volume, then

$$\textit{total heat generated} = q^*(dx\ dy\ dz) \tag{3-15}$$

The law of conservation of energy then states that energies in equations (3-14) and (3-15) must be equal to the rate of energy storage reflected in the time rate of change of the average temperature, t_{avg}, given by

$$\rho c_p \frac{\partial t}{\partial \tau} = \frac{\partial t_{avg}}{\partial x} dx\ dy\ dz \tag{3-16}$$

If we set the equality and divide by the volume of the element, *dx dy dz*, while allowing *dx*, *dy*, and *dz* to go to zero, and t_{avg} to go to t

$$\rho c_p \frac{\partial t}{\partial \tau} = \frac{\partial}{\partial x}\left(k \frac{\partial t}{\partial x}\right) + \frac{\partial}{\partial y}\left(k \frac{\partial t}{\partial y}\right) + \frac{\partial}{\partial z}\left(k \frac{\partial t}{\partial z}\right) + q^* \tag{3-17}$$

This equation represents a volumetric heat balance which must be satisfied at each point in the body, and describes the dependence of the temperature in a solid on the spatial coordinates and on time.

With the results of the thermal diffusivity and specific heat capacity experiments described in Chapter 6, the conductivity of concrete created based on the cementitious mixtures can be calculated by using the relationship

$$k = \alpha \cdot \rho \cdot C_p \tag{3-18}$$

Where,

α = diffusivity m^2/hr
ρ = density kg/m^3
C_p = heat capacity J/gram-°C

The conductivity and heat capacity values of the polystyrene foam were obtained from the manufacturer's specifications, while for the plywood, the typical conductivity and specific heat capacities for plywood used in North America were used.

Convection

Convection refers to the energy transported as a result of macroscopic motion. In other words, the transfer of heat from the surface of a material to a fluid that is moving over it. Figure 3-8 presents an approach to the analysis of convection heat transfer from a surface from which equation 3-19 is derived.

$$q_c = \bar{h} A_s (T_s - T_F) \tag{3-19}$$

where,

q_c = the rate of heat transfer W/m^2-°C
T_s = temperature at the Surface °C
T_F = Fluid temperature °C
A_s = the surface area m^2
$\bar{h}$ = the mean coefficient of heat transfer

The heat lost and gained to the surrounding environment by the hydrating concrete's exposed surface and also the interaction of the foam with ambient conditions is modeled by imposing boundary convection elements. This is conveniently done using the convection element found in DIANA to specify the convection and boundary conditions. The heat flow through the surface of the elements, q^S, due to convection is modeled by the following equation:

$$q^S = h_c (\theta_e - \theta^S) \tag{3-20}$$

where:

h_c = the convection coefficient, W/m^2-°C
θ_e = the external environment temperature, °C
θ^S = the surface temperature of the concrete block, °C

The convection coefficient can be constant, temperature-dependent, or time dependent.

The convection coefficient was calculated using the equation

$$h_c = \begin{cases} 5.6 + 3.95v, & v \le 5\ m/s \\ 7.6v^{0.78}, & v \ge 5\ m/s \end{cases} \tag{3-21}$$

where,

v = the wind speed, m/s

In this research, a constant convection coefficient value of 5.6 W/ m^2-°C or 20106 J/m^2-hr-°C was used for all analyses since all experimentation was conducted in a controlled environment which was maintained at a constant temperature with negligible forced air flow.

Model Geometry

Figure 3-9 shows the model depicting the concrete exposed to ambient conditions at the top surface and with the plywood and polystyrene insulation at the bottom and sides. To improve the efficiency of the analysis, advantage was taken of the double symmetry of the block which allowed for the modeling of one-quarter of the block. The polystyrene insulation, plywood and concrete were explicitly discretized and modeled according to their corresponding thermal properties.

Boundary Conditions

The boundary conditions imposed for the thermal analysis consisted of an initial temperature of the model and the external temperature. Both temperatures were set at the temperatures recorded inside the laboratory on the day each concrete mix was made. Figure 3-10 presents the temperature history of the laboratory during the monitoring of the experimental blocks. The description of the block experiment is presented in Chapter 5.

The average temperature of the laboratory for Blocks 1, 2 and 3 which were cast during the summer months of July and August was approximately 23 °C, while for Block 4 which was cast in October was 20 °C. Figure 3-11 shows the external temperature load of 23 °C that was imposed on the BQ4HT boundary convection elements in the model for Mixture 1.

Table 3-1. Example of direct input of concrete internal heat production

Degree of Hydration	0.10	0.20	0.25	0.40	0.5	0.60	0.75	0.90	1.0
Heat Production Rate (J/m^3-hr)	0.320	0.850	0.960	1.00	0.890	0.400	0.230	0.060	0.00
Total Heat Produced (J/m^3)	3.23e4								
Maximum Value of Heat Production Rate (J/m^3-hr)	7.5e9								
ARRHEN	5000								

Table 3-2. Example of adiabatic temperature rise input

ADIAB	0.0	23.0
	0.1	25.5
	0.2	31.8
	0.3	34.3
	0.4	38.7
	0.5	44.1
	1.0	50.9
	2.0	54.6
	3.0	57.4
	4.0	61.6
	5.0	66.7
	6.0	69.5
	8.0	73.3
	10.0	75.3
	70.0	75.3
ARRHEN	5000	

Table 3-3. Cementitious content of each mixture

Mixture #	1	2	3	4
Percentage of Mixture that is cementitious paste by weight	27.10%	27.10%	27.50%	27.50%

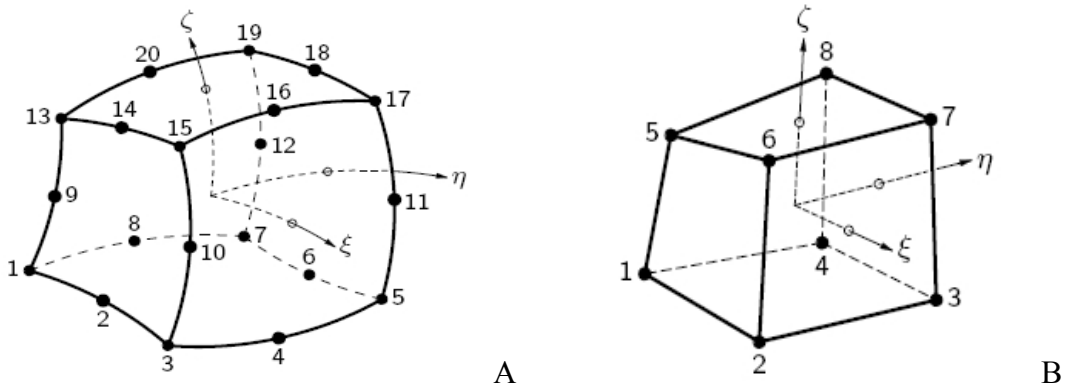

Figure 3-1. Elements used to model early age concrete behavior. A) Twenty-node Isoparametric Solid Brick Element CHX60. B)Eight-node Isoparametric Brick Element HX8HT.

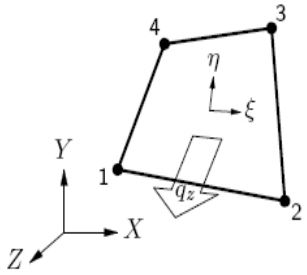

Figure 3-2. Four-node Isoparametric Boundary Element BQ4HT

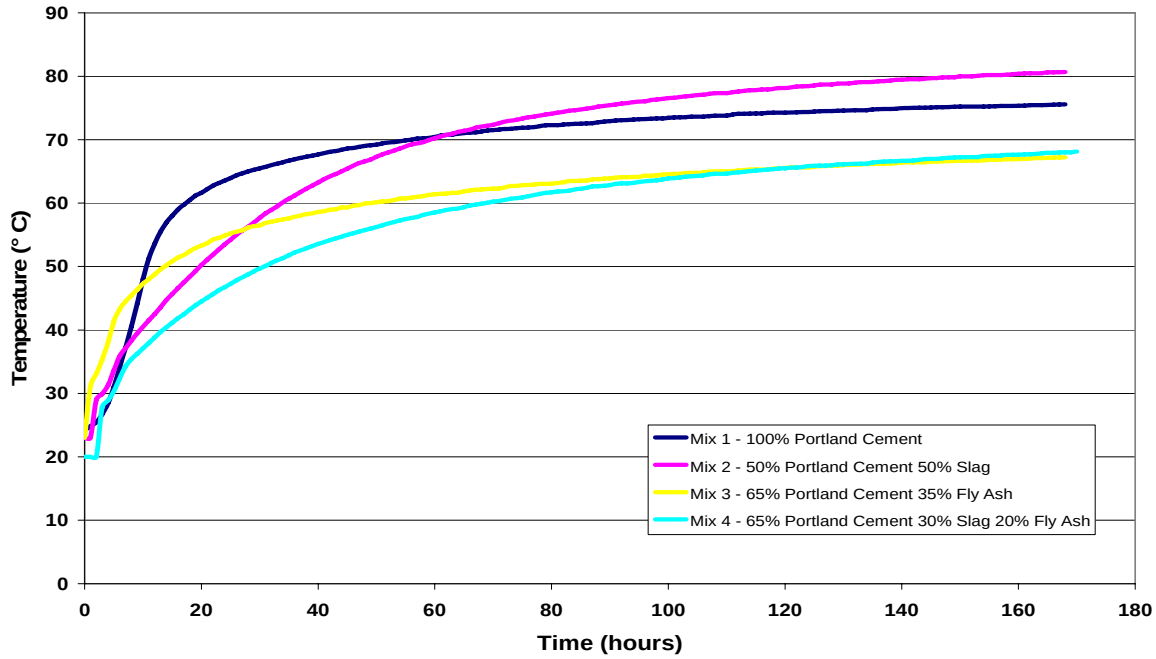

Figure 3-3. Adiabatic temperature rise of each concrete mixture obtained from semi-adiabatic calorimetry testing

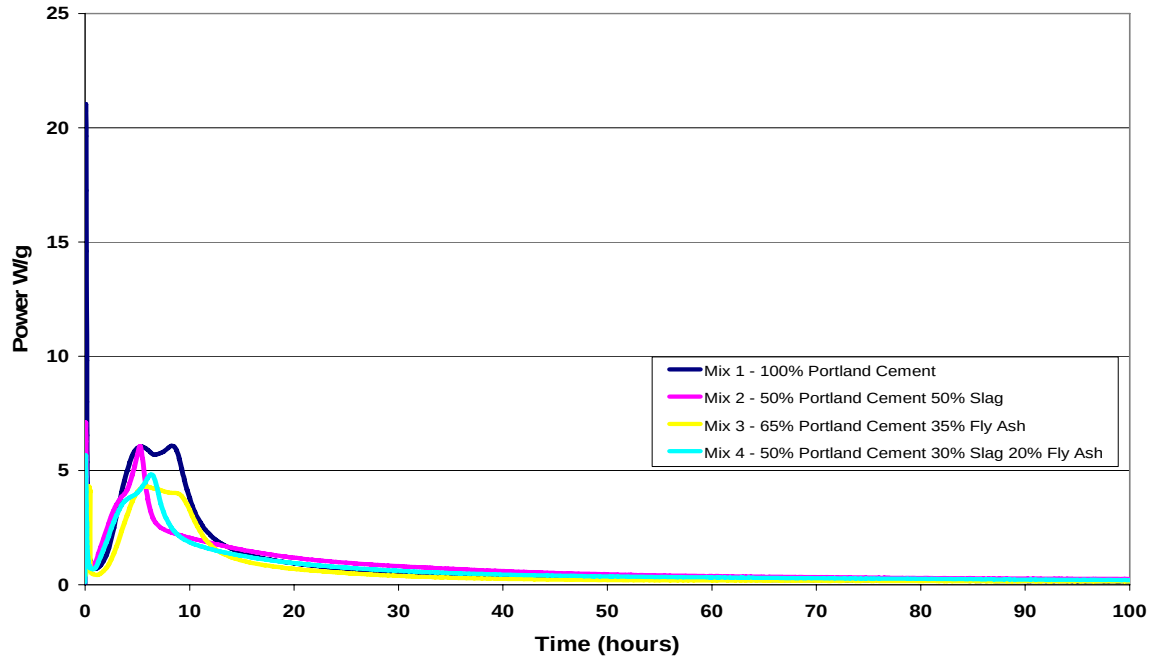

Figure 3-4. Hydration power of each cementitious mixture obtained from isothermal calorimetry testing

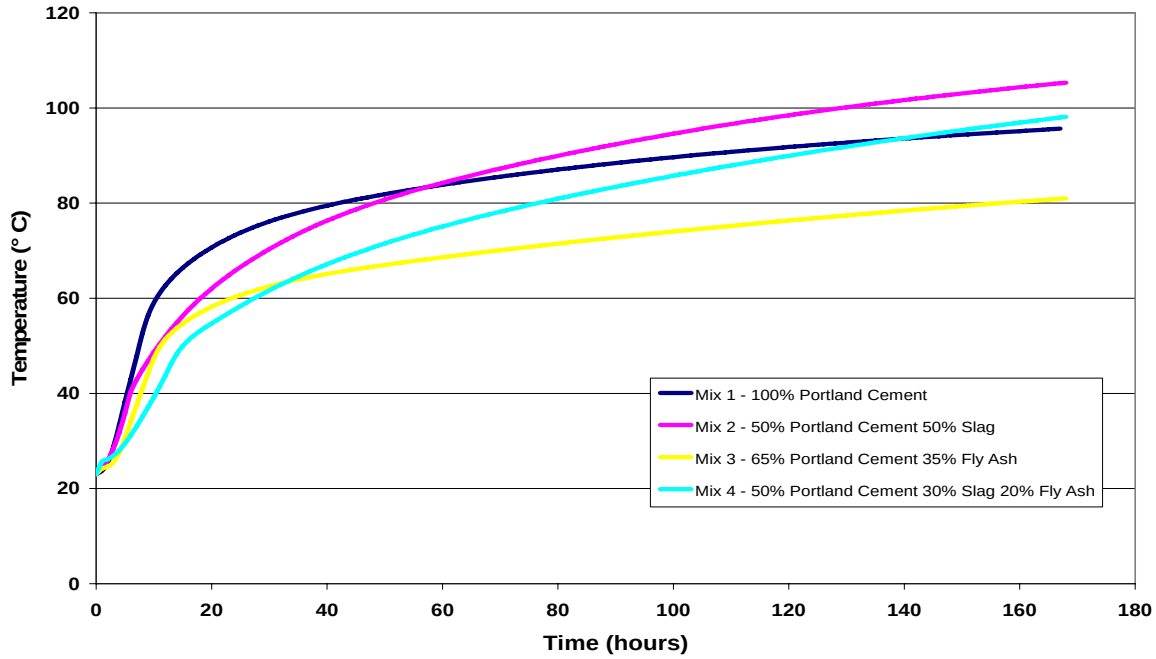

Figure 3-5. Adiabatic temperature rise of each concrete mixture calculated from the hydration power obtained in the isothermal calorimetry testing of cementitious mixtures

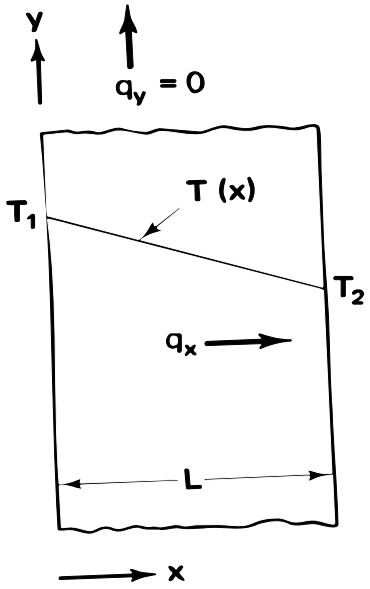

Figure 3-6. One dimensional conduction heat transfer

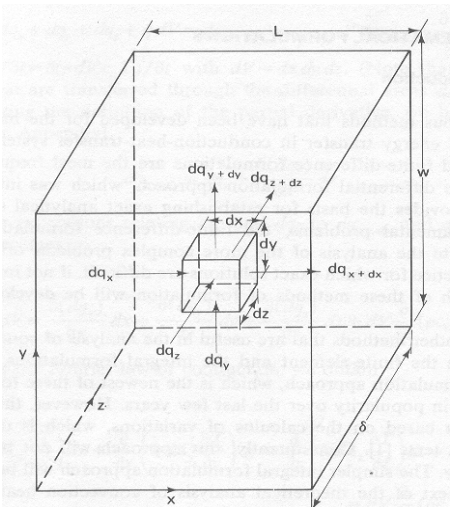

Figure 3-7. Differential volume for a rectangular solid

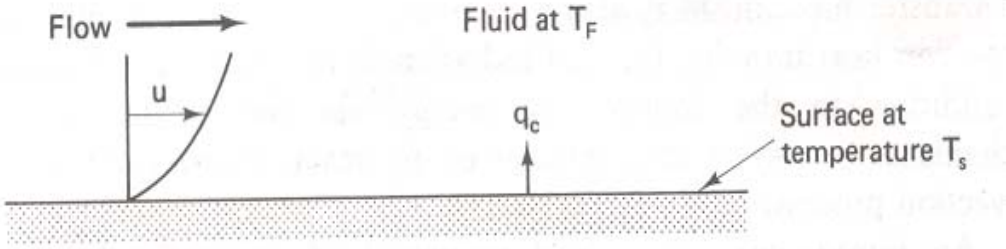

Figure 3-8. Convection heat transfer (Fundamentals of Heat Transfer, Lindon C Thomas)

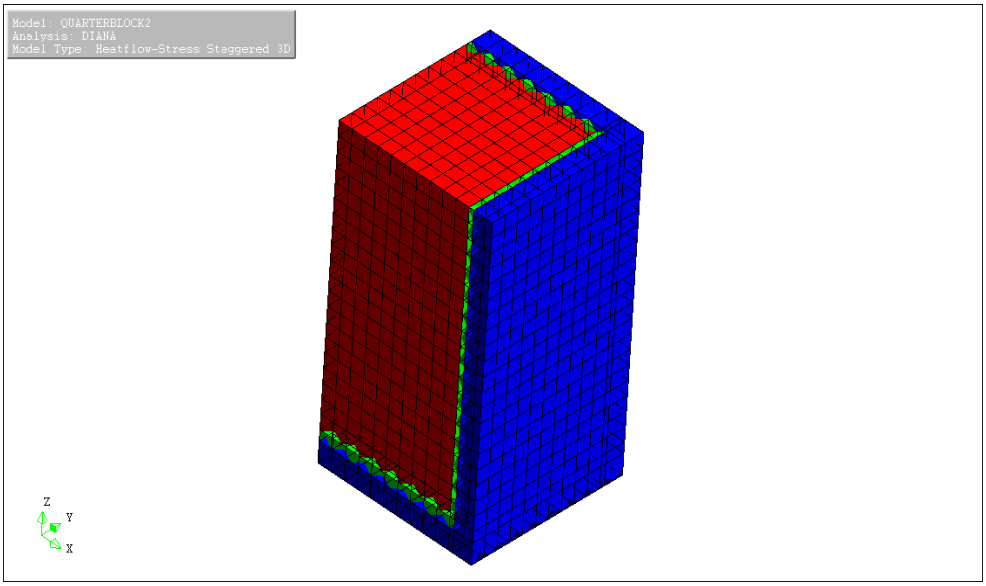

Figure 3-9. Finite element model of concrete block with insulation

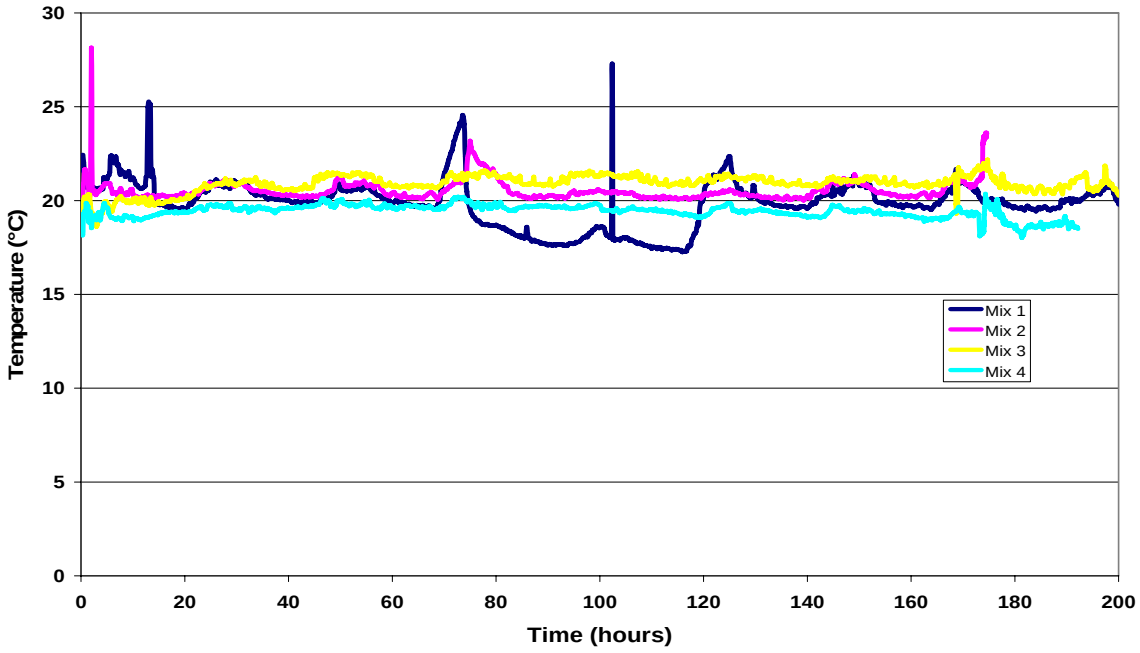

Figure 3-10. Ambient temperatures during experimental block monitoring

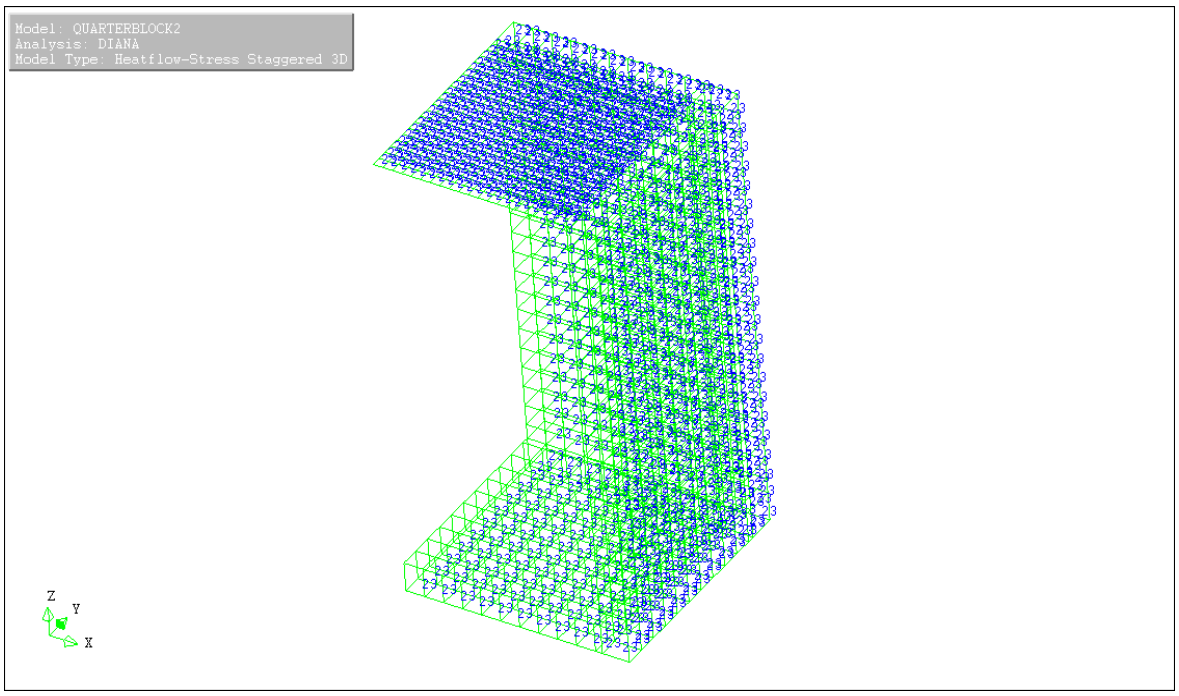

Figure 3-11. External temperatures imposed on finite element model representing the ambient conditions of the laboratory

CHAPTER 4
FINITE ELEMENT STRUCTURAL MODEL

Introduction

Heat produced during the hydration of concrete causes an increase in its temperature. However, because there is the combined effect of the hydration process not being homogeneous and a loss of heat to the surrounding environment, temperature differences will occur throughout the concrete element. These temperature differences can induce thermal strains and stresses that could potentially initiate cracking if they exceed the early age tensile strength of the concrete.

The temperature distribution solution obtained from the thermal analysis is imposed as a thermal load in the structural analysis of the concrete. The mechanical response to the stresses induced by the thermal gradient is greatly dependent on the physical characteristics of the concrete.

This chapter will describe the elements used in DIANA to model the concrete and the physical input parameters required to measure the mechanical behavior.

Element Selection

As stated in Chapter 3, the structural behavior of the concrete block was modeled using the three dimensional twenty-node CHX60 isoparametric solid brick element reproduced here in Figure 4-1. By default, a 3 x 3 x 3 integration scheme is applied, but a 2 x 2 x 2 integration scheme can be used in a patch of more than one element to obtain optimal stress points. The stress and strain distribution is approximated over the volume of the element. Stress σ_{xx} and strain ε_{xx} vary linearly in the x direction and quadratically in the y and z directions. Stress σ_{yy} and strain ε_{yy} vary linearly in the y direction and quadratically in the x and z directions. Stress σ_{zz} and strain ε_{zz} vary linearly in the z

direction and quadratically in the *x* and *y* directions. It utilizes linear interpolation and Gauss integration in its computational scheme.

Material Model

The modeling of the structural behavior presented a few challenges as early age concrete exhibits both an elastic component and a viscous component.

To model the linear elasticity of the concrete, the Young's modulus *E*, Poisson's ratio *v*, and coefficient of thermal expansion α, were directly input into the model. The viscoelastic behavior was modeled based on a Maxwell chain which is also in the form of the direct input of the progression of the Young's modulus with age.

The potential for cracking is tracked by specifying the tensile strength evolution by way of a discrete function that is dependent on time.

Input Parameters

Modulus of Elasticity

Cracking in mass concrete occurs when the tensile stresses induced by the thermal gradients are greater than the tensile strength. The modulus of elasticity (MOE) of concrete is the ratio between the stress and reversible strain and is important because it influences the rigidity of the concrete structure. This linear relationship is known as Hooke's Law and is expressed in Equation 4-1

$$\sigma = E\varepsilon \tag{4-1}$$

Where,

σ = stress (MPa)

E = Young's Modulus (MPa)

ε = linear strain

The elastic limit represents the maximum allowable stress before the concrete will crack and undergo permanent deformation.

In heterogeneous multiphase materials like concrete, the modulus of elasticity increases as it hydrates, which is detrimental to the concrete because the probability of cracking increases as the modulus increases.

Poisson's Ratio

Poisson's ratio is the ratio of the lateral strain to the axial strain within the elastic range of the concrete. According to Mehta and Monteiro (1976), Poisson's ratio has no consistent relationship with the curing age of the concrete. Values obtained during the testing for compression modulus of elasticity was consistently 0.2, which is within the universally accepted range of 0.15 and 0.20 for concrete.

Coefficient of Thermal Expansion

The coefficient of thermal expansion is used to describe the sensitivity of concrete expansion or contraction to changes in temperature. It is defined as the change in unit length per degree of temperature change (Mehta and Monteiro 1976). The value of the coefficient of thermal expansion is particularly important in mass concrete because the strain induced during the cooling period is dependent on both the magnitude of the change in temperature and the coefficient of thermal expansion.

Tensile Strength

In normal concrete applications, the low tensile strength of concrete is usually of little concern because reinforcing steel bars, which have high tensile strength values, are used to increase the overall strength of the structure. However, in mass concrete applications, the use of steel is either impractical, such as in the case of dams, or due to

the size of the structure, the spaces between the steel are large creating elements that are weak in tension.

There are two tests commonly used to estimate the tensile strength of concrete. They are the ASTM C 78 third-point flexural loading test, and the ASTM C 496 splitting tension test, both of which are described in Chapter 6.

Symmetry and Boundary Conditions

The boundary conditions imposed for the structural analysis of the quarter block consisted of the restriction of displacements along the symmetry planes. The base of the block was modeled as being in a fixed support condition and so displacements along the Z direction were also restricted. Both conditions are presented in Figure 4-2.

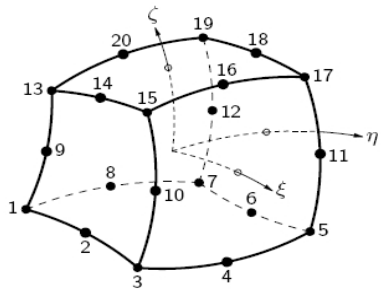

Figure 4-1. Twenty-node Isoparametric Solid Brick element CHX60

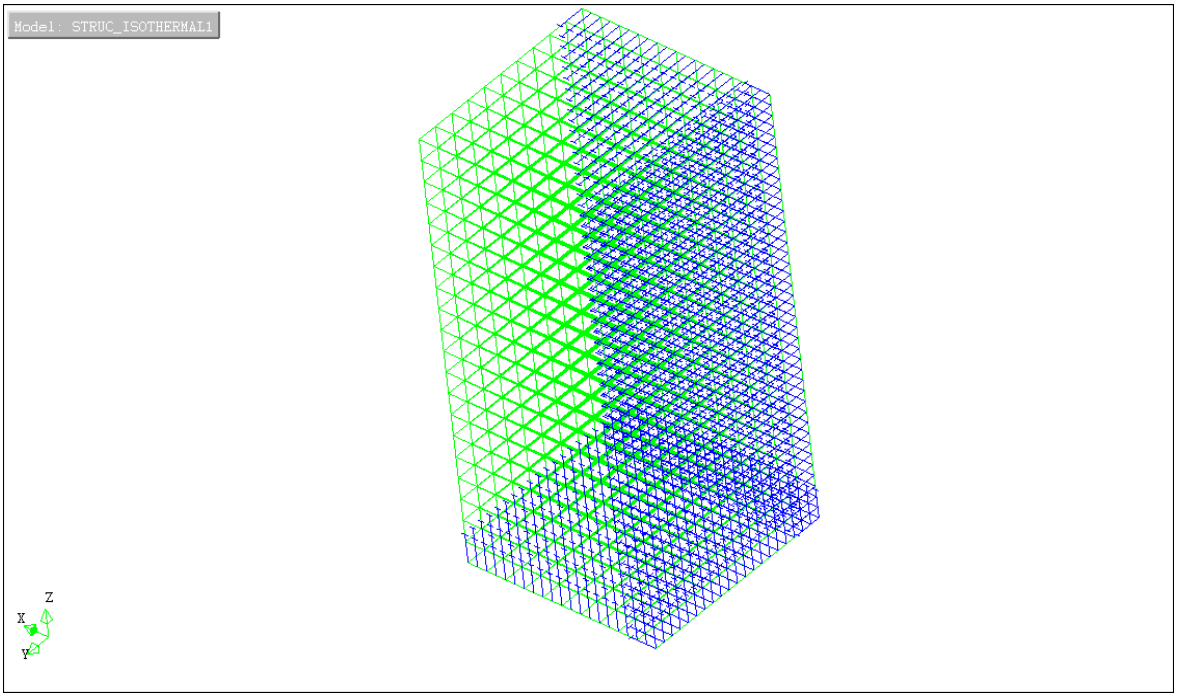

Figure 4-2. Symmetry conditions and supports of model

CHAPTER 5
BLOCK EXPERIMENT

Introduction

To verify that the finite element model created is effective in modeling the early age behavior of hydrating mass concrete, four different mixes of concrete, typical of use in mass concrete applications in Florida, were produced. Each mixture was used to make large concrete blocks with dimensions that qualify them to be characterized as massive concrete elements. Measurements of the temperature and strain at predetermined locations within the blocks were recorded until the equilibrium temperature was achieved. These temperatures and strains will then be compared with the results obtained from the finite element model.

Concrete Mix Design

All of the four concrete mixes used in this study had a water to cementitious material ratio of 0.5 to allow for compatibility with isothermal calorimetry testing that will be used to determine the activation energies and heat of hydration of each concrete mix.

Mix 1 consisted of 100% Type I Portland cement concrete; Mix 2 had 50% of the Portland cement mass replaced by ground granulated blast-furnace slag; Mix 3 contained 65% Portland cement and 35% Class F fly ash; and Mix 4 was a blend of 50% Portland cement, 30% granulated blast furnace slag, 20% Class F fly ash. The mix designs for each block are shown in Table 5-1. The coarse and fine aggregates were adjusted according to the volumetric differences caused by the varying densities of each cementitious material.

Block Geometry

Two 42” x 42” x 42” (1.07m x 1.07m x 1.07m) forms were created for pouring of the experimental concrete blocks. The geometry of the blocks is presented in Figure 5-1. The side faces and base of both blocks consisted of a 0.75 inch thick plywood formwork surrounded by a

three inch thick layer of polystyrene plates. However, one of the blocks had a cover with the same make up as the sides placed on its top surface after pouring was completed in an effort to simulate a fully adiabatic process, while the top face of the other block was left open and exposed to environmental conditions. Figure 5-2 is a photograph of the two blocks after the concrete had been poured.

Instrumentation for Data Collection

The two concrete blocks were instrumented for the monitoring of early age temperatures and strain at predetermined locations. The data acquisition equipment consisted of Type K thermocouples with an accuracy of ±2.2 °C and embedded strain gages.

The layout of the thermocouples and strain gages are presented in Figure 5-3 through Figure 5-5. The thermocouple data and the strain data were recorded in order to validate the finite element model's ability to accurately predict the early age behavior of the concrete block specimens

Temperature Profiles

The location of the thermocouples in the blocks were chosen to capture the temperature difference between the center of the block and the exposed surface, as well as to monitor the near surface temperature gradient to determine if it would contribute to thermal cracking of the concrete. The thermocouples at the sides and bottom of the block were placed to validate the effectiveness of the insulation and by extension the thermal boundary conditions that would be used in the finite element model.

The temperatures measured by the thermocouples placed along the center of the uncovered concrete block of mix 1 are presented in Figure 5-6. It can be seen that, as expected, the highest temperature, 67 °C at 20 hours after pouring, was measured at the center of the block (21 inches below the top surface). The peak temperature measured at the bottom of the block (42

inches below the top surface), also 67 °C, but occurring 33 hours after the concrete is poured, shows that the assumption that the bottom is insulated is valid. It is also shown, as expected, that the lowest temperatures were recorded in the thermocouples located nearest to the exposed top surface of the concrete block.

The temperature data shown in Figure 5-7 provide the temperature profiles measured by the thermocouples located 2 inches from the side surface of the uncovered block. The maximum temperature of 65 °C is again recorded at the thermocouple located 21 inches below the top surface. This temperature is 2.0 °C less than the temperature recorded at the center of the block, which is within the thermal tolerance of ±2.2 °C of the thermocouples. This again serves to validate the assumption of the sides of the block being well insulated.

The temperature profile for the uncovered concrete block with a cement replacement of 50% ground granulated blast-furnace slag is presented in Figure 5-8. As expected in concrete containing slag, the section of the profile representing the increasing temperatures has a slope that is less than that obtained in the concrete containing 100% Portland cement. This is due to ground granulated blast-furnace slag having a very slow rate of hydration reaction. It is interesting to note that while the peak temperature for this concrete was approximately the same as the concrete containing 100% Portland cement in mix 1, it occurred 40 hours after being poured, approximately twice as long.

Figure 5-9 shows the temperatures measured in the concrete of mix 3 in which 35% of the Portland cement was replaced by fly ash. The temperature increase trend in this block shows a lower heat of hydration rate as compared with what was obtained in mix 1 containing 100% Portland cement. The peak temperatures at each location were lower in mix 3.

The combined effects of the ground granulated blast-furnace slag and the fly ash on the hydration rate and peak temperatures of the concrete respectively, is seen in the temperature-time plots of mix 4 presented in Figure 5-10. The slope of the profile during the temperature increase period is very similar to the trend observed in mix 2, showing a slower rate of temperature rise as compared with mix 1 and mix3. The peak temperature in mix 4 was much lower than those of mixes 1 and 2, similar to that of mix 3.

Table 5-1. Mix designs of concrete used in the large-scale blocks

Material	Mix 1 100% Portland Cement (lb/yd^3)	Mix 2 50% Portland-50% Slag (lb/yd^3)	Mix 3 65% Portland-35% Fly Ash (lb/yd^3)	Mix 4 50% Portland-30% Slag-20% Fly Ash (lb/yd^3)
Cement	681	341	443	341
GGBF Slag	0	341	0	204
Fly Ash	0	0	238	136
Water	341	341	341	341
Fine Agg.	1095	1088	1036	1050
Course Agg.	1650	1668	1660	1650

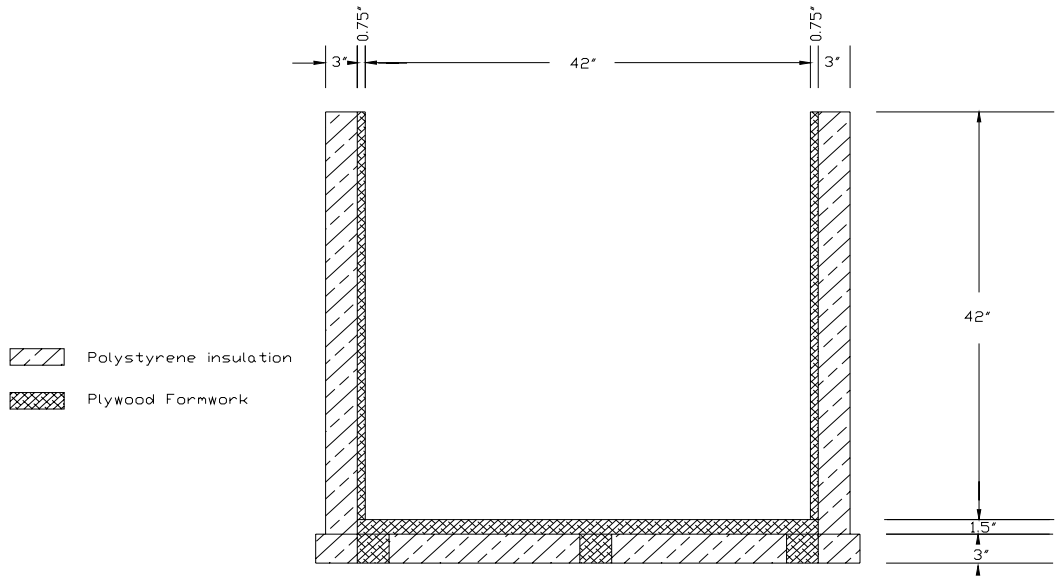

Figure 5-1. Experimental block geometry

Figure 5-2. Uninsulated (left) and insulated (right) mass concrete block specimens

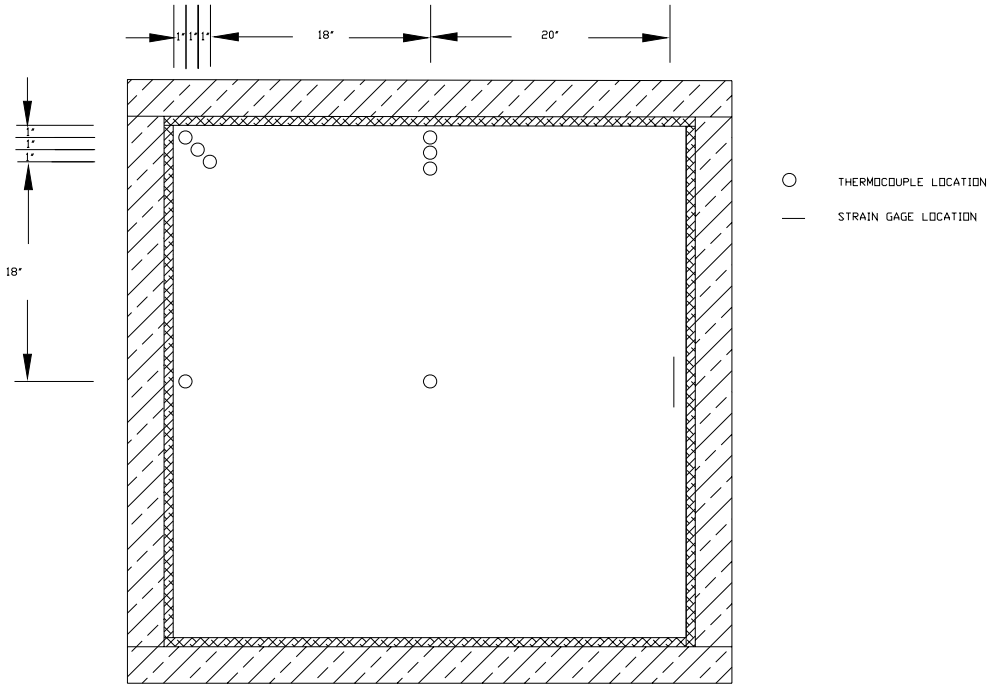

Figure 5-3. Thermocouple location (Plan)

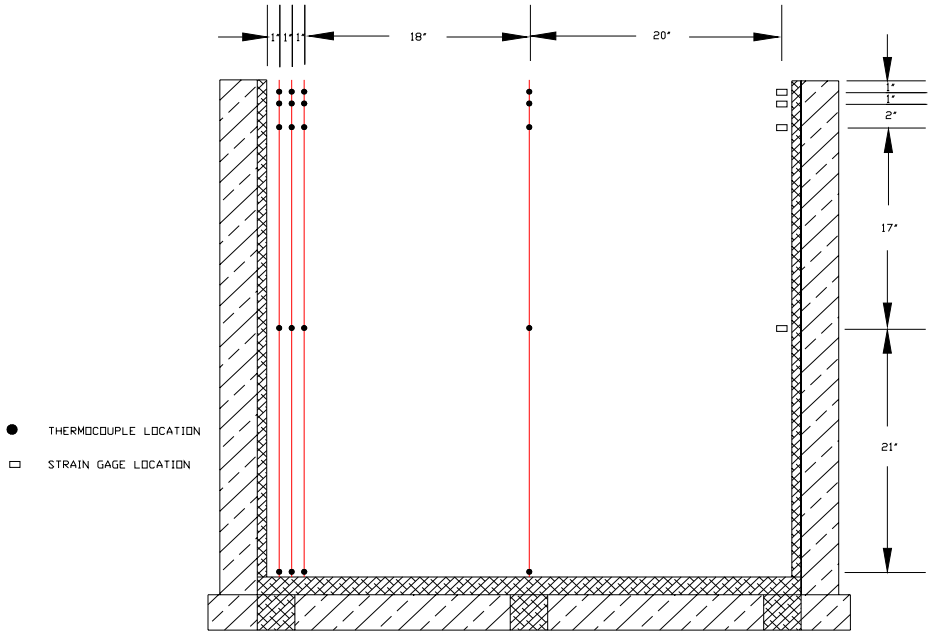

Figure 5-4. Thermocouple location (Section)

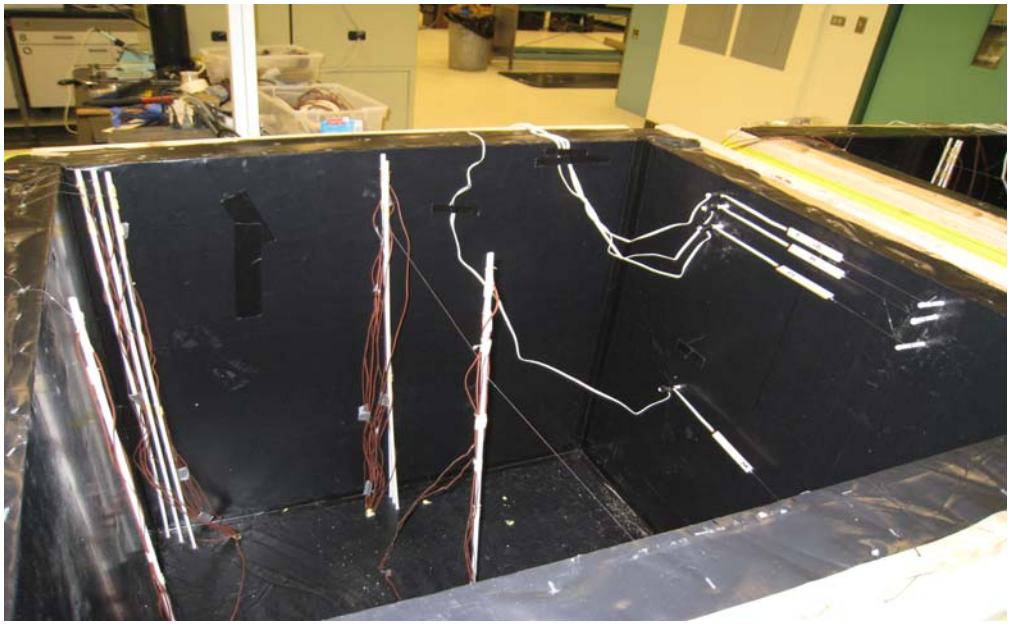

Figure 5-5. Instrumentation layout for experimental block

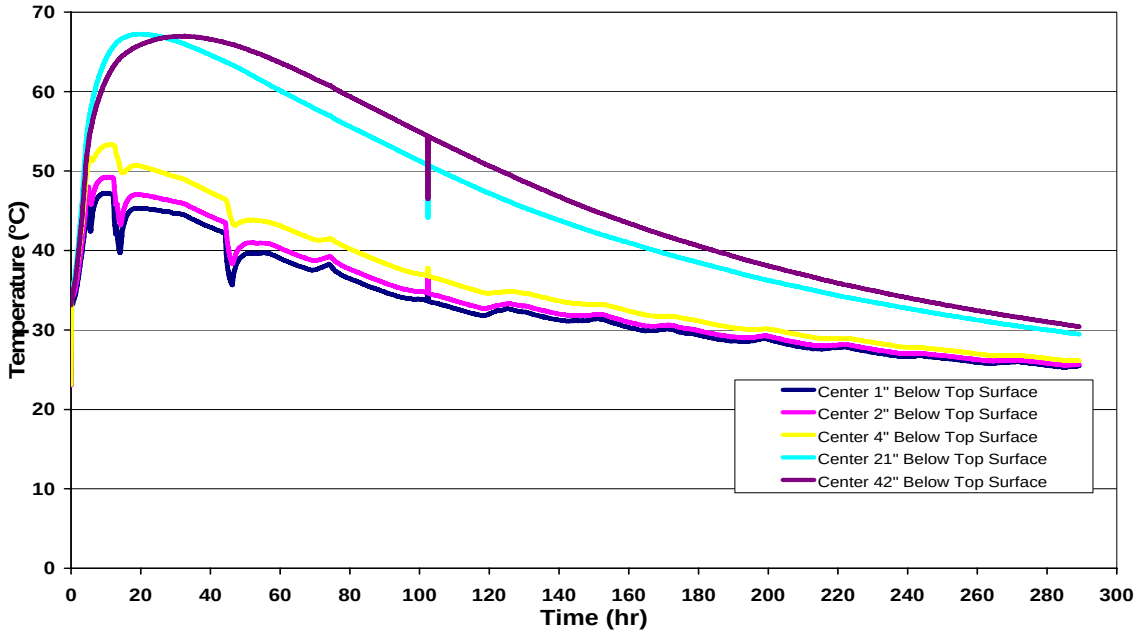

Figure 5-6. Temperatures along the center line of the uncovered concrete block mix 1

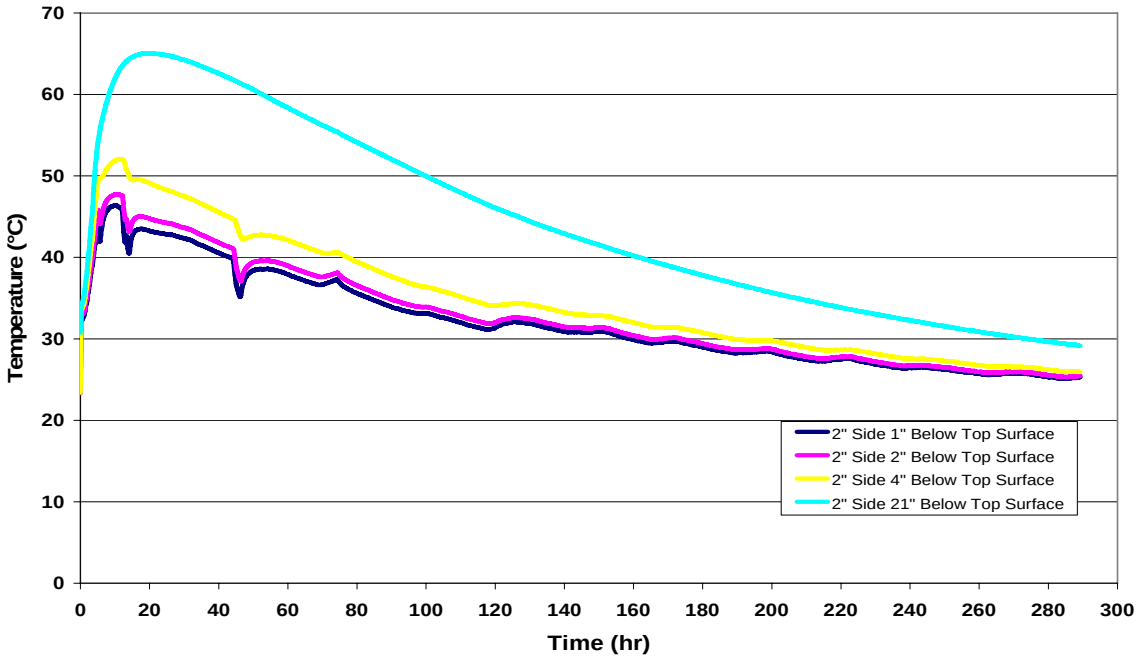

Figure 5-7. Temperatures 2" from the side of the uncovered block in mix 1

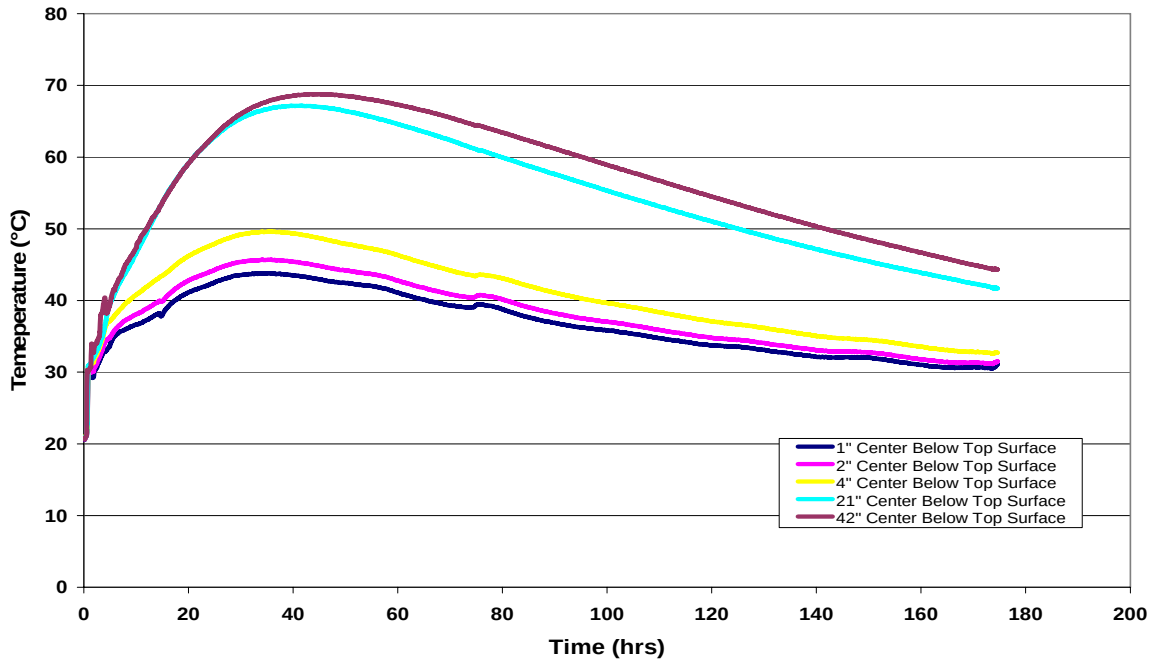

Figure 5-8. Temperatures along the center line of the uncovered block in mix 2

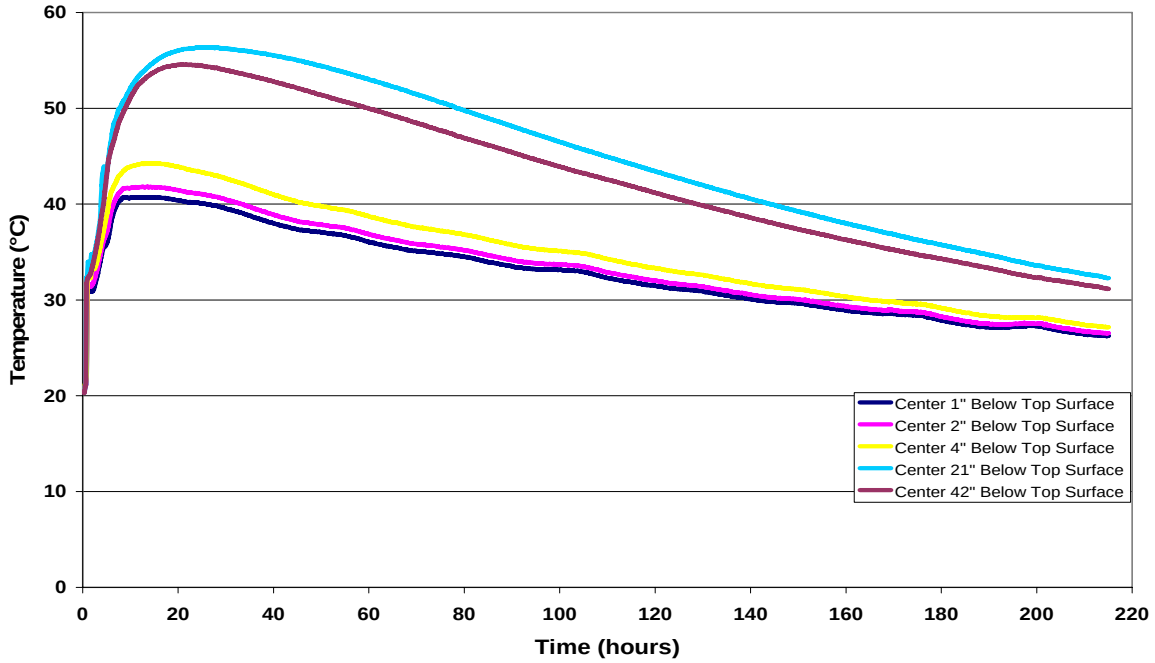

Figure 5-9. Temperatures along the center line of the uncovered block in Mix 3

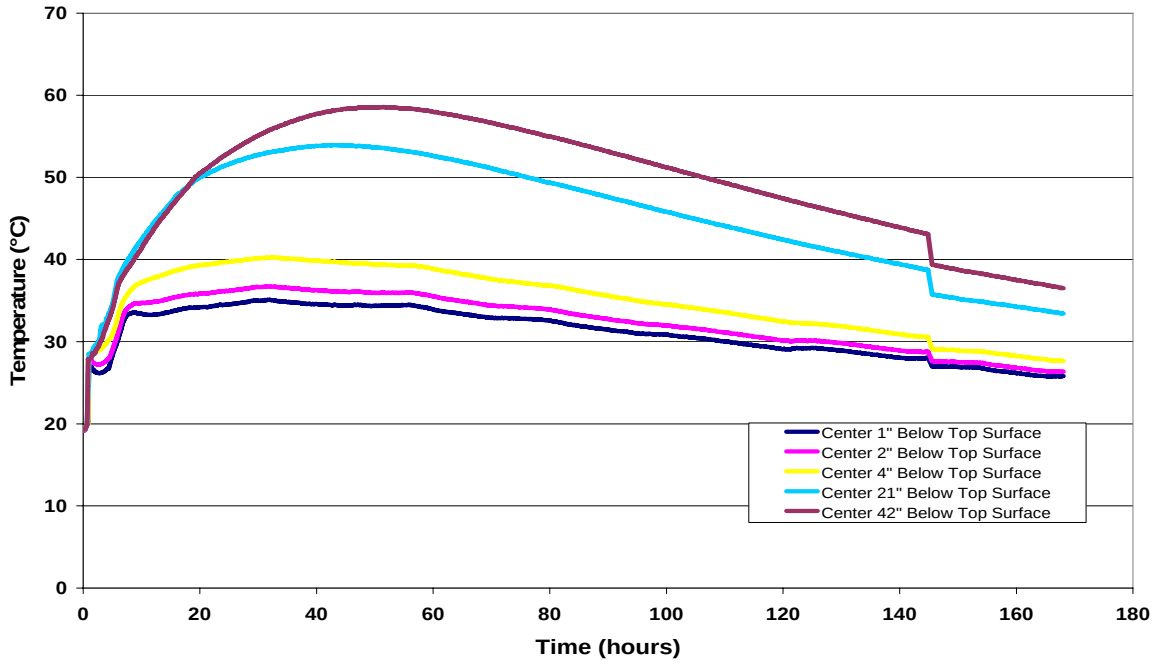

Figure 5-10. Temperatures along the center line of the uncovered block in mix 4

CHAPTER 6
MATERIAL TESTS AND PROPERTIES

Introduction

The laboratory testing of the concrete mixtures used to create each of the experimental blocks focused on characterizing and relating the heat production, maturity, physical and strength properties of concrete at early ages. The results obtained were used as input parameters for the finite element model of the blocks.

Heat of Hydration

The determination of the heat generated during the hydration of the concrete is essential for the characterization of its thermal behavior at early ages. Two of the experimental methods in use today, Semi-Adiabatic Calorimetry and Isothermal Calorimetry testing, were utilized in this research.

Semi-Adiabatic Calorimetry

A Semi-Adiabatic Calorimeter is defined as "a calorimeter where the maximum heat losses are less than 100J/(K·h)" (RILEM , 1997 p451). Semi-adiabatic calorimetry is used in this research instead of adiabatic testing because producing a true adiabatic testing system is extremely difficult and technically advanced as it requires a controlled supply of heat to the system over time. The Semi-adiabatic calorimetry system is a purely passive one which only requires the monitoring of time, temperature and the heat flux for the acquisition of temperature data. The system consists of an insulated cylinder which contains two thermocouples and a heat-flux sensor. One of the thermocouples is embedded into the concrete specimen in the center of the calorimeter while the other thermocouple is located on the exterior. The heat flux sensor is embedded within the

insulation of the semi adiabatic calorimeter. Figure 6-1 presents the energy history recorded from the concrete produced from mix 1.

Isothermal Conduction Calorimetry

Isothermal conduction calorimetry is a very useful testing method for the determination of the heat energy that is evolved from the hydration of a cementitious material over time. It provides a direct measurement of the heat generated by a specimen, avoiding the errors associated with methods that utilize chemical analyses. The resulting data from the heat-flow sensor in the calorimeter is a voltage signal (in the order of milli-volts) that is proportional to the thermal power from the sample. The integral of the thermal power over the time of the test is the heat of hydration of the specimen. For this research, a relatively small sample (6 grams) of the cementitious material used in each mass concrete block was taken and tested in the isothermal calorimeter. The specimens were tested at temperatures of 15 °C, 23 °C, 38 °C, and 49 °C. The data curves produced by the test at each temperature were analyzed for the energy rise versus time, as presented in Figure 6-2. This plot shows a trend of the energy rise with respect to time being significantly larger as the test temperature is increased. However, Figure 6-3 indicates that regardless of the test temperature, the values for the energy rise with respect to equivalent age are virtually equal. Therefore, from this observation we can obtain the relationship between energy rise and temperature rise which can then be used in the input for the finite element model.

Figures 6-4 to Figure 6-6 show the energy rise with respect to equivalent age for mixes 2, 3 and 4 respectively. All except the plot for mix 2 indicate that the values of the energy rise with respect to equivalent age are essentially same. The reason for the

anomaly in mix 2 is not fully understood but is attributed to the high replacement of Portland cement (50%) with ground granulated blast-furnace slag.

The full procedures and explanation of the Semi-Adiabatic Calorimetry and Isothermal conduction calorimetry tests are described by Ferraro (Dissertation, 2009).

Specific Heat Capacity

Specific heat is the amount of heat required per unit mass to cause a unit rise of temperature. The specific heat capacity testing in this research is being conducted with a calorimeter similar to the apparatus used by De Schutter and Taerwe, 1995, shown in Figure 6-7. It contains an interior bath of oil and an exterior bath of polypropylene glycol. These liquids were chosen because of their ability to rapidly transfer heat.

A known flux of heat energy (E1) is supplied to the interior bath containing oil and the resulting temperature increase ($\Delta\theta 1$) observed. The stir paddle is used to distribute the heat evenly throughout the interior bath. The cementitious material was then added to the oil bath and energy (E2) was again supplied to the bath. The resulting change in temperature of the cementitious material ($\Delta\theta 2$) is the final temperature minus the initial temperature of the cementitious material at introduction to the bath. The specific heat capacity of cementitious material then calculated using the following formula.

$$C = \frac{1}{m_c}\left(\frac{E2}{\Delta\theta 2} - \frac{E1}{\Delta\theta 1}\right) \tag{6-1}$$

Thermal Diffusivity

Thermal diffusivity is a measure of the ease or difficulty with which concrete undergoes temperature change (ACI 207.2). Diffusivity is directly related to the type of aggregate used and the density of the concrete. The higher the diffusivity value, the easier it is for the concrete to gain or lose heat.

Three cylindrical 6 x 12” concrete specimens instrumented with thermocouples at the center of their mass are removed from the moist cure room where they were maintained at a temperature of 73 °F ± 2 °F (θ_0) and 100% relative humidity and placed in a water bath at temperature $\theta_0 + \Delta\theta$. As the cylinders are heated by the hot water, the temperature $\theta(t)$ at the center axis of the specimens are measured with respect to time until they reach a steady temperature of 176 °F. The results of the three cylinders are averaged, and inserted in the following equation:

$$\log[(\theta_0 + \Delta\theta - \theta(t))/\Delta\theta] \quad (6\text{-}2)$$

Plotted as a function of time, the curve becomes linear after some time, and the slope of this curve is directly related to the thermal diffusivity. The results of the test show that thermal diffusivity of the concrete used in the first three blocks varies as concrete ages, presented in Figure 6-8.

Flexural Strength

The flexural strength of concrete is a measure of the tensile strength of the concrete. It is also often referred to as the modulus of rupture (MOR). Beam specimens, shown in Figure 6-9, with dimensions of 6 x 6 x 22 in. are cast from the concrete used in the mass concrete blocks. The flexural strength of the concrete in this research was measured by applying two point loads to the unreinforced beam at 1/3 and 2/3 of the loaded span length of 18 inches, as shown in Figure 6-10. A load rate of 30 lbs/sec , which is approximately 6% of the ultimate load as specified in ASTM C78, is applied to the beams so as to not induce significant creep, while restricting the occurrence of premature rupture.

Figure 6-11 shows the stress and strain distribution, according to Bernoulli's theorem. The modulus of rupture (MOR) of the beam cross-section shown is taken as the maximum stresses in the extreme fibers.

Figure 6-12 is a graphical representation MOR versus time for the companion beam specimens cast from each mixture. The results are consistent with typical findings where the mixture containing 100% Portland cement gained flexural strength the fastest while the mixture in which 35% of the Portland cement is replaced by fly ash gains flexural strength the slowest. The mixture containing 50% slag and the mixture containing the ternary blend gained flexural strength at a rate between the mixtures with 100% Portland cement and 35% fly ash.

Splitting Tensile Strength

The splitting tensile strength test was performed on 4 x 8 in. cylinders specimens, sampled from each concrete mixture, in accordance with ASTM C496, the set up of which is shown in Figure 6-13. The tests were carried out at ages of 1, 2, 3, 7, 14 and 28 days and are presented in Figure 6-14 were the strength development over time of the concrete of each mix is observed. As was the case in the flexural beam test, the concrete containing 100% Portland cement gained strength the fastest, the concrete with 35% fly ash gained strength the slowest, while the concretes that contained 50% slag and the ternary blend gained strength at a rate between them.

The results obtained from the splitting tension test were used as the inputs for the finite element model of the experimental concrete blocks. These results were chosen because they are the smaller than the results obtained from the flexural test and therefore are more conservative.

Modulus of Elasticity and Poisson's Ratio Testing

The compressive modulus of elasticity and Poisson's ratio of concrete was determined using the ASTM C469 standard test method. The rate of development of the modulus of elasticity with age, obtained from the compression testing of 4 inch by 8 inch cylinder samples taken from each concrete mix used in the experimental blocks is presented in Figure 6-15.

The stress-strain relationship obtained from the middle third section of the beams during the flexural tests described previously was used to calculate the tensile modulus of elasticity of the respective concrete mixtures, shown in Figure 6-16. This was done because cracking in mass concrete is primarily a phenomenon of tensile action, which is also the failure mode of the flexural test beams.

The compressive modulus, which was higher of the two types of modulus of elasticity, was used in the finite element analysis as it is the more conservative description of the stress-strain relationship of the concrete.

Coefficient of Thermal Expansion Testing

The results of testing for the coefficient of thermal expansion of the concrete mixtures used in this research are shown in Figure 6-17. There was very little change in the values for each mix over the first seven days, which is the duration of the analysis of the finite element model. It was thus decided that a constant input value for the coefficient of thermal expansion of each model block was sufficient for the analysis.

Summary of Material Properties

The thermal properties of the concrete are listed in Table 6-1. The effect of the ground granulated blast-furnace slag on the thermal behavior of the concrete in mix 2 and mix 4 is evident. The slower adiabatic temperature increases observed in the

experimental blocks with these mixes can be attributed to the high activation energies, which is the energy that must be overcome in order for the hydration reaction to occur. Table 6-2 presents the thermal conductivities and heat capacities of the plywood and polystyrene insulation used in the formwork of the block.

The mechanical properties used to describe the strength development of the concrete are listed in Table 6-3. The effect of the ground granulated blast-furnace slag and fly ash on the early age strength of the concrete in mixtures 2, 3 and 4 is evident. The tensile strength at day one in each mix is extremely low, confirming the theory that the benefit of lower rates of temperature rise produced by the use of supplementary cementitious materials occurs at the expense of lower ductility, in a higher elastic modulus to strength ratio, and a reduced strain capacity.

The constant values of Poisson's ratio and the coefficient of thermal expansion are presented in Table 6-4.

Table 6-1. Thermal properties of concrete

	CONDUCTIVITY (J/m-hr-°C)	HEAT CAPACITY (J/m^3-°C)	ACTIVATION ENERGY (J/mol)
Mixture 1	7920	2675596	34235
Mixture 2	4418	2017434	50400
Mixture 3	5883	2603101	32982
Mixture 4	4838	2024985	37330

Table 6-2. Thermal properties of plywood and polystyrene

	CONDUCTIVITY (J/m-hr-°C)	HEAT CAPACITY (J/m^3-°C)
Plywood	540	85440
Polystyrene	224.85	20824

Table 6-3. Mechanical properties of concrete

	Time (Days)	Modulus of Elasticity (MPa)	Tensile Strength (MPa)
Block 1 (100% Portland Cement)	1	13445	1.25
	2	16892	1.66
	3	18064	1.93
	7	20236	2.206
	14	22248	2.972
	28	25213	3.303
Block 2 (50% Portland 50% Slag)	1	8618	0.255
	2	13170	0.807
	3	14893	1.23
	7	19443	2.31
	14	21481	2.45
	28	24921	2.99
Block 3 (65% Portland 35% Fly ash)	1	9791	0.669
	2	13996	0.931
	3	14479	1.28
	7	16547	1.63
	14	18985	1.91
	28	25235	3.30
Block 4 (50% Portland 30% Slag 20% Fly Ash)	1	7722	0.393
	2	10963	0.765
	3		1.01
	7	16905	1.82
	14	20053	2.20
	28	23352	2.85

Table 6-4. Mechanical properties of concrete

	Poisson's Ratio	Coefficient of Thermal Expansion (in/in -°C)
Block 1	0.19	9.16E-06
Block 2	0.20	1.11E-05
Block 3	0.20	1.11E-05
Block 4	0.20	1.004E-05

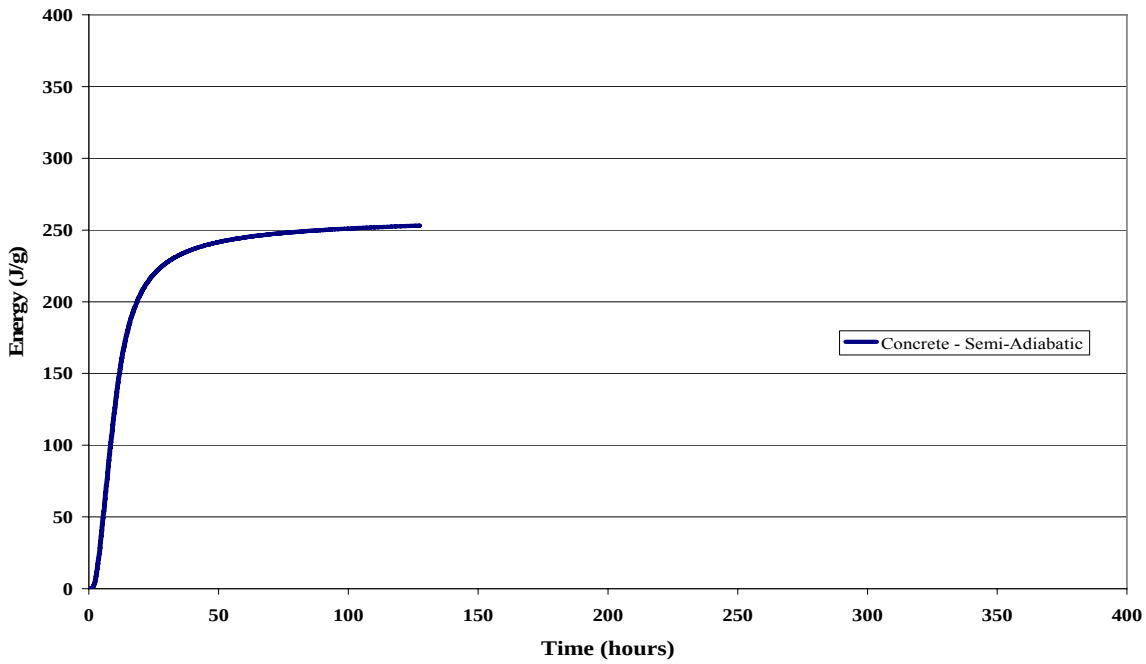

Figure 6-1. Resultant semi-adiabatic calorimetric energy curve for mix 1

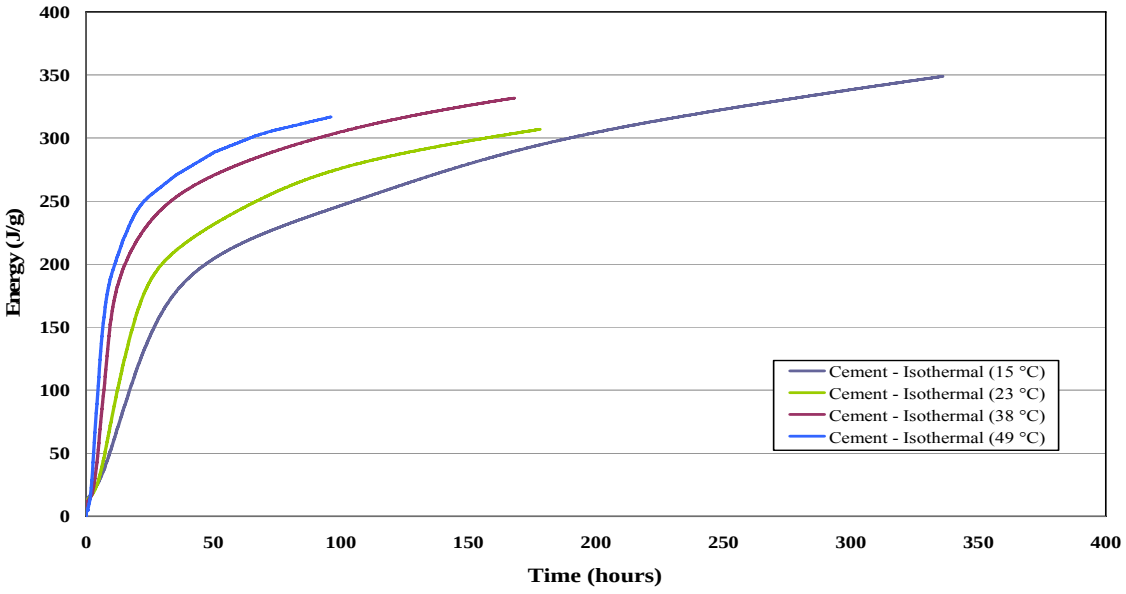

Figure 6-2. Resultant isothermal calorimetric curves with regard to energy versus time for mix 1

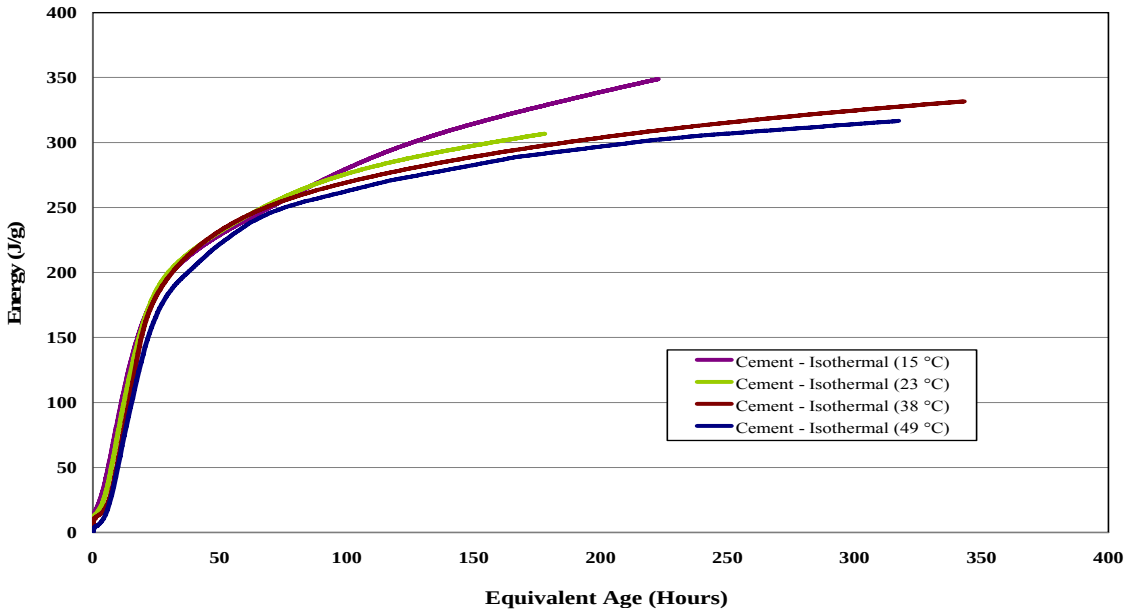

Figure 6-3. Resultant isothermal calorimetric curves with regard to energy versus equivalent Age for mix 1

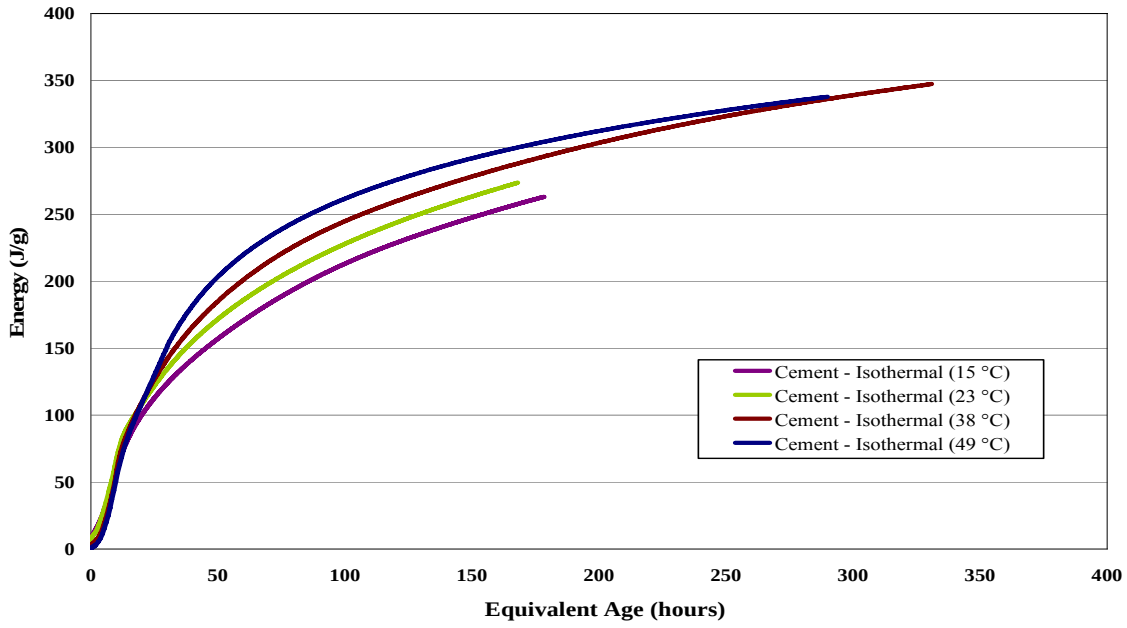

Figure 6-4. Resultant isothermal calorimetric curves with regard to energy versus equivalent Age for mix 2

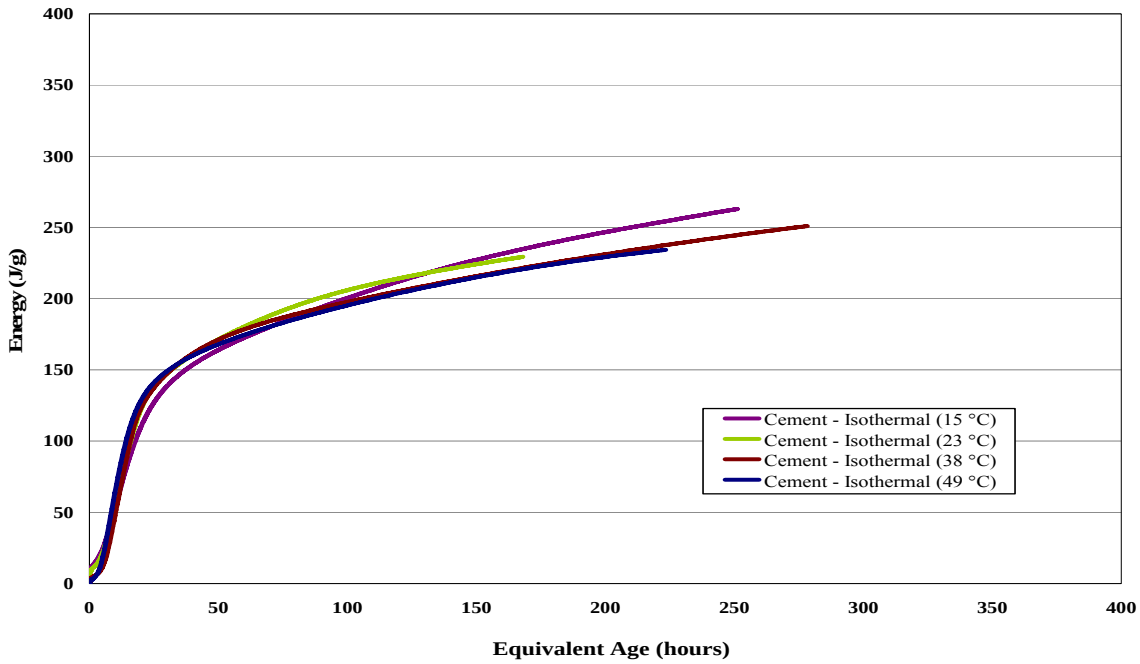

Figure 6-5. Resultant isothermal calorimetric curves with regard to energy versus equivalent Age for mix 3

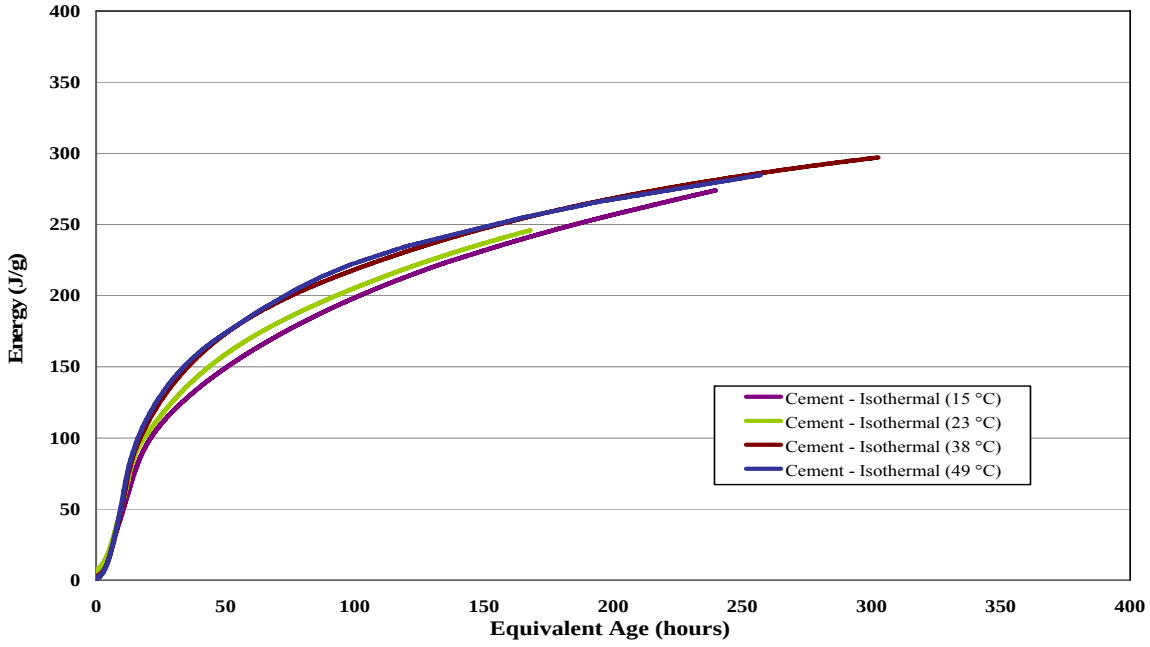

Figure 6-6. Resultant isothermal calorimetric curves with regard to energy versus equivalent Age for mix 4

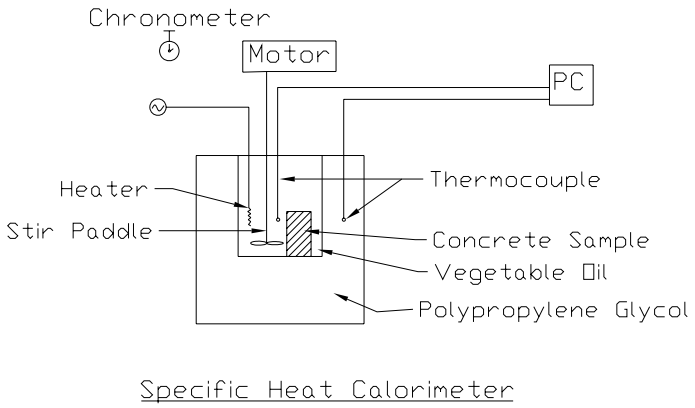

Figure 6-7. Schematic of the specific heat capacity calorimeter

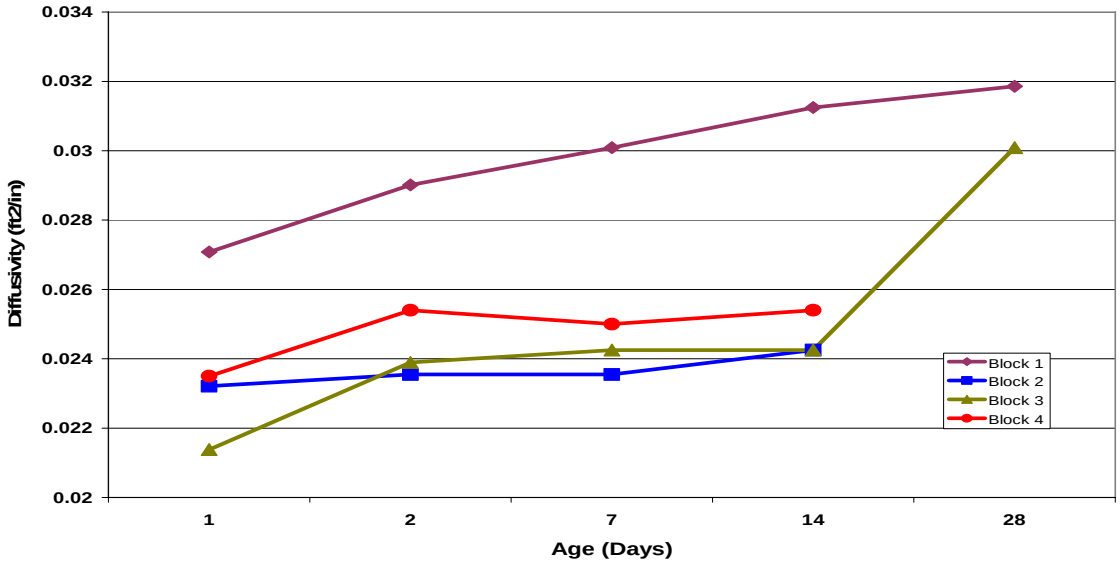

Figure 6-8. Thermal diffusivity vs. age of the experimental blocks

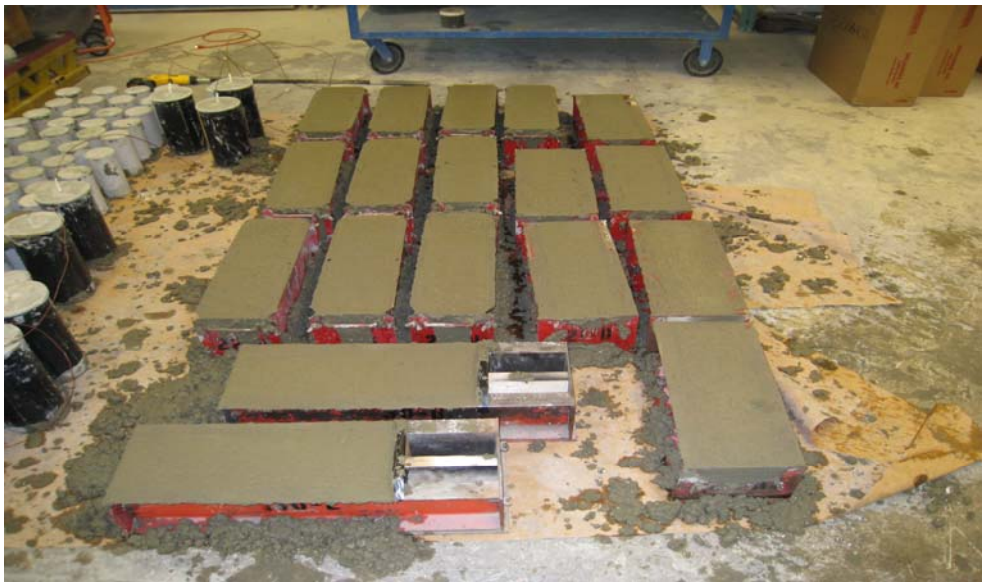

Figure 6-9. Beam specimens for flexural strength testing

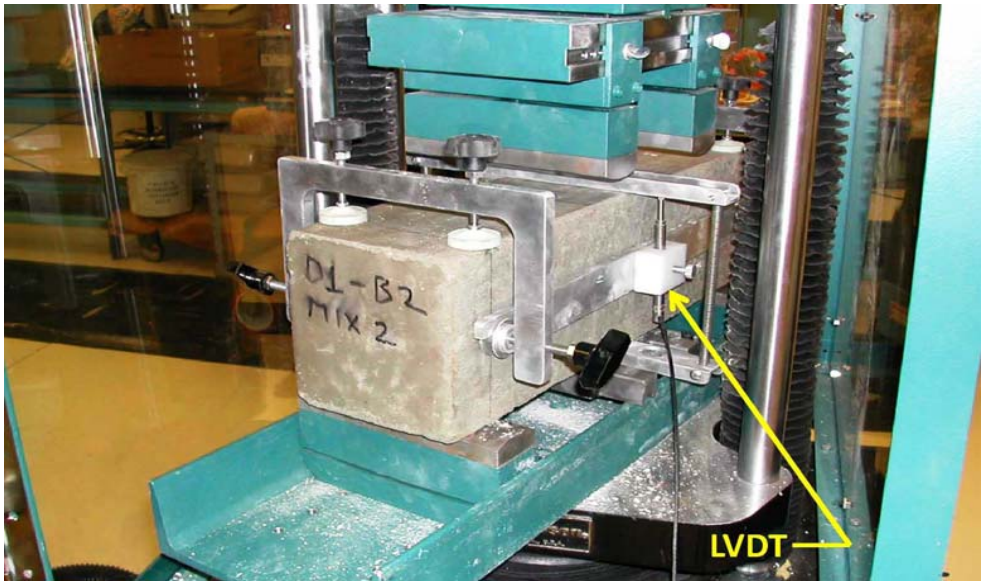

Figure 6-10. Beam specimen undergoing flexural strength testing

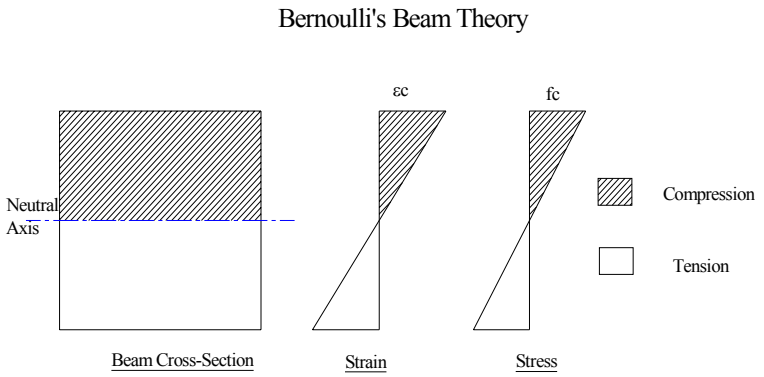

Figure 6-11. Theoretical stress and strain distribution through beam cross section

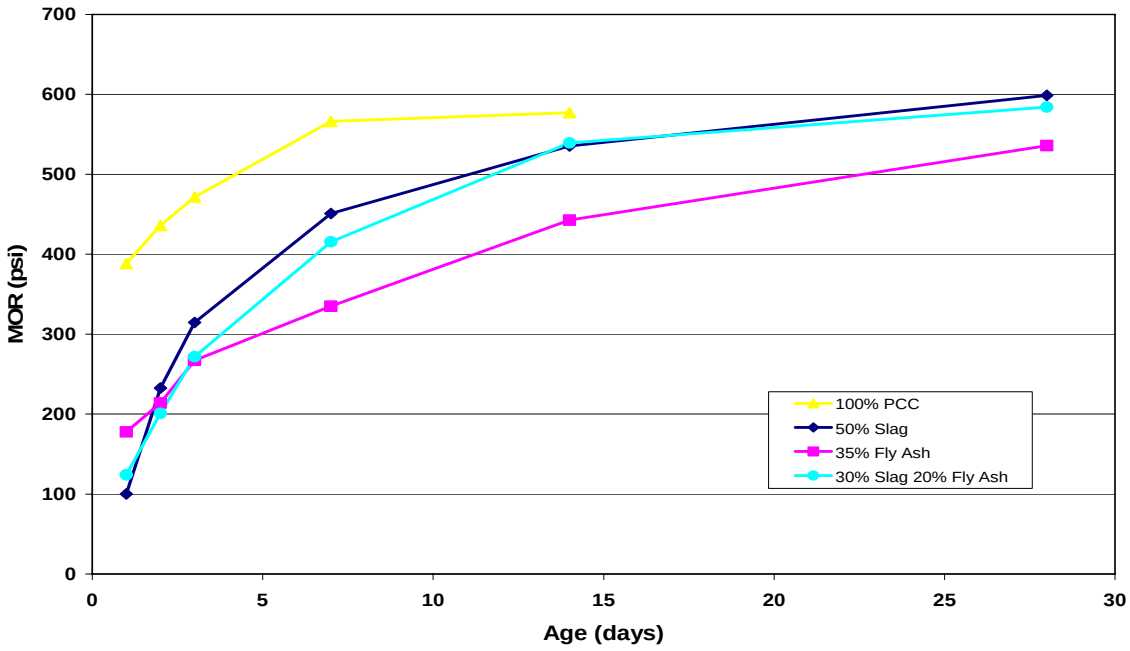

Figure 6-12. The modulus of rupture of the beam specimens taken from mixtures 1, 2, 3 and 4

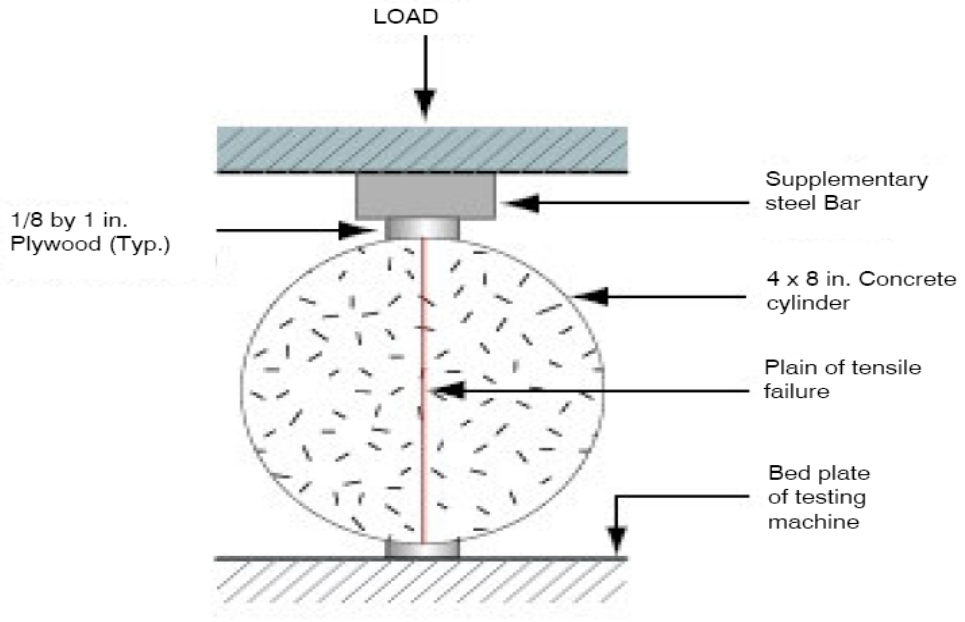

Figure 6-13. Diagrammatic arrangement of splitting tension test ASTM C496

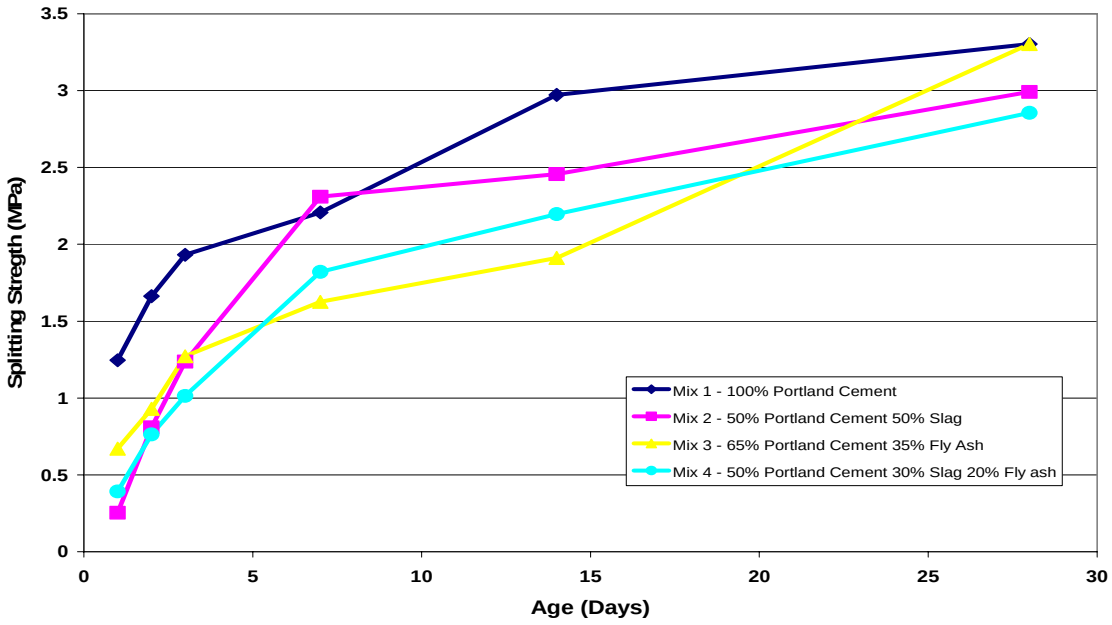

Figure 6-14. Splitting tensile strength of concrete used in mixtures 1, 2, 3 and 4

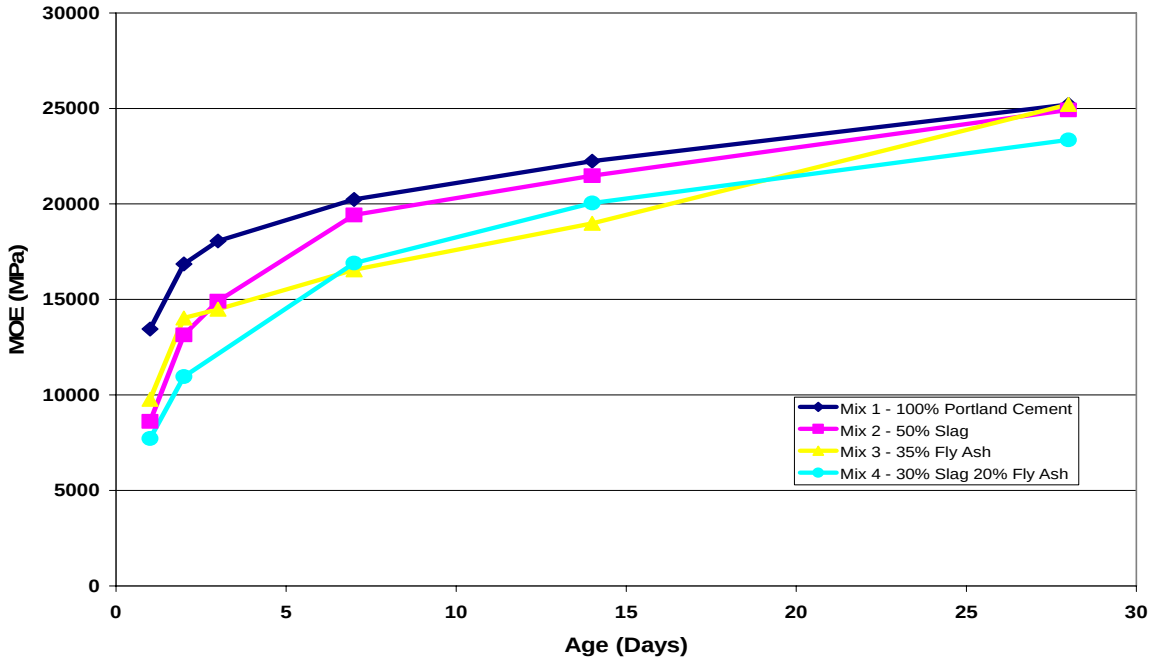

Figure 6-15. Compressive modulus of elasticity versus time

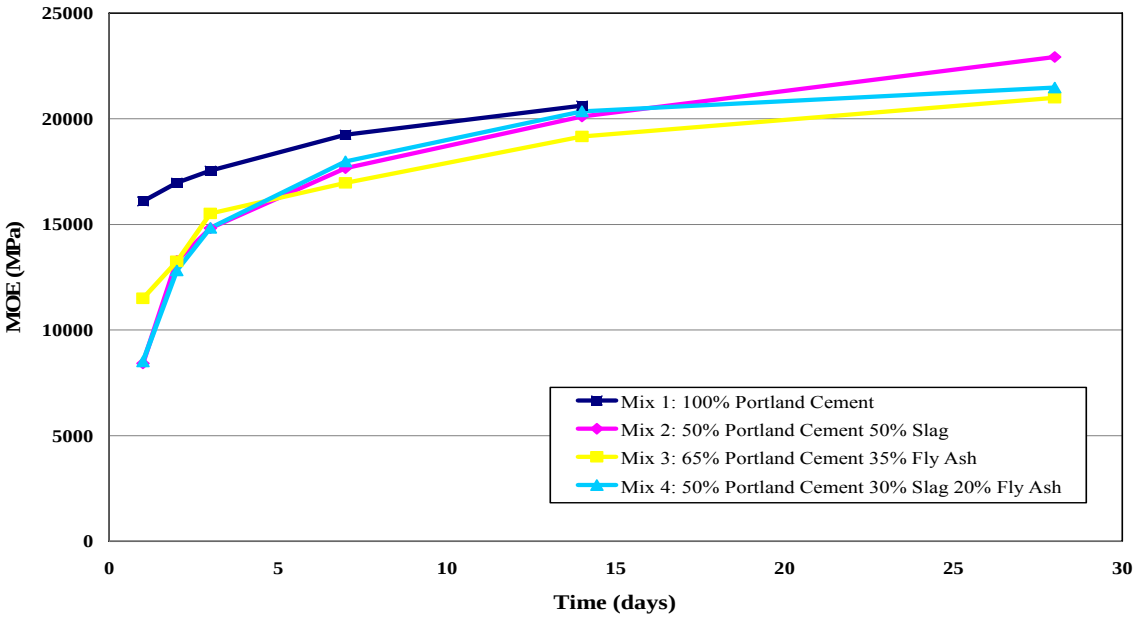

Figure 6-16. Tensile modulus of elasticity versus time

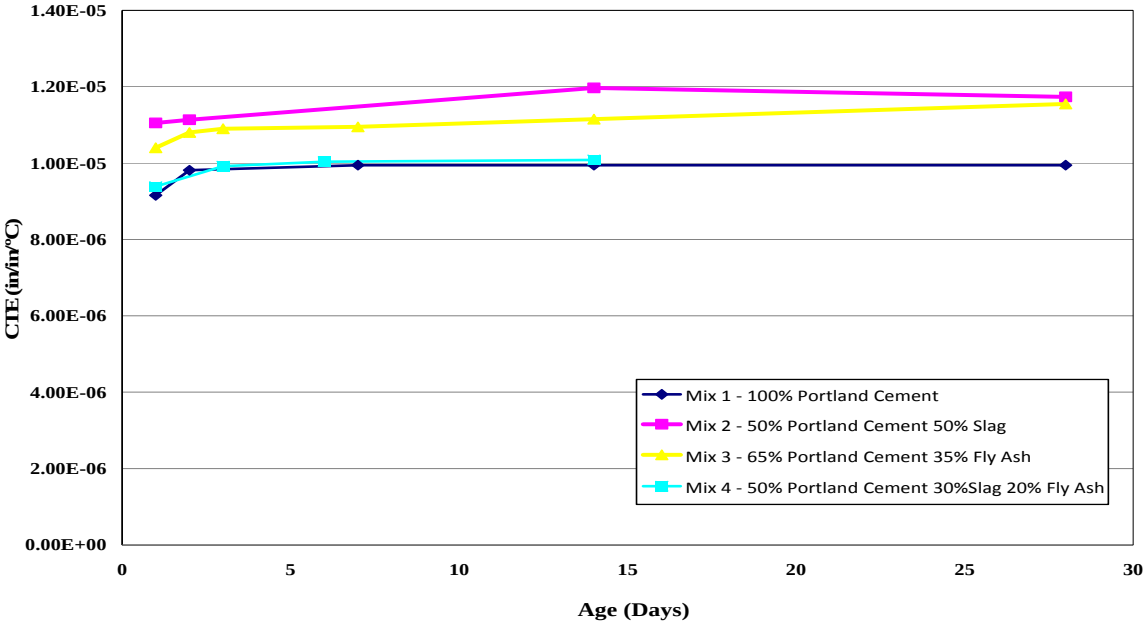

Figure 6-17. Coefficient of thermal expansion versus time for each mixture

CHAPTER 7
THERMAL ANALYSIS RESULTS

Introduction

In this chapter, the temperatures calculated in the model block using the energy input from Semi-Adiabatic and Isothermal calorimetry testing are presented and discussed. The results are compared with temperatures in the experimental block measured by embedded thermocouples. The locations of the thermocouples in the block were presented in Chapter 5. They are duplicated in Figure 7-1 and Figure 7-2 for convenience.

The degree of hydration and the equivalent age with respect to actual time at the top (Element 5069) and central (Element 4069) regions of the model block were conducted and are presented in Figures 7-3 and 7-4 respectively. The equivalent age of each point in the concrete is calculated according to the Arrhenius-type equation

$$t_e = \int_0^t e^{\frac{Ea}{R}\left(\frac{1}{T_{ref}} - \frac{1}{T(t)}\right)} dt \qquad (7\text{-}1)$$

Where:

t_e = equivalent age at the reference temperature, hours
T(t) = average temperature of concrete at time t, °C
T = reference temperature, °C
E_a = activation energy of concrete, J/mol
R = universal gas constant, 8.3144 J/mol-°C

It can be seen from these two plots that the rate of hydration and hence the maturity of concrete varies within the block due to the different time-temperature histories of the hydrating cement.

Figure 7-5 shows the quarter block of hydrating concrete with insulation on the bottom and sides at time step 1.

Semi-Adiabatic Calorimetry Finite Element Results

Points 2 inches, 4 inches, and 21 inches below the top surface along the centerline of the block were chosen for the analysis. These locations were chosen because various DOT specifications for mass concrete generally limit the temperature differential, measured between temperature sensors, between the midpoint and a point 2 inches inside the exposed face.

Figures 7-6 through to 7-17 show the comparison of the temperatures measured in the experimental blocks of each mixture, with the temperature profiles with respect to time produced by the analysis with DIANA.

The trends for the increase and decrease temperature produced by the finite element model for the block containing Mixture 1 were similar to the trend recorded experimentally at all three locations. The time lag in the finite element model with respect to the experimental temperatures can be attributed to the delivery of the concrete over an hour after the commencement of mixing whereas the beginning of the hydration reaction was captured by the semi-adiabatic calorimetry test. Usually the semi-adiabatic test is conducted on a sample of concrete obtained directly from the batch used in the block, however at the time of delivery for mixture 1 the FDOT computer server experienced a communication failure delaying the initiation of the semi-adiabatic test per the IQ drum by approximately 7 hours. To correct this discrepancy, the mixture was recreated in the lab at a starting temperature of 23 °C, and new specimens were created and used in the semi-adiabatic test.

Figure 7-6 presents the temperatures 2 inches below the exposed top surface of the block. The peak temperature of 49.5 °C calculated by the model is identical to the peak temperature of 49.3 °C measured in the experimental block. On the face of it, this is an impressively accurate simulation, however the fact that the concrete in the experimental block spent over an hour in the delivery truck means that some energy which cannot be measured was lost to the environment.

Another factor that should be taken into consideration is that a companion test that monitored cracking with the aid of acoustic emissions apparatus was being conducted. The dips in experimental block's temperature represents each time the plastic cover was lifted off to place the sensors.

Figure 7-7 presents the temperatures 4 inches below the top surface. The peak temperatures of 52 °C in the model and the peak temperature of 53.34 °C measured in the experimental block lie within the ±2.2 °C accuracy of the thermocouples used. Again, the peak temperature in the experimental block is affected by the energy lost while the concrete was in the delivery truck and the lifting off of the cover when placing the acoustic emission sensors.

The block temperatures 21 inches below the top surface of the block are presented in Figure 7-8. At this distance from the surface, there seems to be little effect from the cover being lifted off to place the acoustic emission sensors. The peak temperature of 67.2 °C measured in the experimental block is 6 °C higher than the temperature calculated by finite element model. It is important to reiterate that the trends in temperature gain and loss are similar.

The results for mixture 2 show that the finite element model again produced an increasing temperature trend similar to that measured in the experimental block. The calculated temperatures in the model, shown in Figure 7-9, peaked at 39.6 °C, thirty-eight hours after the start of the analysis. This is a significant 6 °C lower than the peak temperature of 45.7 °C occurring at 35 hours, measured in the experimental block.

Figure 7-10 presents the temperatures 4 inches below the top surface where a similar difference between the model and experimental temperatures is observed. The temperature in the model peaked at 39 hours with a value of 42.4 °C while the experimental block peaked at 49.6°C in 33.6 hours. An even more significant difference between the analytical and experimental peak

temperatures is observed 21 inches below the top surface of the block, 55 °C and 67 °C respectively, as presented in Figure 7-11.

The results for mixture 3 show better correspondence between the finite element model and the experimentally measured temperatures. Both the increase and decrease in temperature trends are similar. At a depth of 2 inches below the top surface the calculated peak temperature in the model, shown in Figure 7-12, was 40.2 °C, while the peak temperature measured in the experimental block at the same depth was 41.8 °C. Figure 7-13 shows that at 4 inches below the top surface the peak temperatures were 42.5 °C and 44.3 °C in the model experimental block respectively. The temperatures at 21 inches are presented in Figure 7-14. Although the temperature trends are similar, the peak temperature in the model is 51.6 °C while the experimentally measured temperature was 56.4°C, a difference of 4.5 °C which is greater than the accuracy range of the thermocouples.

The results for mixture 4 presented in Figure 7-15 through to Figure 7-17 show the same trends as was reported previously for Mixtures 1 and 3 where at depths of 2 inches and 4 inches below the top surface, the difference between the calculated peak temperatures in the model and the measured peak temperatures in the experimental blocks were within the accuracy of ±2.2 °C of the thermocouples. However at 21 inches, the difference increases to approximately 4 °C.

Isothermal Calorimetry Finite Element Results

Figures 7-18 through to 7-29 show a comparison of the temperature profiles with respect to time measured in the experimental block, with those obtained from the analytical finite element model using the energy input from the isothermal calorimetry tests. Again, the locations within the block chosen for analysis are 2 inches, 4 inches, and 21 inches below the top surface along the centerline of the block.

The temperature-time histories of mixture 1 at 2 inches below the top surface produced by the finite element model and measured in the experimental block are presented in Figure 7-18. The increases in temperature for both are identical however the predicted peak temperature in the model is 54.6 °C while the experimentally measured peak temperature was 49.3 °C. As reported earlier, the dips in the experimental block's temperature represent each time the plastic cover placed over the block (to prevent evaporation of the surface water) was lifted off to place the sensors used by the crack monitoring acoustic emissions apparatus. This no doubt affected the peak temperature of points close to the top surface of the block.

Figure 7-19 shows the comparison of the temperature profiles 4 inches below the top surface. Again the peak temperature measured experimentally is affected by the removal of the plastic cover. The increase and subsequent decrease in temperatures however are identical

At 21 inches below the top surface, the effect of the removal of the plastic cover is negligible, and it can be seen in Figure 7-20 that the peak temperature of 69 °C calculated in the finite element model is only 2 °C greater than the 67.2 °C measured experimentally.

Figure 7-21 shows the comparison between temperatures calculated in finite element model and those measured experimentally in the block containing mixture 2. Figure 7-22 is the comparison at 4 inches and Figure 7-23 at 21 inches.

The maximum temperatures obtained in the model at the three locations are all within 2°C of the temperatures recorded experimentally. Considering that the accuracy of the thermocouples used measure the temperatures in the experimental block ±2.2 °C, it can be concluded that the model has exactly modeled the behavior of the experimental block.

The results for mixture 3 show good correspondence between the finite element model and the experimentally measured temperatures. Both the increase and decrease in temperature

trends are similar. At a depth of 2 inches below the top surface, the calculated peak temperature in the model, shown in Figure 7-24, was 43.6 °C, while the peak temperature measured in the experimental block at the same depth was 41.8 °C. Figure 7-25 shows that at 4 inches below the top surface the peak temperatures were 46.4 °C and 44.3 °C in the model and experimental block, respectively. The temperatures at 21 inches are presented in Figure 7-26. Although the temperature trends are similar, the peak temperature in the model is 56.7 °C while the experimentally measured temperature was 56.4 °C, an insignificant difference of 0.3 °C.

The trend of the temperature increases obtained from the model of the block with mixture 4 differed from what obtained in the experimental block, as shown in Figures 7-27 through Figure 7-29. The reason for this difference is unknown but the fact that the peak temperatures obtained at 2 inches, 4 inches and 21 inches were all within 2.2 °C of the peak temperatures measured in the experimental block , and the decreasing trend is also similar provided enough comfort that the temperature gradient within the block was properly modeled.

Summary of Findings

The semi-adiabatic calorimeter was designed to obtain the temperature rise of the concrete in the field, therefore was never intended to serve as a high precision instrument. The temperature results for each of the mixtures modeled were less than the temperatures measured experimentally. This suggests an underestimation of the adiabatic temperature rise of the concrete mixtures and by extension confirms that not all the energy evolved from the concrete was measured.

The adiabatic temperature input from the isothermal calorimetry tests produced temperature profiles that were very similar to the temperatures measured experimentally. In some cases the temperatures in the model were higher than what obtained in the experimental

block. Accordingly, the temperatures obtained from isothermal calorimetry can be considered conservative, and thus the preferred input for modeling concrete.

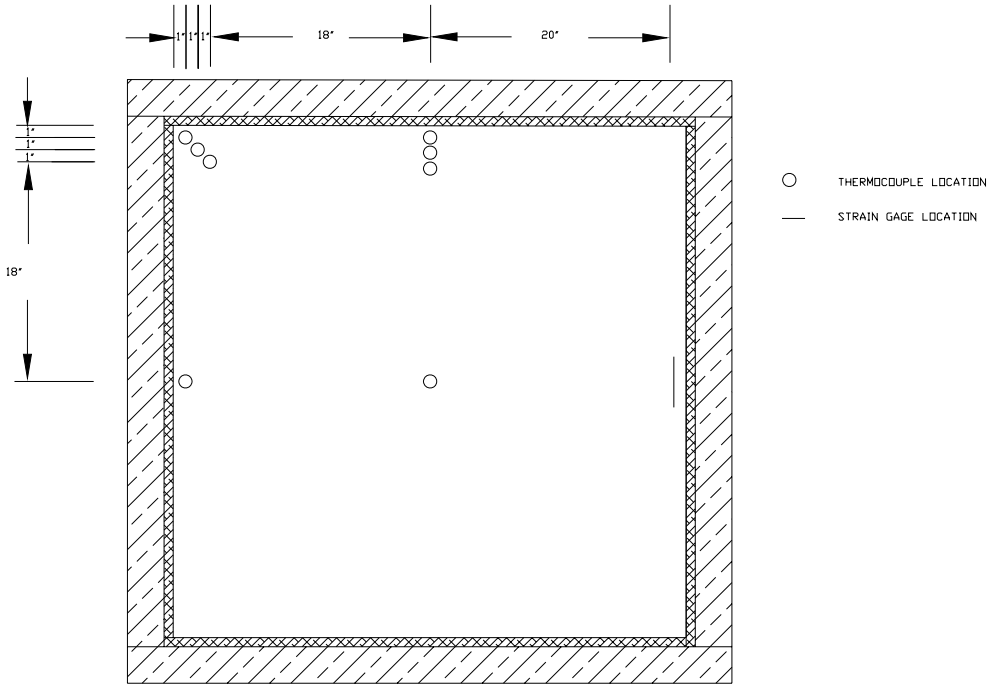

Figure 7-1. Thermocouple location (Plan)

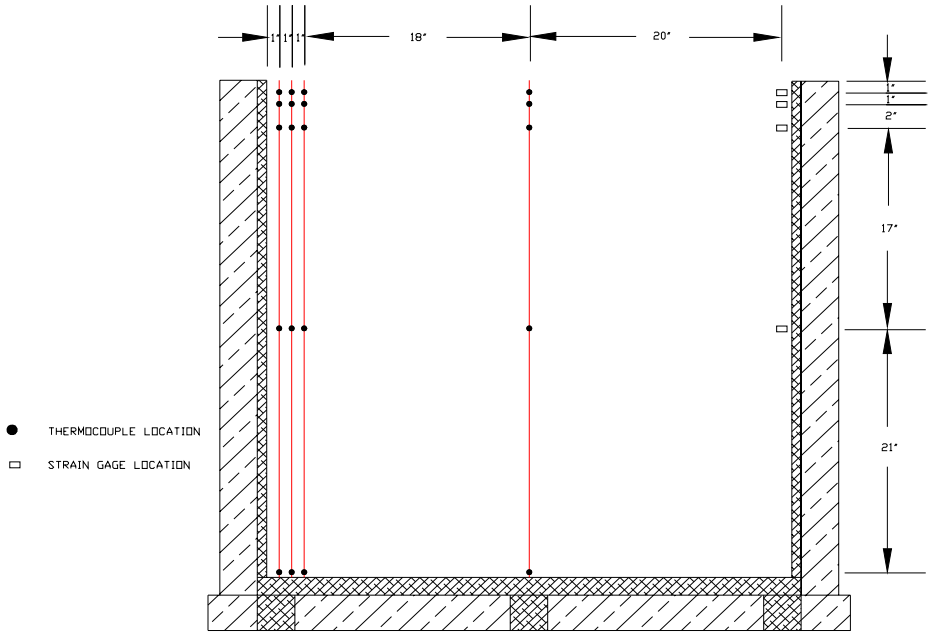

Figure 7-2. Thermocouple location (Section)

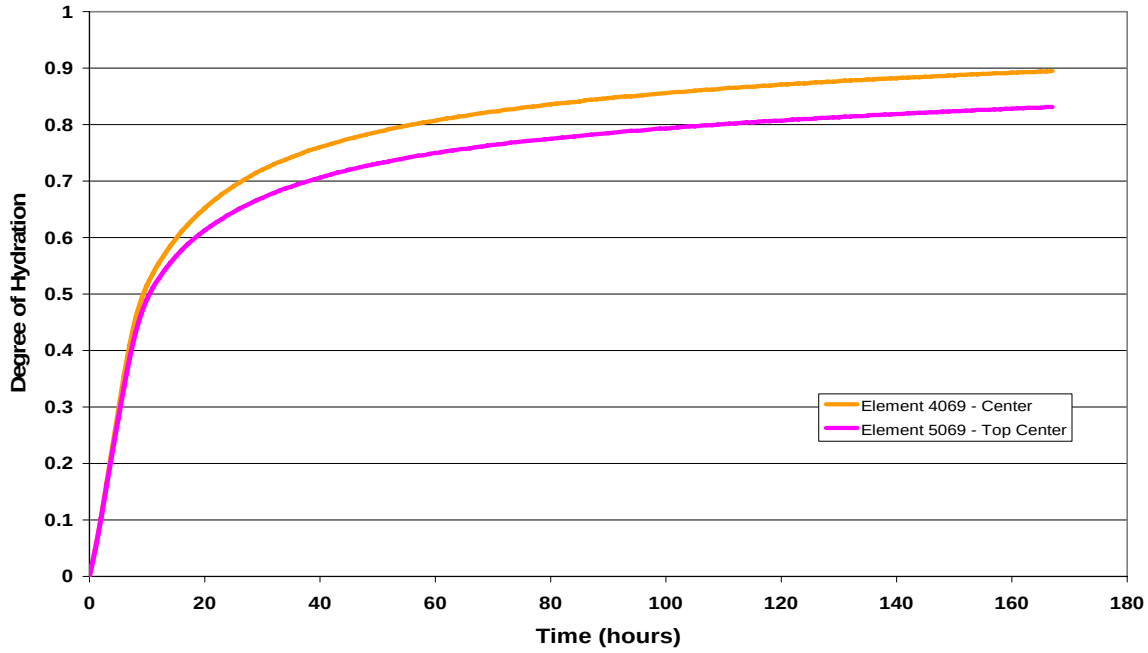

Figure 7-3. Degree of hydration at the center and top of the block in mixture 1

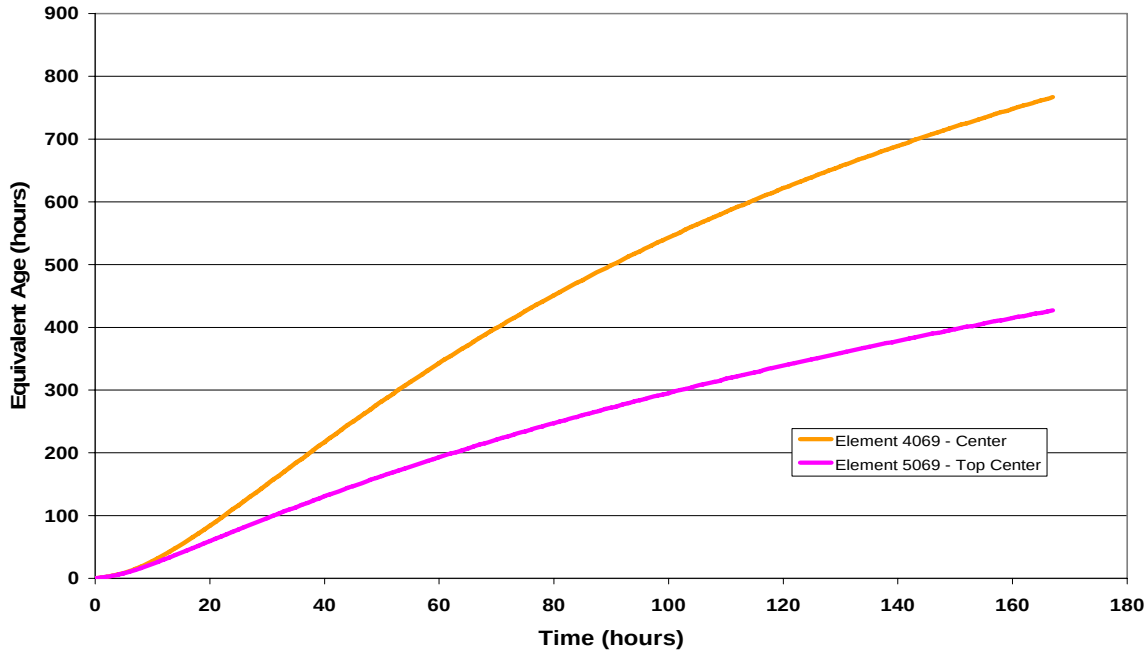

Figure 7-4. Equivalent age at the center and top of the block in mixture 1

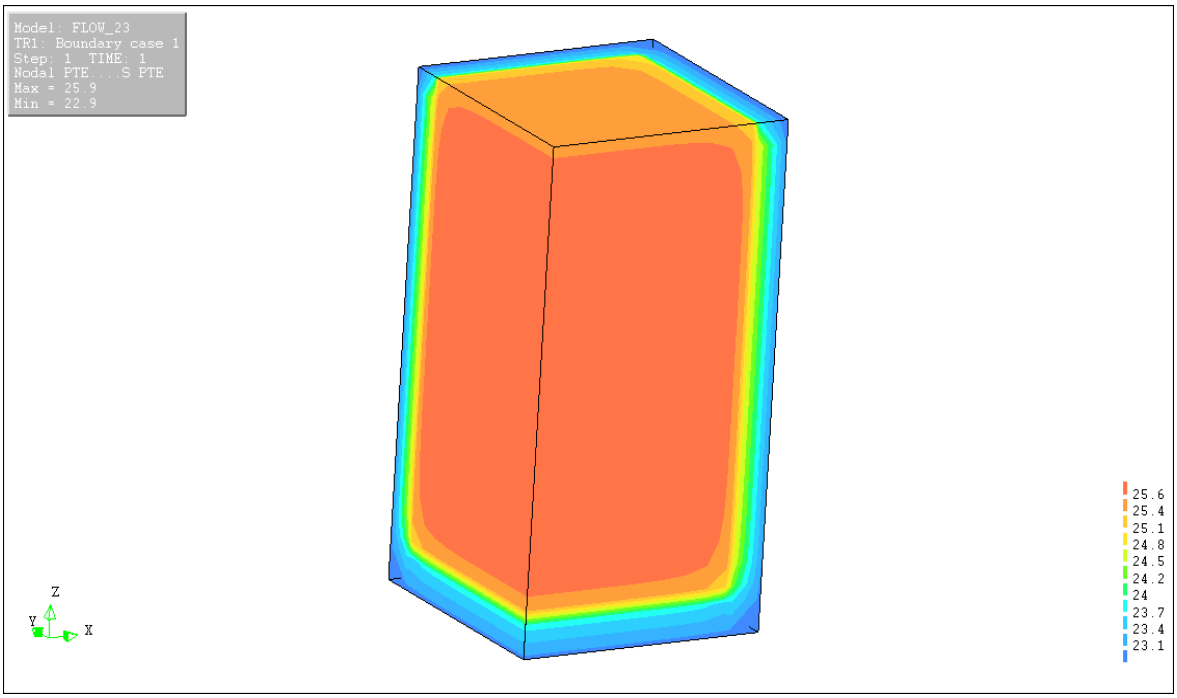

Figure 7-5. Concrete quarter block with insulation at time step 1

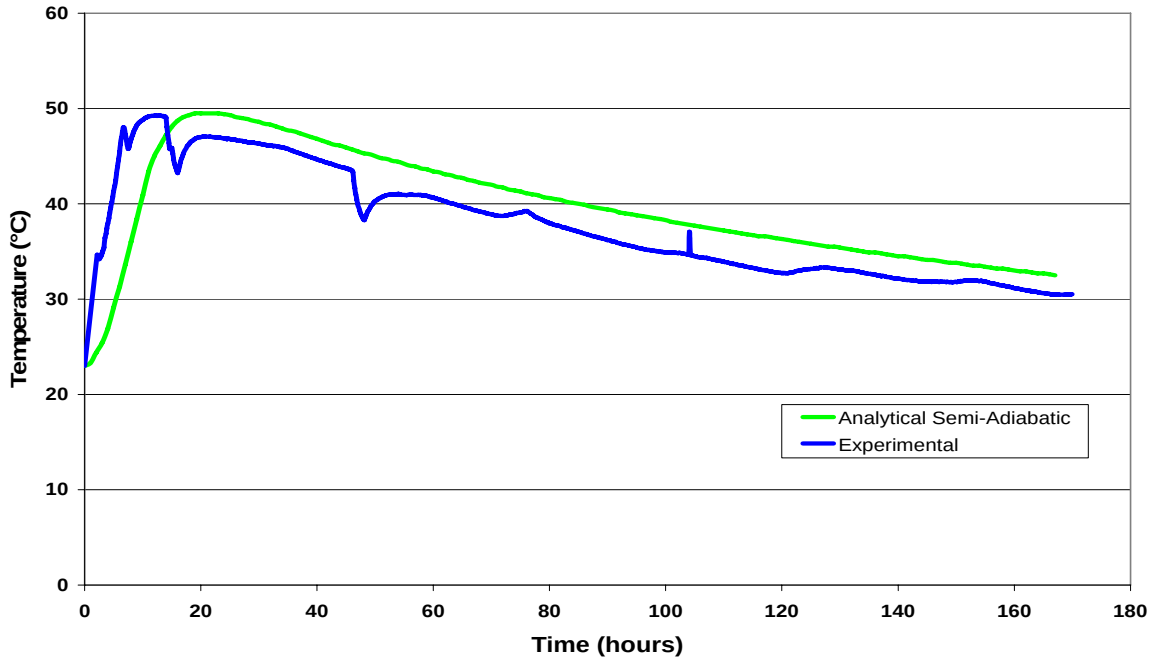

Figure 7-6. Semi-adiabatic and experimentally measured temperature-time histories at the center of the block, 2" below the exposed top surface of mixture 1

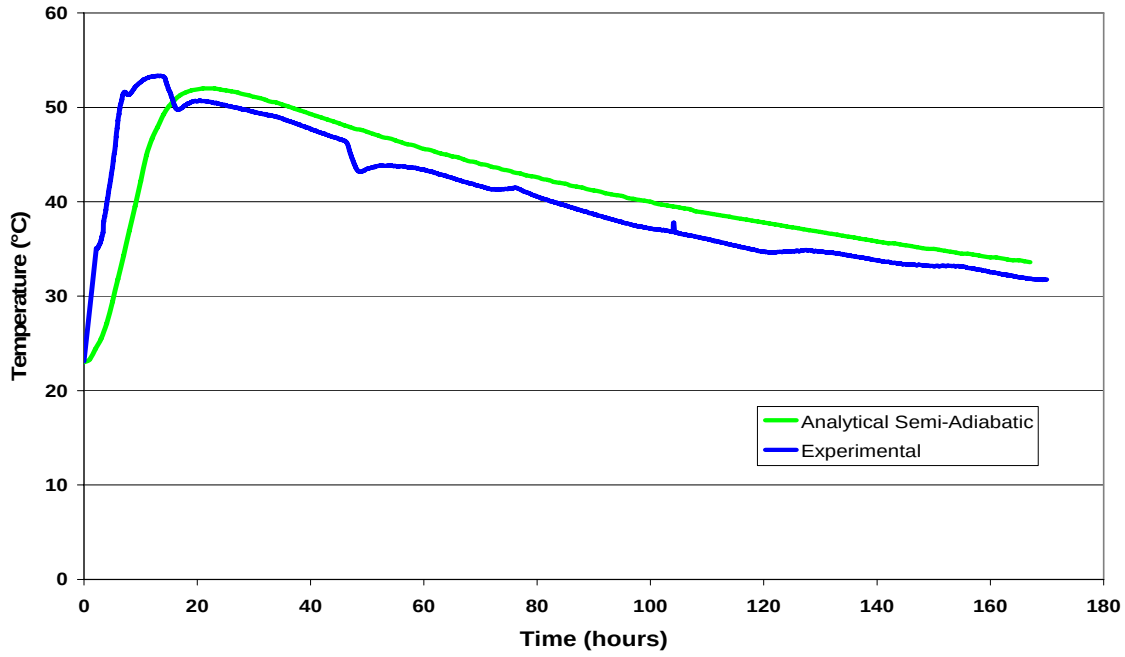

Figure 7-7. Semi-adiabatic and experimentally measured temperature-time histories at the center of the block, 4" below the exposed top surface of mixture 1

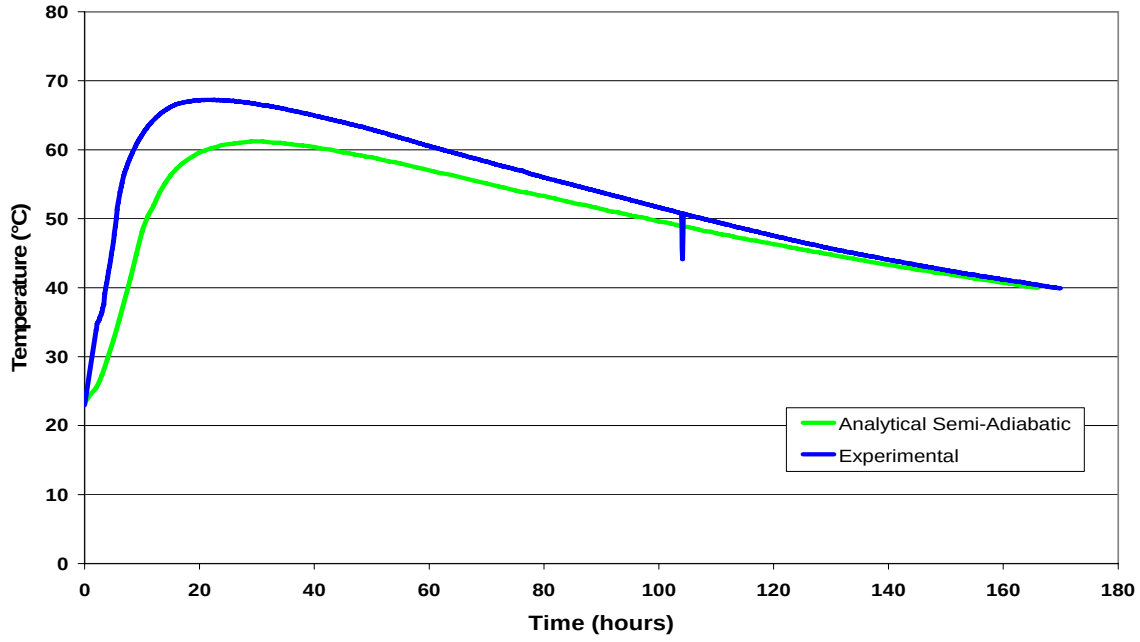

Figure 7-8. Semi-adiabatic and experimentally measured temperature-time histories at the center of the block, 21" below the exposed top surface of mixture 1

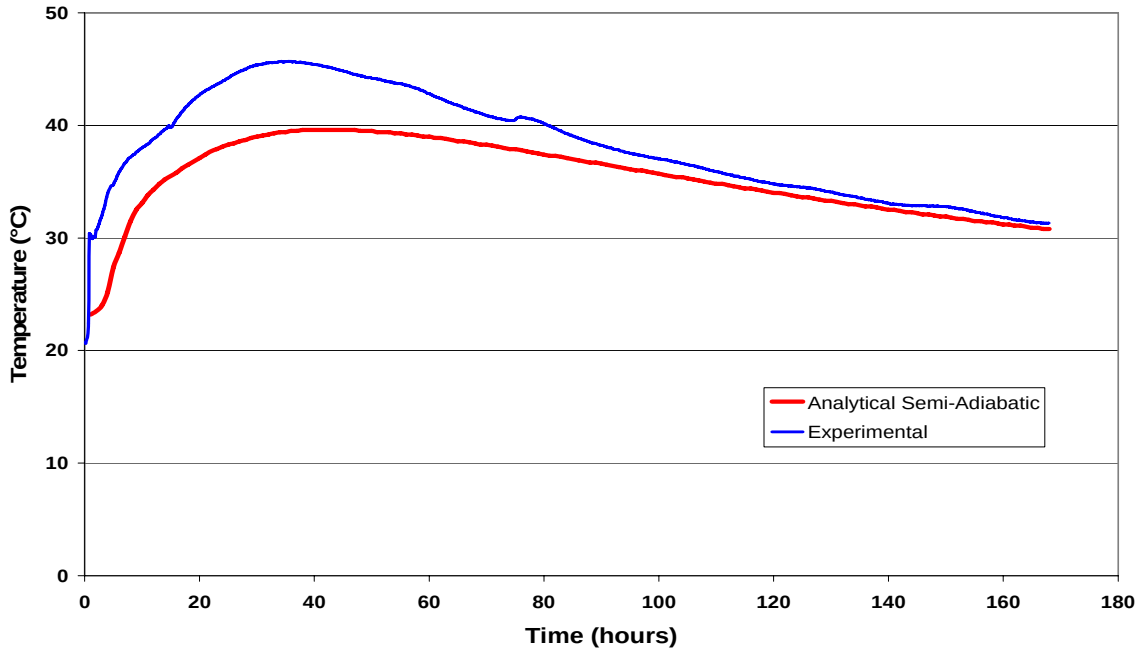

Figure 7-9. Semi-adiabatic and experimentally measured temperature-time histories at the center of the block, 2" below the exposed top surface of mixture 2

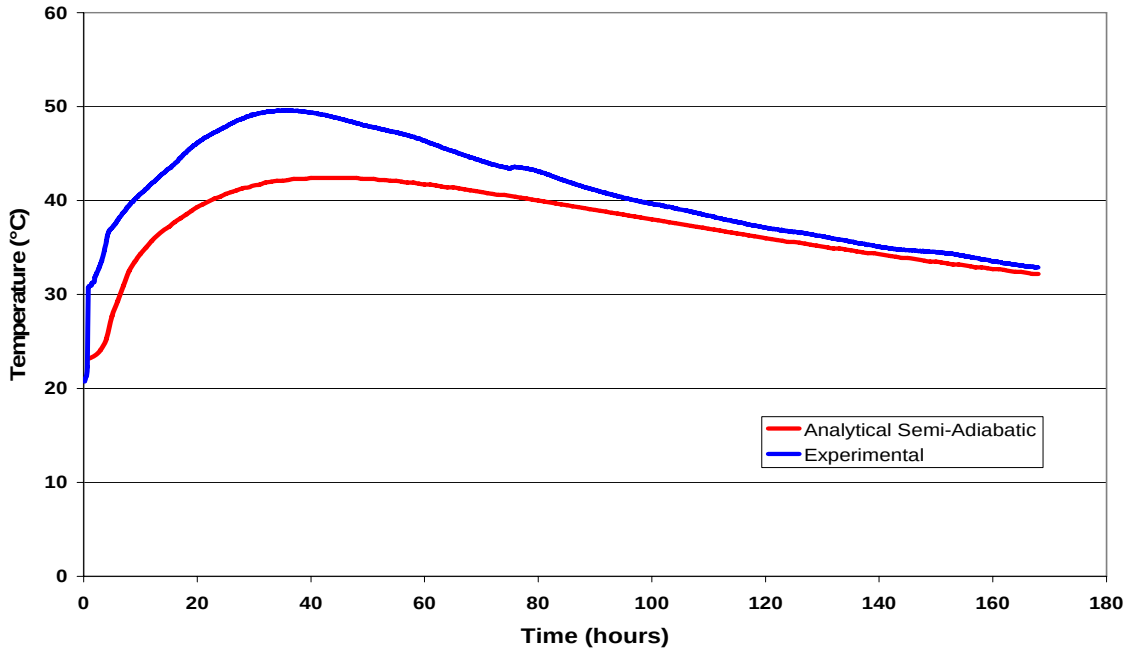

Figure 7-10. Semi-adiabatic and experimentally measured temperature-time histories at the center of the block, 4" below the exposed top surface of mixture 2

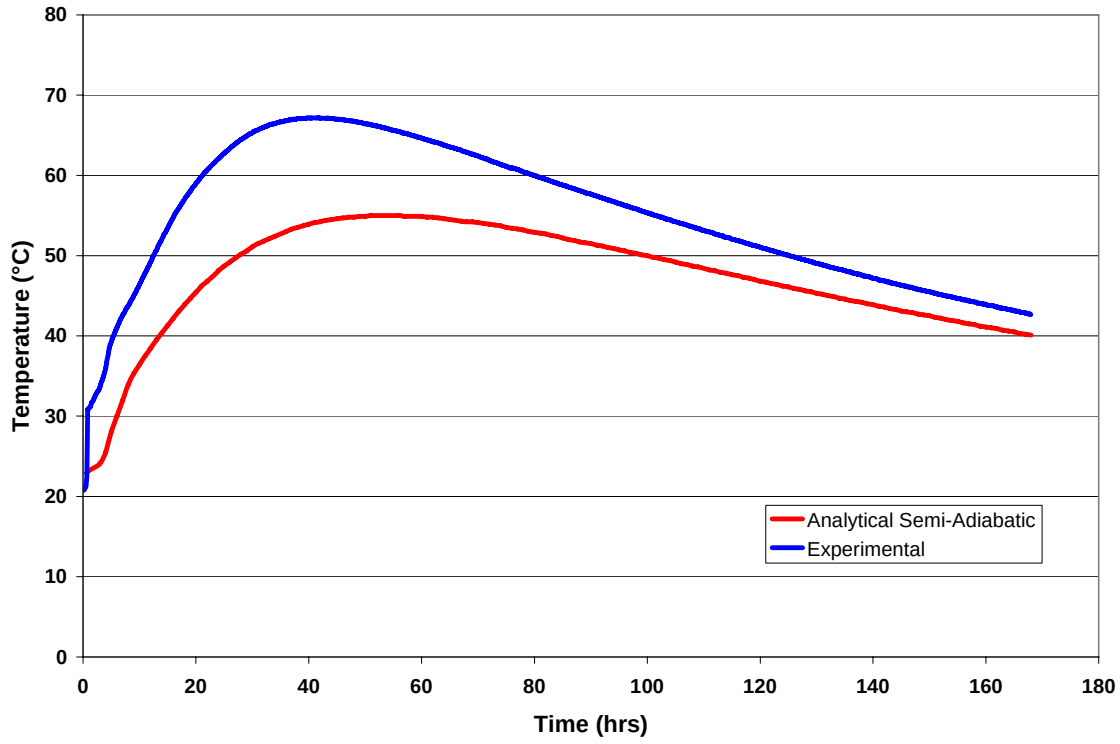

Figure 7-11. Semi-adiabatic and experimentally measured temperature-time histories at the center of the block, 21" below the exposed top surface of mixture 2

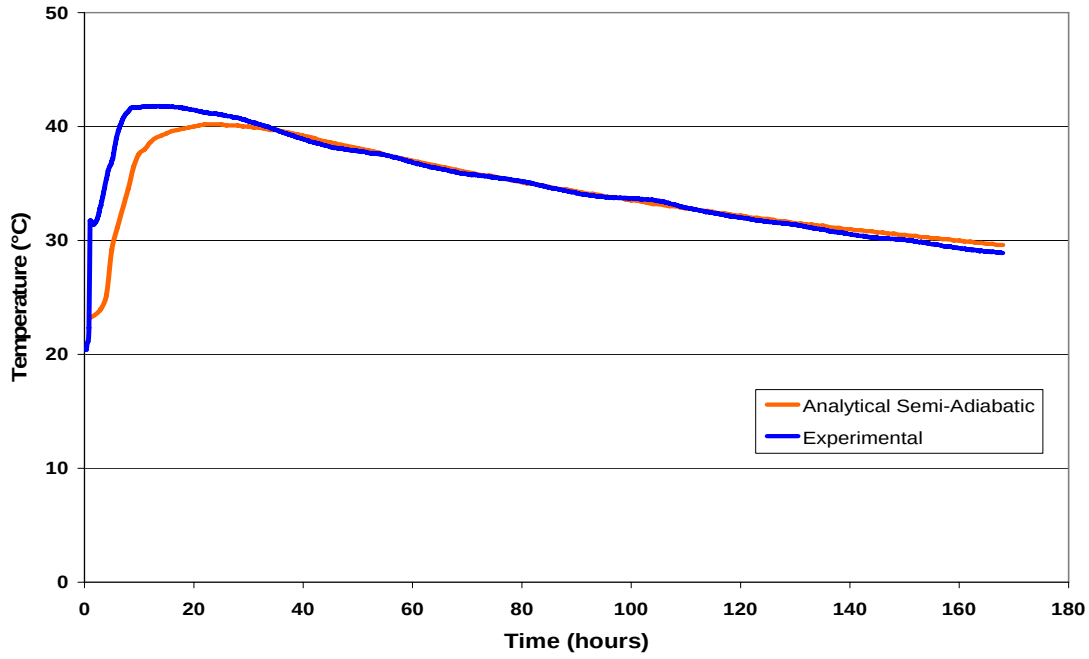

Figure 7-12. Semi-adiabatic and experimentally measured temperature-time histories at the center of the block, 2" below the exposed top surface of mixture 3

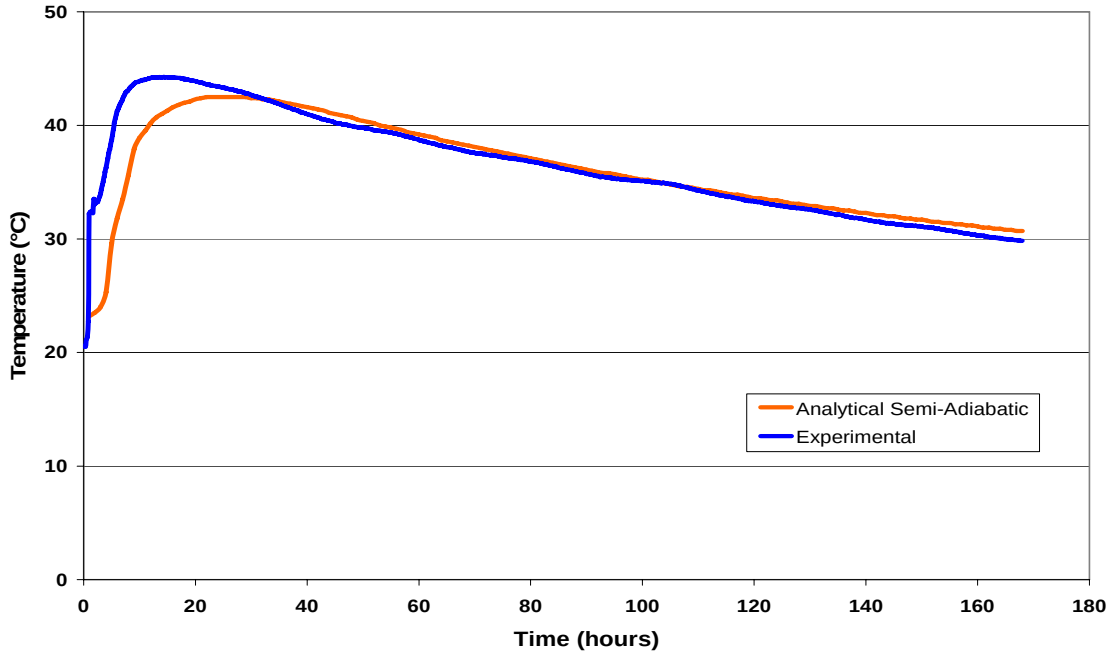

Figure 7-13. Semi-adiabatic and experimentally measured temperature-time histories at the center of the block, 4" below the exposed top surface of mixture 3

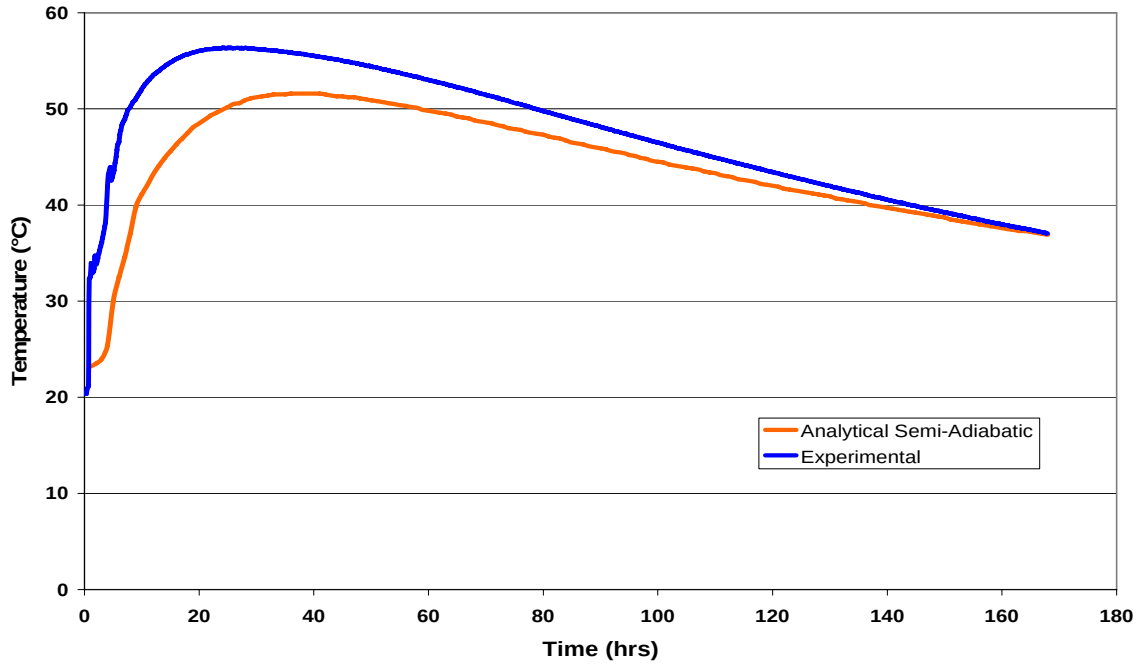

Figure 7-14. Semi-adiabatic and experimentally measured temperature-time histories at the center of the block, 21" below the exposed top surface of mixture 3

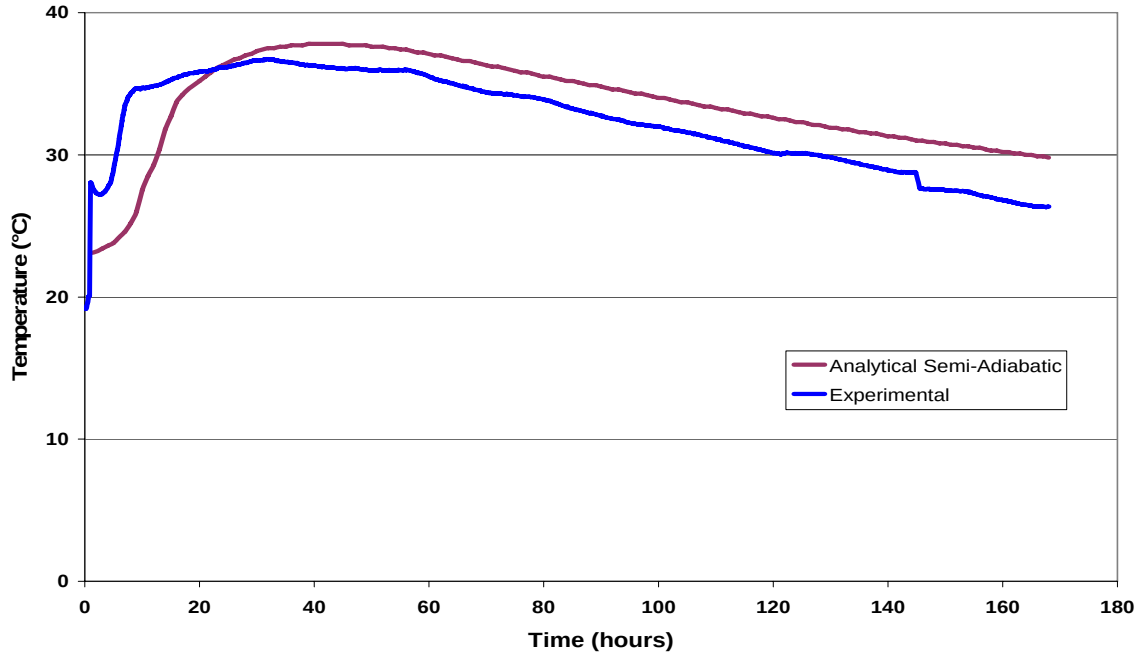

Figure 7-15. Semi-adiabatic and experimentally measured temperature-time histories at the center of the block, 2" below the exposed top surface of mixture 4

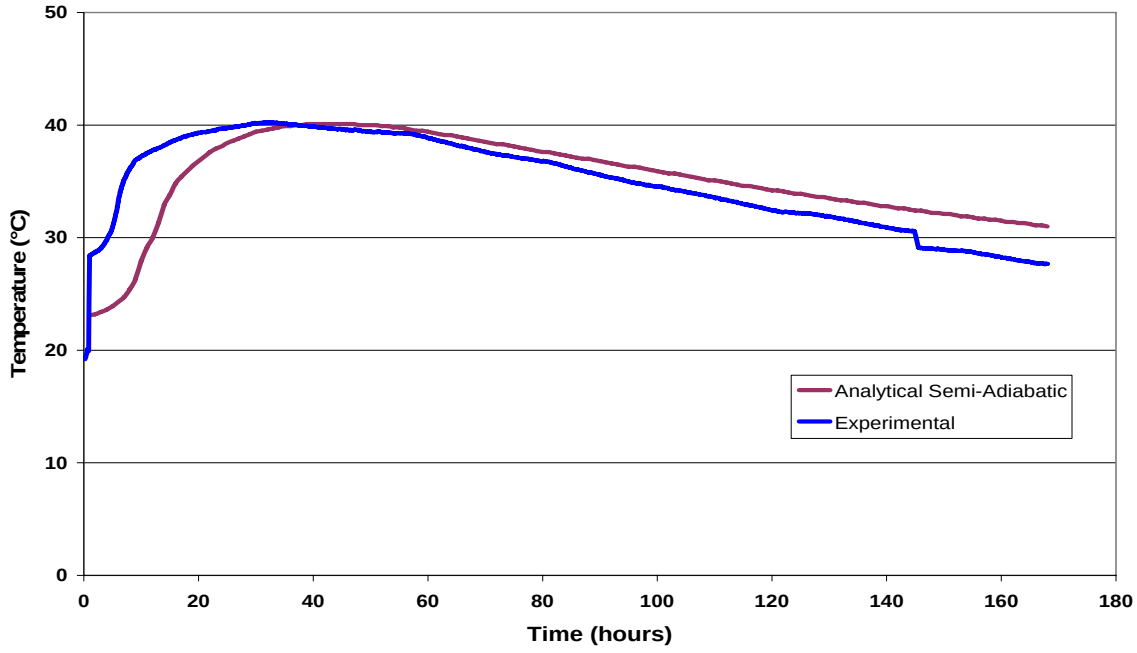

Figure 7-16. Semi-adiabatic and experimentally measured temperature-time histories at the center of the block, 4" below the exposed top surface of mixture 4

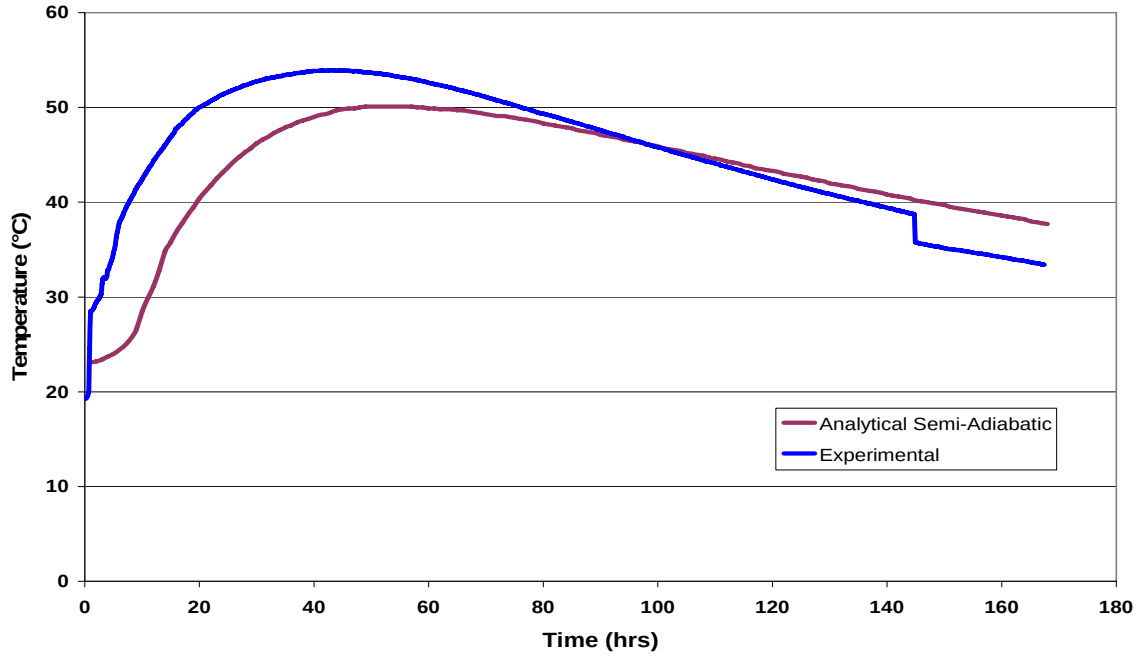

Figure 7-17. Semi-adiabatic and experimentally measured temperature-time histories at the center of the block, 21" below the exposed top surface of mixture 4

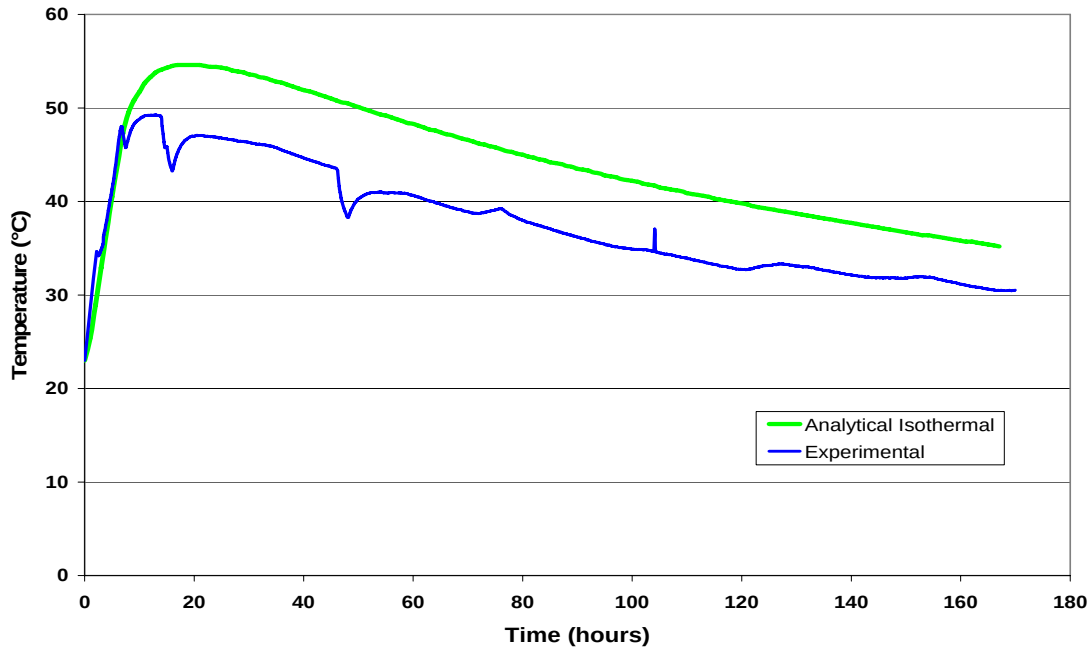

Figure 7-18. Isothermal and experimentally measured temperature-time histories at the center of the block, 2" below the exposed top surface of mixture 1

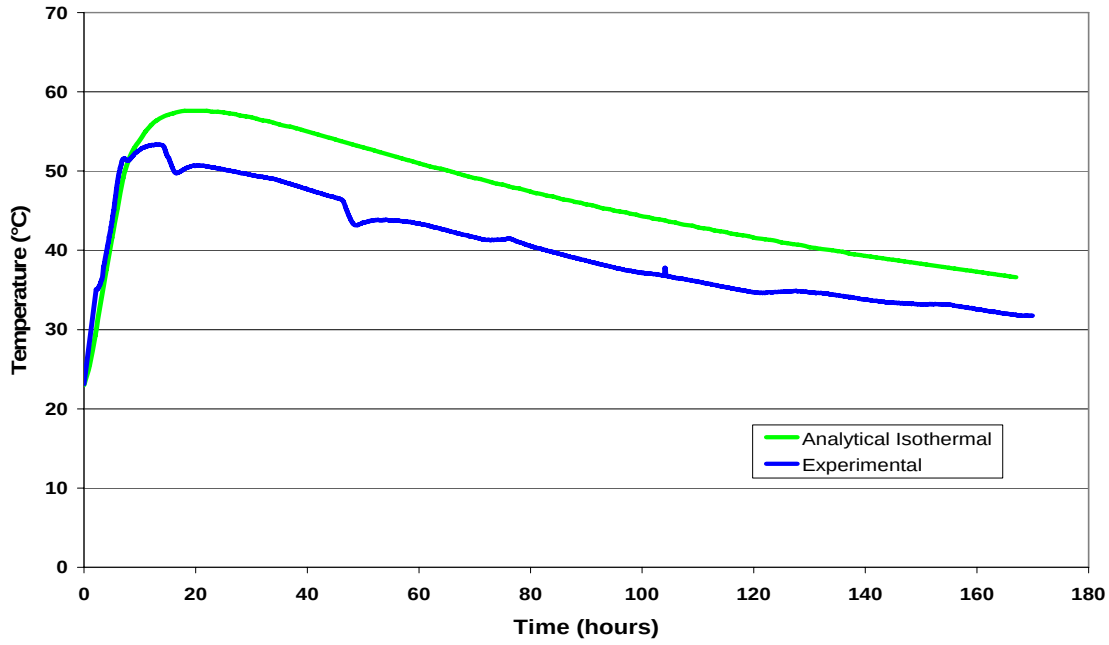

Figure 7-19. Isothermal and experimentally measured temperature-time histories at the center of the block, 4" below the exposed top surface of mixture 1

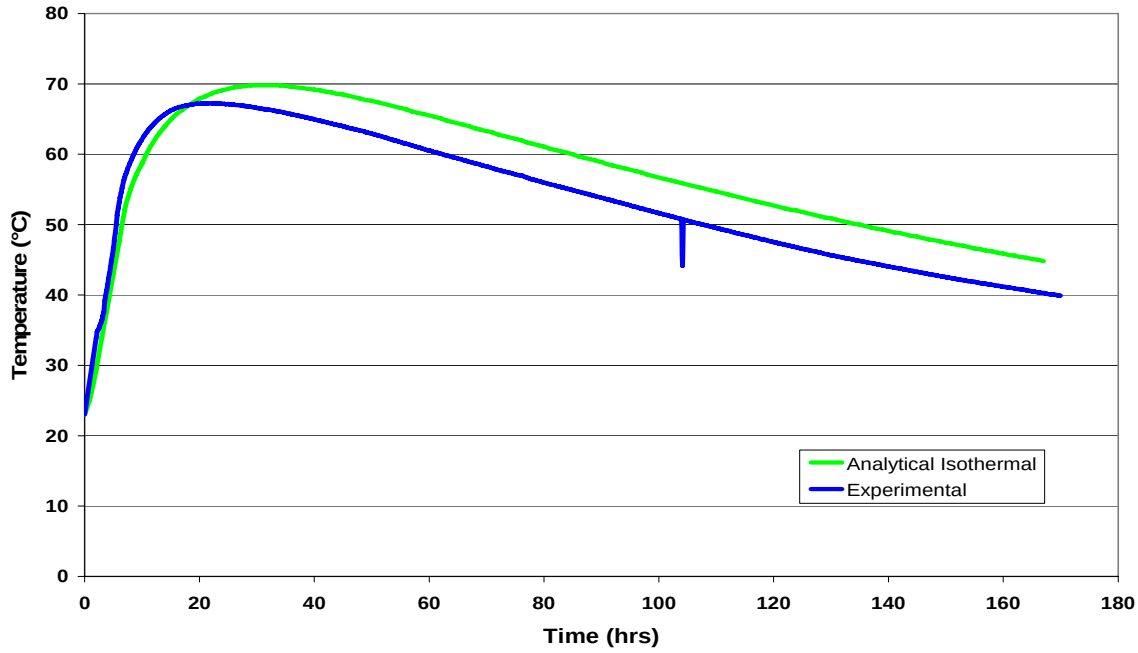

Figure 7-20. Isothermal and experimentally measured temperature-time histories at the center of the block, 21" below the exposed top surface of mixture 1

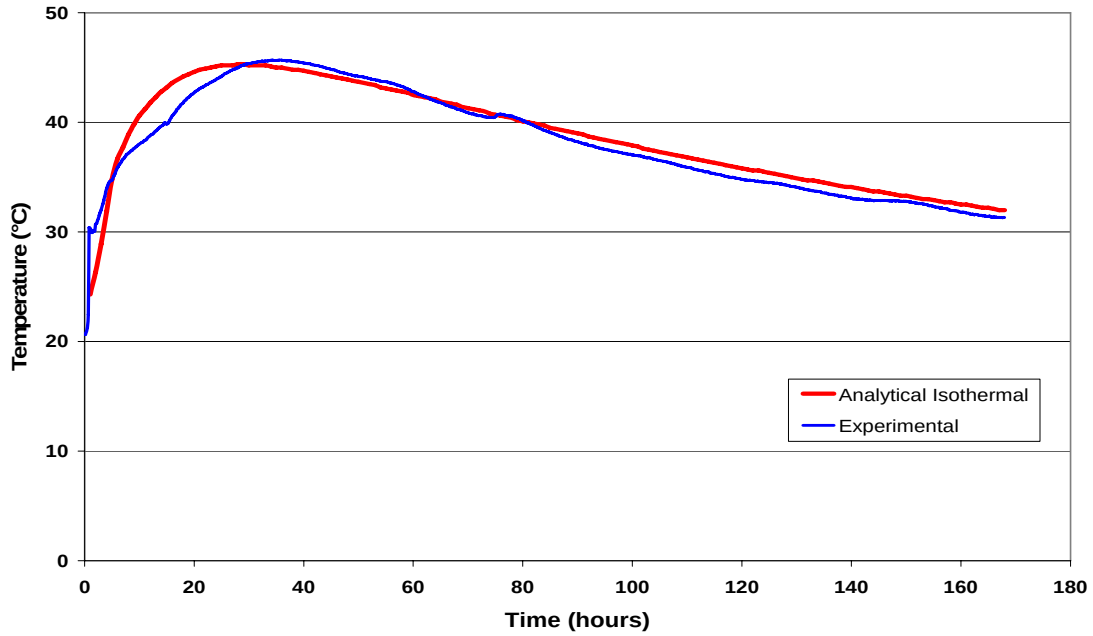

Figure 7-21. Isothermal and experimentally measured temperature-time histories at the center of the block, 2" below the exposed top surface of mixture 2

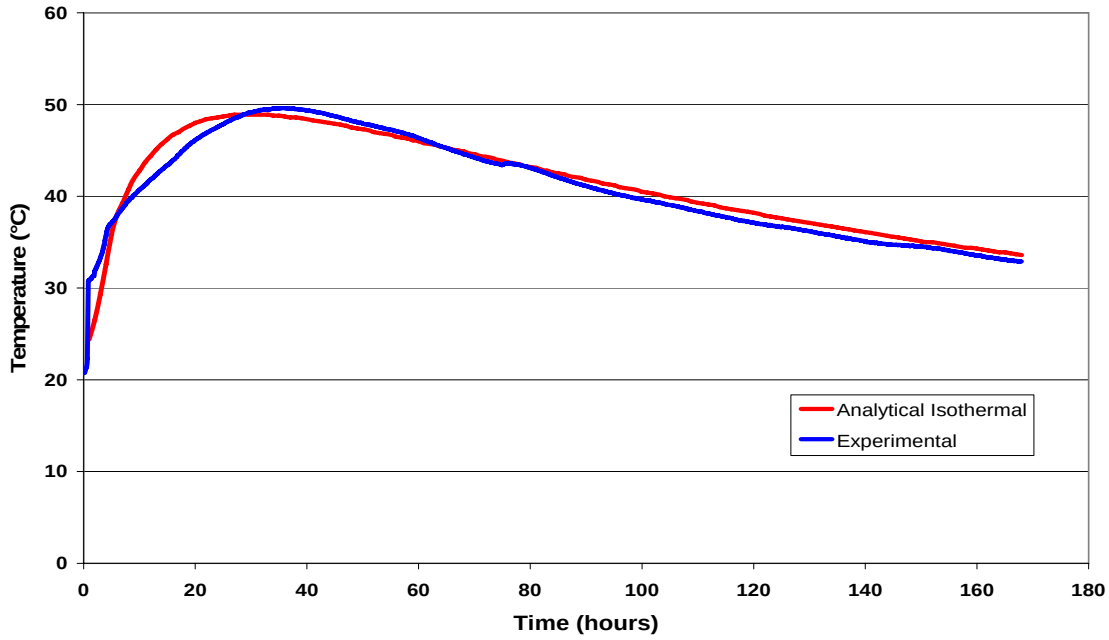

Figure 7-22. Isothermal and experimentally measured temperature-time histories at the center of the block, 4" below the exposed top surface of mixture 2

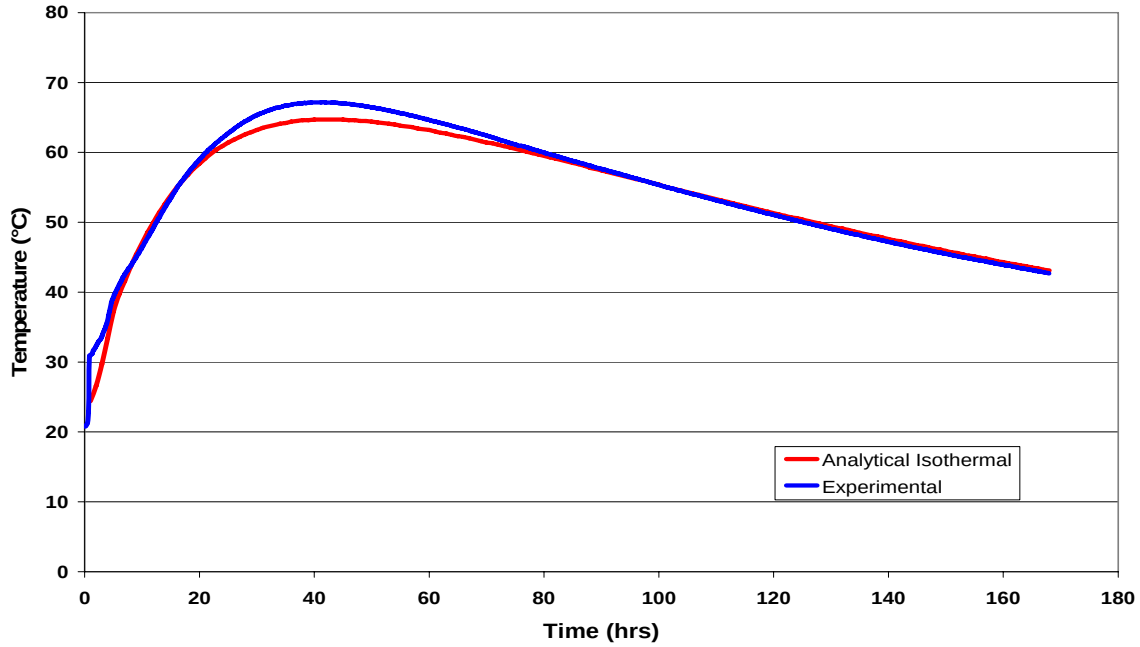

Figure 7-23. Isothermal and experimentally measured temperature-time histories at the center of the block, 21" below the exposed top surface of mixture 2

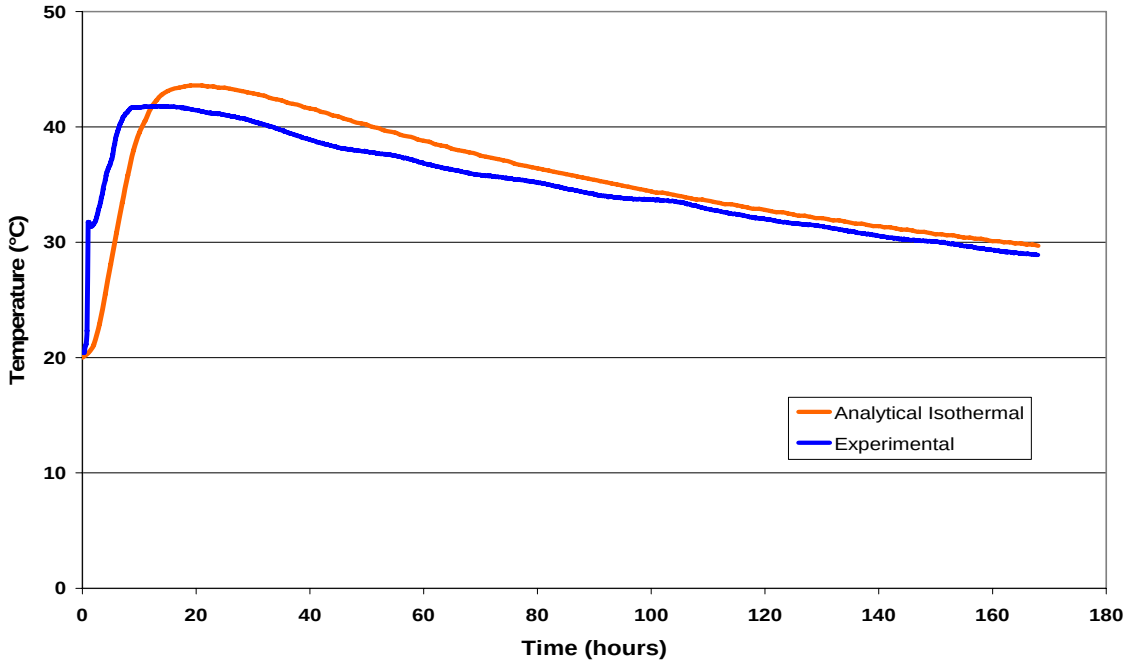

Figure 7-24. Isothermal and experimentally measured temperature-time histories at the center of the block, 2" below the exposed top surface of mixture 3

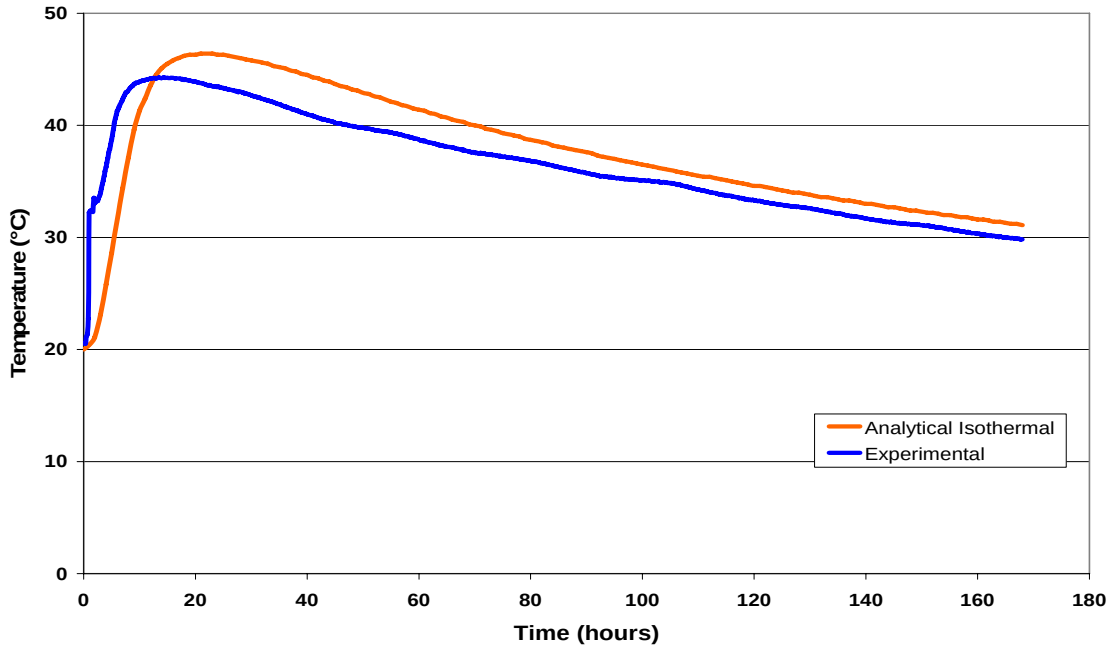

Figure 7-25. Isothermal and experimentally measured temperature-time histories at the center of the block, 4" below the exposed top surface of mixture 3

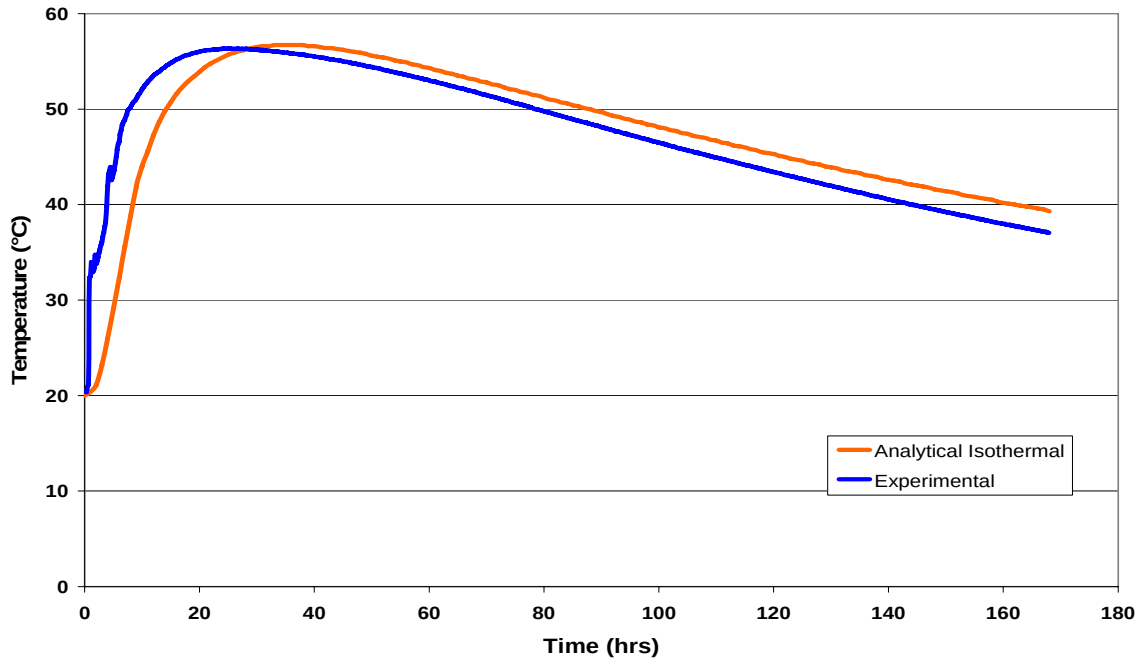

Figure 7-26. Isothermal and experimentally measured temperature-time histories at the center of the block, 21" below the exposed top surface of mixture 3

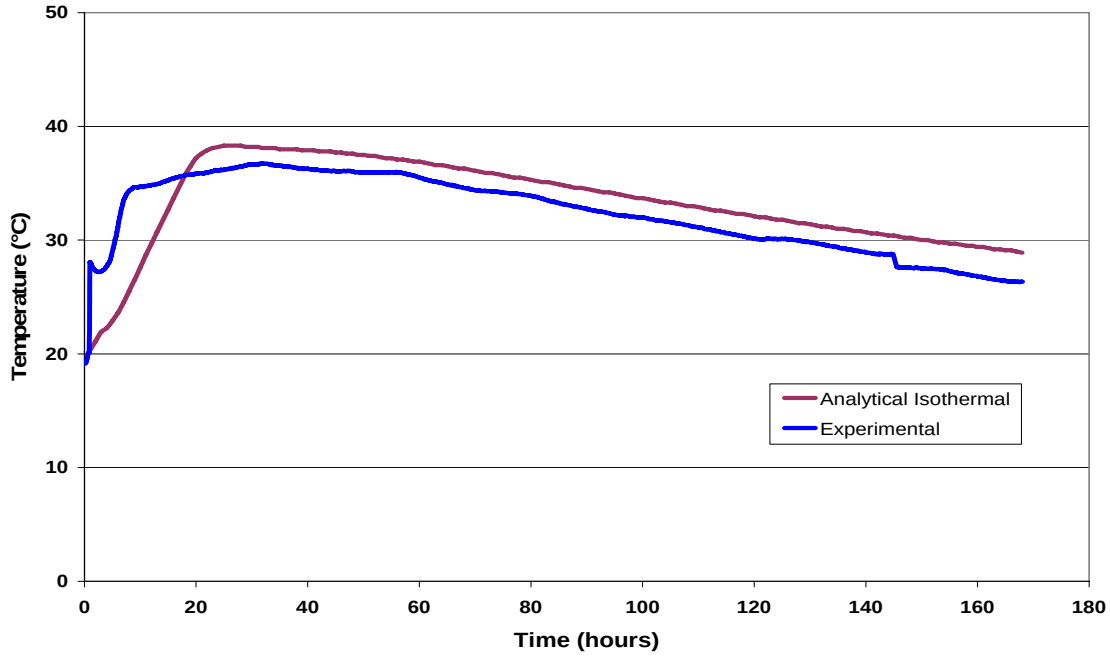

Figure 7-27. Isothermal and experimentally measured temperature-time histories at the center of the block, 2" below the exposed top surface of mixture 4

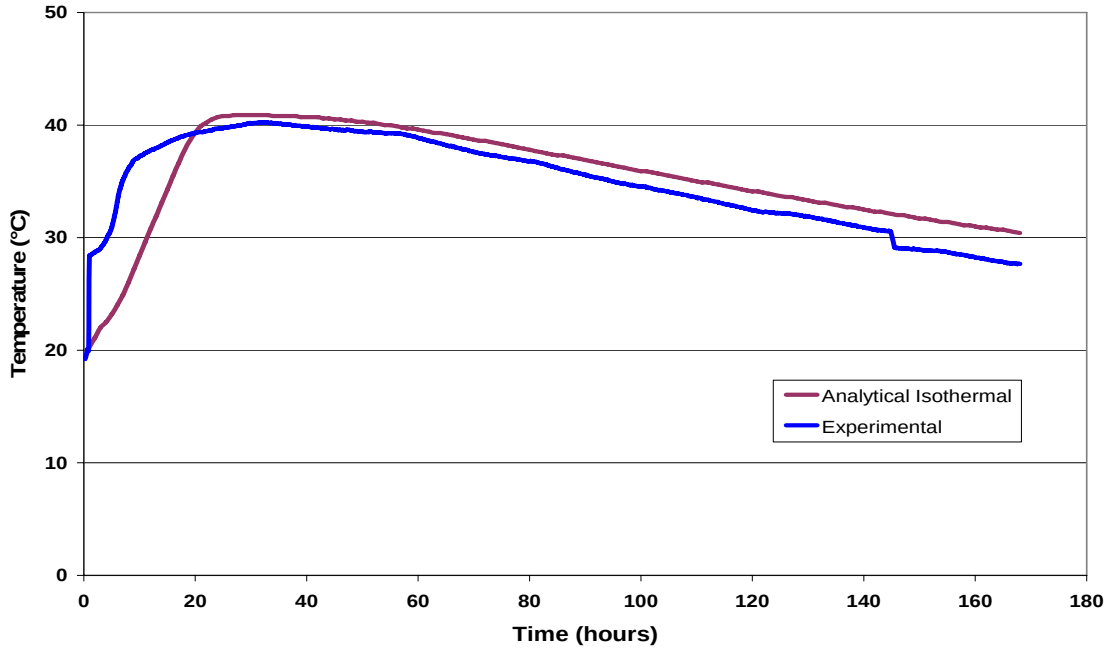

Figure 7-28. Isothermal and experimentally measured temperature-time histories at the center of the block, 4" below the exposed top surface of mixture 4

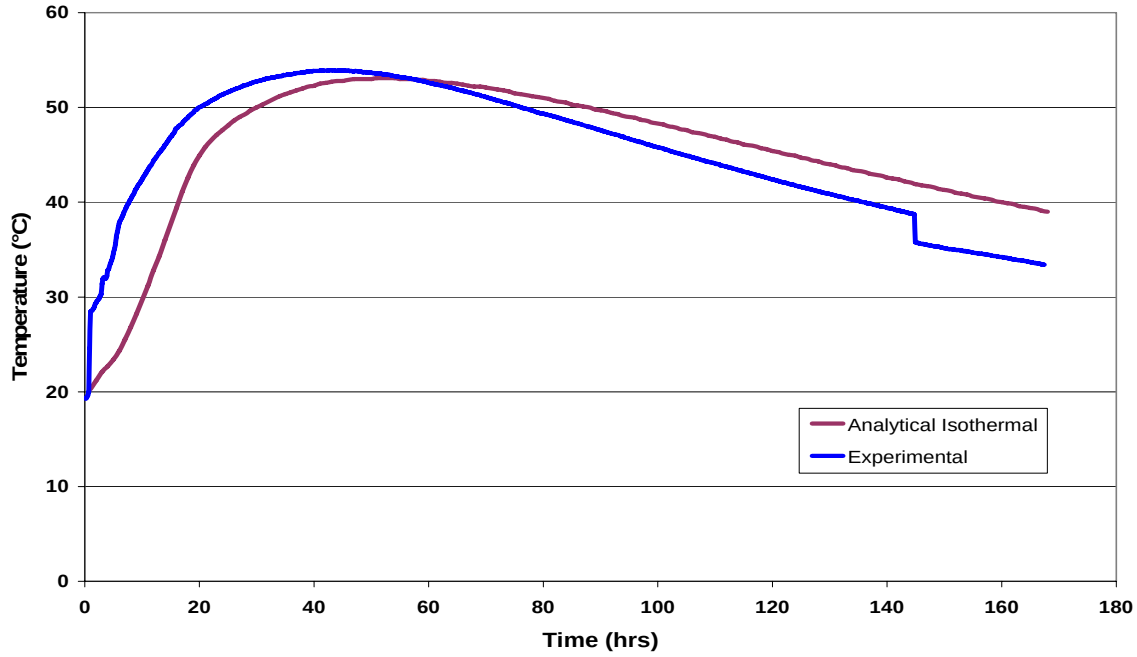

Figure 7-29. Isothermal and experimentally measured temperature-time histories at the center of the block, 21" below the exposed top surface of mixture 4

CHAPTER 8
STRUCTURAL ANALYSIS RESULTS

Stress Results

In this chapter, the stresses and strains induced by the differences in temperature within the hydrating concrete using the isothermal calorimetry data are presented and discussed. As stated earlier, these temperature gradients are produced when the heat being generated in the concrete is dissipated to the surrounding environment causing the temperature at regions close to the surface of the concrete to be lower than the temperature at the interior of the concrete. At the same time the heat generated is a function of the temperature and time history of the concrete, therefore individual locations in the concrete will experience different levels of heat. Figure 8-1 shows the location of the elements that will be analyzed for their stress and strain states during the hydration process. These locations were chosen because the largest tensile and compressive actions will be experienced at the top and central region of the concrete respectively.

Figure 8-2 presents the calculated stress in the X-X plane, occurring in the block with Mixture 1, with respect to time of Element 4069 (node 638) and Element 5069 (node 508) which are located at the center and top center of the finite element model respectively. The plot shows that the model accurately predicts Element 5069 undergoes tensile (positive) stresses as the concrete hydrates and expands, while Element 4069 experiences compressive stresses. This is consistent with the theory that a faster hydrating central region of a massive concrete structure will be in compression as it tries to expand but is restricted by the less mature concrete around it. Figure 8-3 presents the calculated stress in the X-X plane with respect to time of Element 4259 (node 1208) and Element 5159(node 618), which are located at the center edge and top edge of the finite element model respectively. Element 5159 undergoes tensile (positive) stresses as the concrete hydrates and expands. Element 4259 also acts in tension as it is being pushed against by

the expanding inner concrete. As expected, the maximum tensile stress of 1.34 MPa occurs at the top edge of the block in Element 5159.

The effect on the induced stresses in the concrete of Mixture 2 which contains slag is shown in Figure 8-4 and Figure 8-5. The peak tensile stresses in Element 5069 (0.97 MPa) and Element 5159 (1.18 MPa), at the top of block, were slightly less than the tensile stresses experienced in Mixture 1 containing 100% Portland cement, but occurred approximately 10 hours later. The similarities in peak tensile stress values is a result of the closeness of the peak temperatures in each mixture, while the time difference can be attributed to the slow rate of hydration, and hence slow rate of temperature increase, in the concrete. Interestingly the stresses across the top of the block transition to compressive stresses 150 hours after placement. The stress at the center edge of the block (Element 4259) acts in tension, as was the case in Mixture 1. The stress in Element 4069 begins in compression but becomes tensile after 164 hours of hydration.

The stresses produced in Mixture 3 were similar in trend to those obtained in Mixture 1. This is to be expected given that the rate of temperature rise in Mixture 3 was steep as was the case of the temperature rise in Mixture 1. Figure 8-6 shows that the highest tensile stress experienced at the top center of the block (Element 5069) was 0.878 MPa occurring 26 hours after concrete placement, while the maximum compressive stress of, 0.358 MPa, at the center of the block (Element 4069) occurred 40 hours after placement. The maximum tensile stress value of 1.10 MPa again occurred at the top edge of the block (Element 5159) as shown in Figure 8-7.

Figure 8-8 shows the stresses calculated in the top center and center of the block containing Mixture 4, while Figure 8-9 presents the stresses at the edge. The tensile stresses induced in this block were significantly less than the stresses in Mixture 1and Mixture 3, but

slightly larger than the stresses in Mixture 2. The rate of temperature rise of Mixture 4 like Mixture 2, both of which were presented in Chapter 7, was slow. Therefore this reduction in tensile stresses can likely be attributed to the presence of the ground granulated blast-furnace slag.

Cracking Potential

Cracking in concrete will occur when the tensile stresses, induced by the temperature gradients, exceed the low tensile strength that exists at early ages. The probability of cracking is measured by the function presented in Equation 8-1 called the cracking index.

$$I_{cr}(t) = \frac{f_t(t)}{\sigma_I(t)} \tag{8-1}$$

Where,

I_{cr} = the crack index
f_t = the tensile strength
σ_I = the maximum principal stress

I_{cr} is given a value of 100 if $\sigma_I \leq 0.01 f_t$. If I_{cr} falls below 1.0 this is an indication that cracking has been initiated.

A plot of the progression of the crack index along the center line of the block in Mixture 1 is presented in Figure 8-10. It shows that almost immediately after the concrete hardens, the crack index for Element 5069 is less than 1.0, indicating that the tensile stress at the top surface edge exceeded the tensile strength of the concrete, and hence cracking has occurred. Element 4069, which is at the center of the block is always in a compressive state, therefore has a constant crack index of 100. Figure 8-11 shows the crack indices for the center edge (Element 4259) and top edge (Element 5159) respectively. Element 4259 only just remains above 1.0, while Element 5159 shows a high probability that cracking occurs during the first 25 hours. This was confirmed

by a close examination of the experimental block that contained mixture 1, shown in Figure 8-22, where cracking can be observed at all the top surface edges.

In Mixture 2, cracking occurs at the top center of the block approximately 10 hours after pouring, as shown in Figure 8-12. The same figure also shows that while the center of block goes into tension after 80 hours, the concrete is in a mature state and the tensile strength is well developed. Figure 8-13 shows the crack indices at the edge of the block. As was expected, cracking occurs at the top edge of the block, however the center edge of the block just barely stays above the crack threshold.

Mixtures 3 and 4 act in a similar manner to Mixture 1, where their centers are constantly in compression and hence have negligible risks of cracking. In Mixture 3, the crack indices in Element 5069 and Element 5159 suggest that cracking will occur, shown in Figures 8-14 an 8-15 respectively. While Figure 8-16 and 8-17 show that for Mixture 4 the tensile stresses that develop in these elements will not exceed their tensile strength and hence will not crack.

It appears that the ratio of substitution of cementitious materials used in the concrete of Mixture 4 is effective in mitigating the cracking risk in massive concrete elements.

Temperature Difference and Cracking

As previously stated, the requirements for the control of heat generation and in particular the maximum allowable temperature difference in mass concrete vary on a state by state basis. Currently, there is no agreement on what should be the maximum allowable temperature differential between the center of a mass concrete element and its surface so as to reduce the occurrence of thermal cracking. The critical temperature differences for the mixtures used in this project are determined from the results of the finite element analyses on each block.

Figure 8-18 shows the plot of the temperature difference between the center and surface of the block with Mixture 1. The calculated tensile stresses at the surface exceeded the early age tensile strength value of 1.25 MPa at a temperature differential of 17.3 °C.

Cracking in Mixture 2, which contained ground granulated blast-furnace slag, occurred when the temperature differential reached about 3.2 °C, as shown in Figure 8-19. This is significantly less than the differential in Mixture 1, which shows that although the addition of slag to Portland cement slowed the rate of temperature rise, it also caused the concrete to have a lower early age tensile strength of 0.255 MPa. This was to the detriment of the integrity of the structure.

The temperature differential of 8.4 °C at which cracking initiated in Mixture 3, shown in Figure 8-20, was larger than the differential in Mixture 2. In this case, although the fly ash lowered the peak temperature of the concrete, as shown in Figure 7-12 through to Figure 7-14, it did not have any effect on rate of initial temperature rise, and therefore a low value of the tensile strength caused the concrete to crack at a lower temperature differential than the block with mixture 1.

Although the crack index for Mixture 4, presented in Figure 8-17, shows that thermal cracking does not occur, it was only just avoided. It was therefore decided to still investigate the relationship between the temperature difference and induced stress at the surface of the block. Figure 8-21 shows the plot of this relationship, and it can be seen that the induced stress reaches the 24 hour (Day 1) tensile strength of 0.393 MPa when the temperature differential is 20.6 °C, 26 hours after being poured.

Summary of Findings

The investigation of the structural response of the concrete used in each Mixture to the internal heat generation and resulting temperature distribution found that:

- The concrete mixture containing 100% Portland cement had the highest induced stress but also cracked at the highest temperature difference.

- Although the ground granulated blast furnace slag had a slower rate of temperature increase, it cracked at a very low temperature differential. This was due to the lower tensile strength typical of slag concrete.

- The percent fly ash substituted for Portland cement did not have much effect on the induced stresses. Cracking occurred at a temperature differential of 8.4° C which also low and which is also due to the concrete's low tensile strength.

- The mixture proportion of 50% Portland cement, 30% slag and 20% fly ash effectively reduces the probability of thermal cracking due to hydration reaction. Never the less, the temperature differential at which cracking could occur is derived as 20.6 °C.

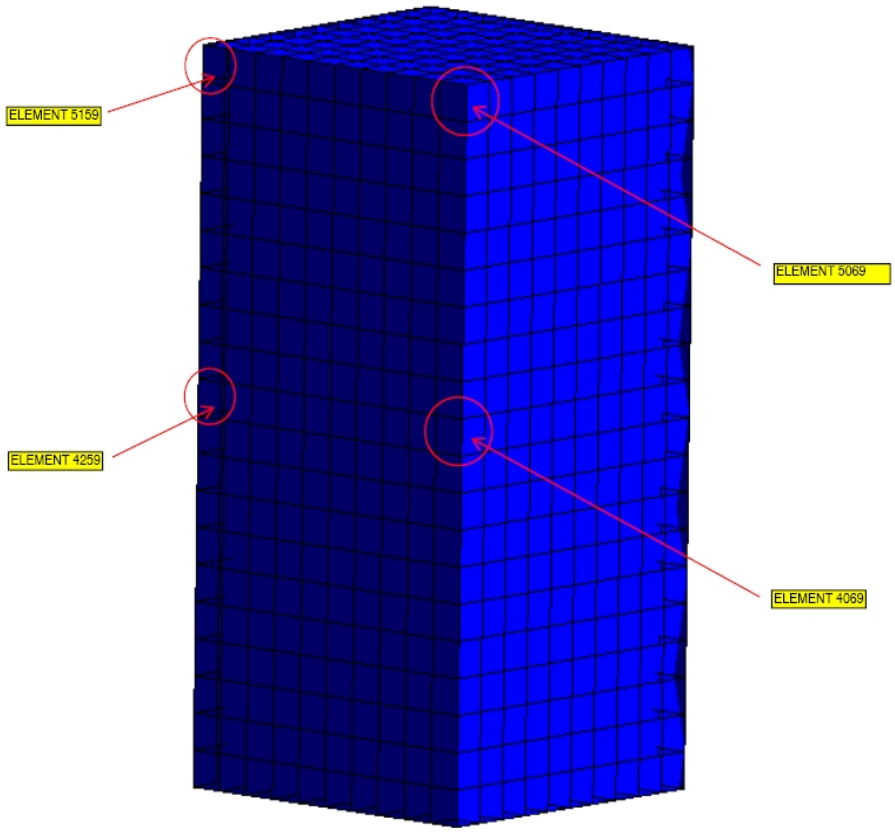

Figure 8-1. Location of elements analyzed for stress

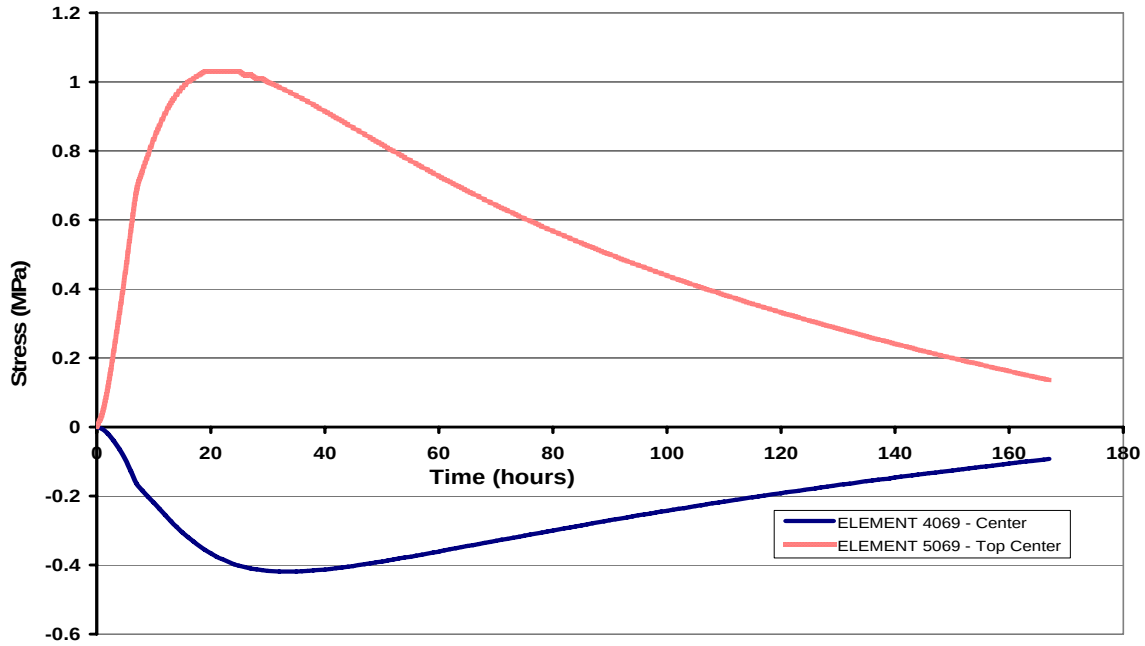

Figure 8-2. Stress state at the top center and center of the finite element concrete block with mixture 1

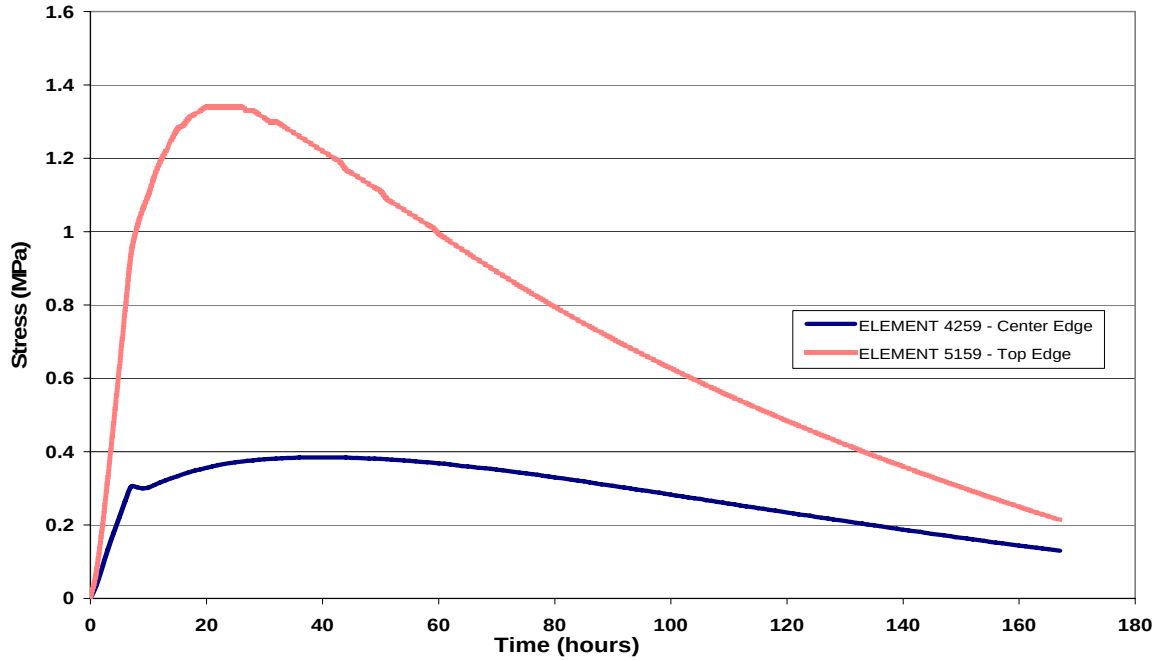

Figure 8-3. Stress state at the top edge and center edge of the finite element concrete block with mixture 1

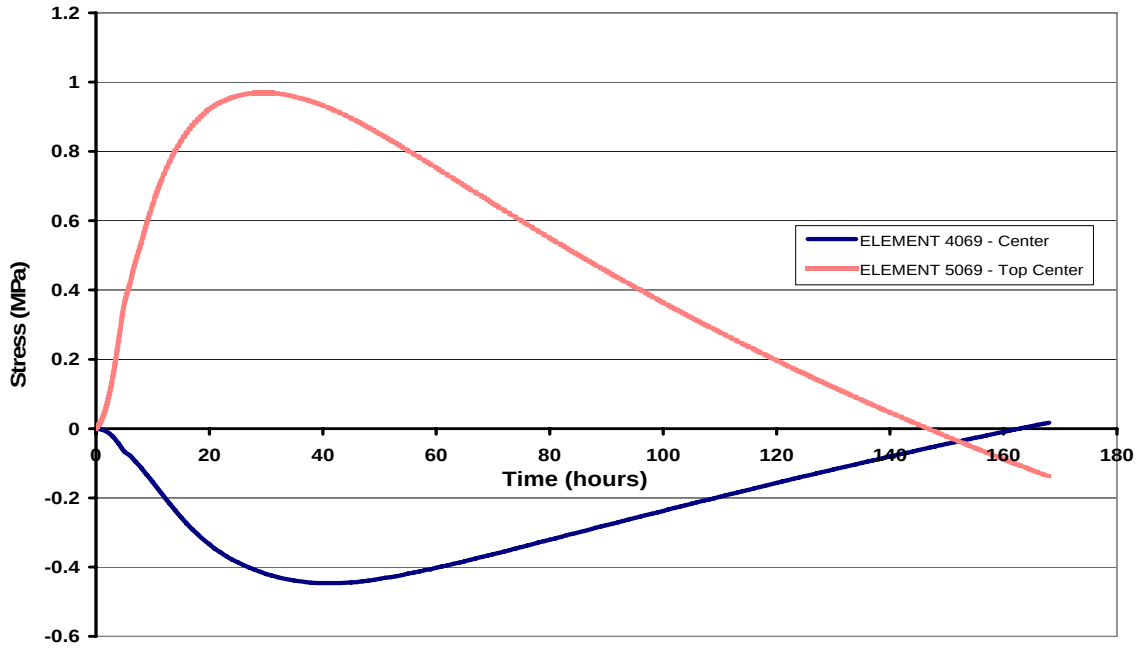

Figure 8-4. Stress state at the top center and center of the finite element concrete block with mixture 2

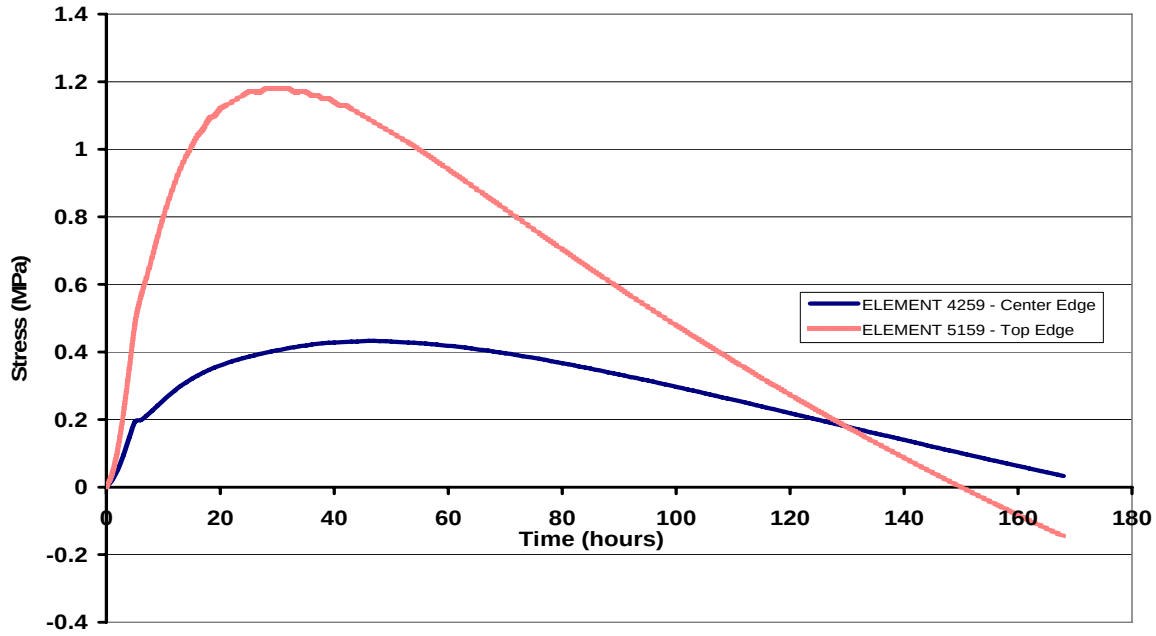

Figure 8-5. Stress state at the top edge and center edge of the finite element concrete block with mixture 2

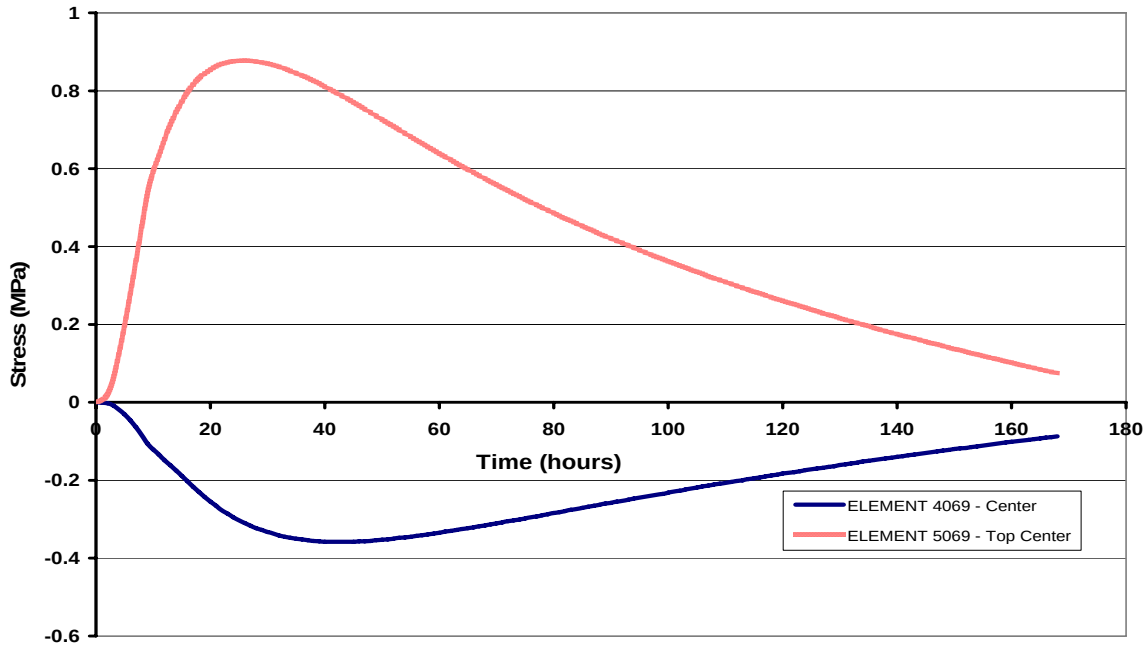

Figure 8-6. Stress state at the top center and center of the finite element concrete block with mixture 3

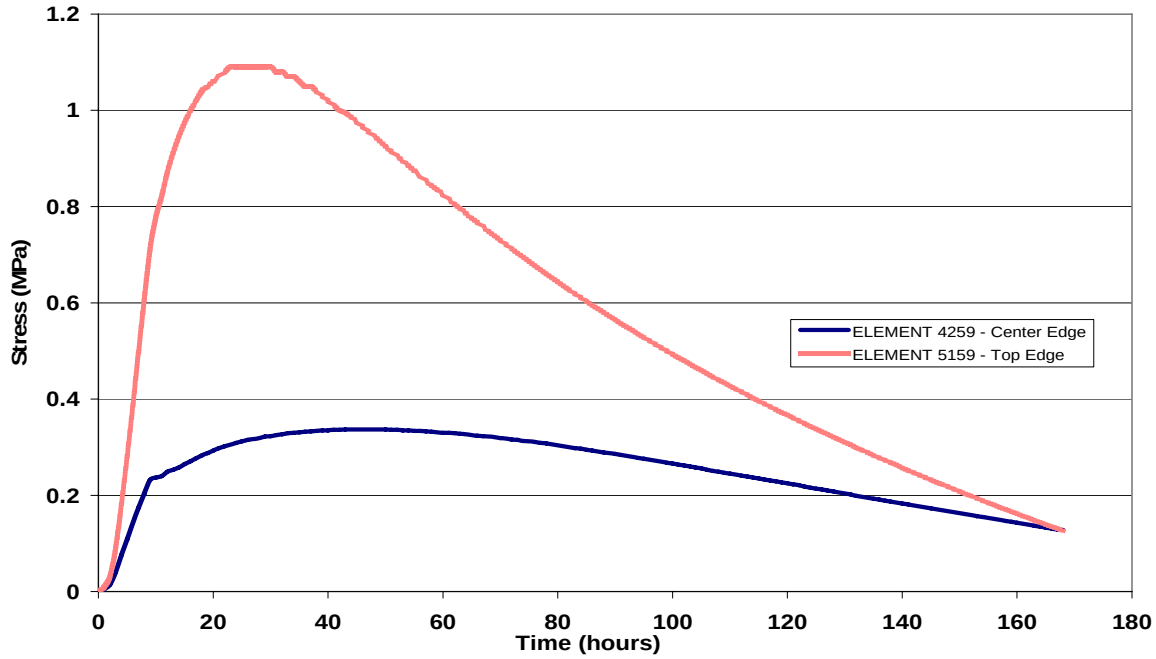

Figure 8-7. Stress state at the top edge and center edge of the finite element concrete block with mixture 3

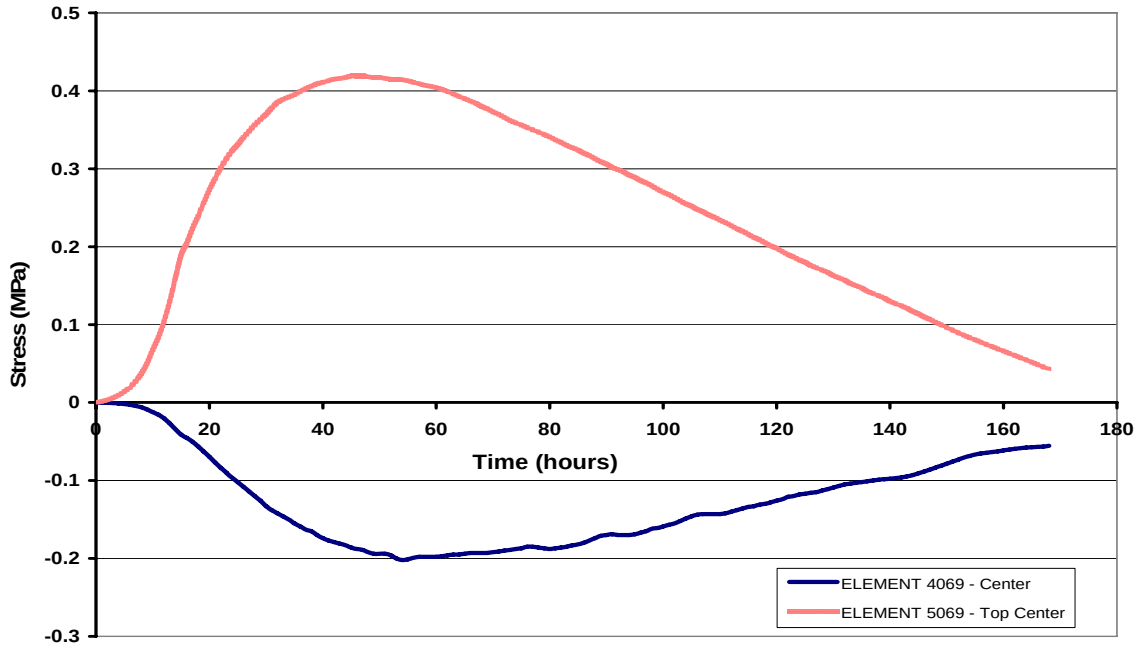

Figure 8-8. Stress state at the top center and center of the finite element concrete block with mixture 4

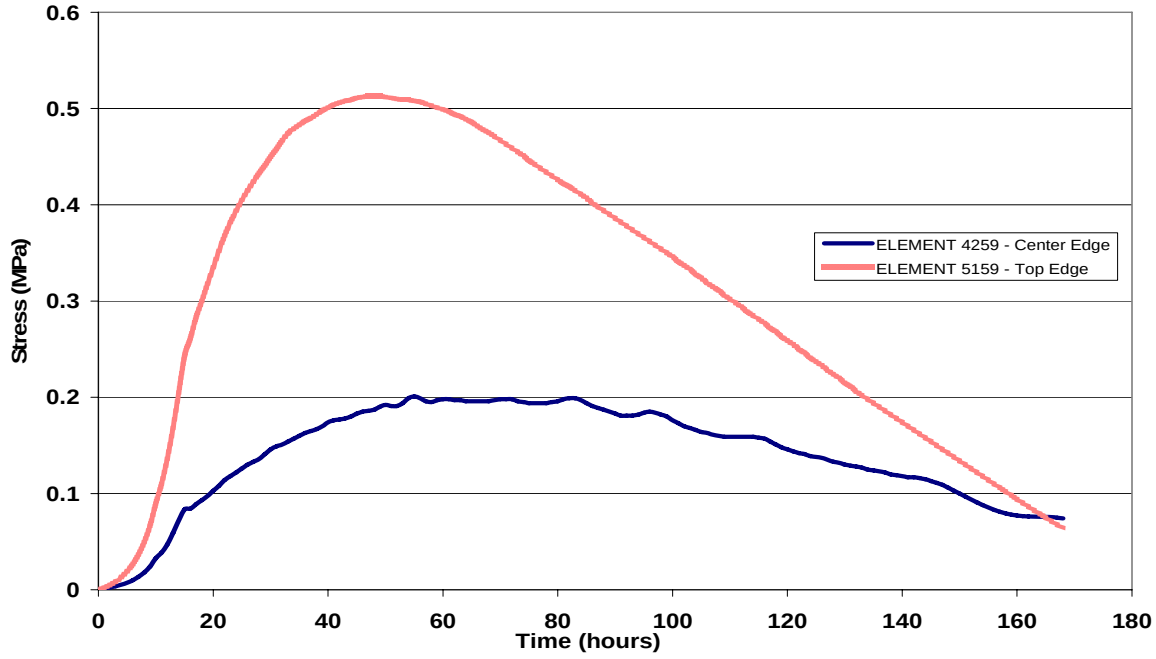

Figure 8-9. Stress state at the top edge and center edge of the finite element concrete block with mixture 4

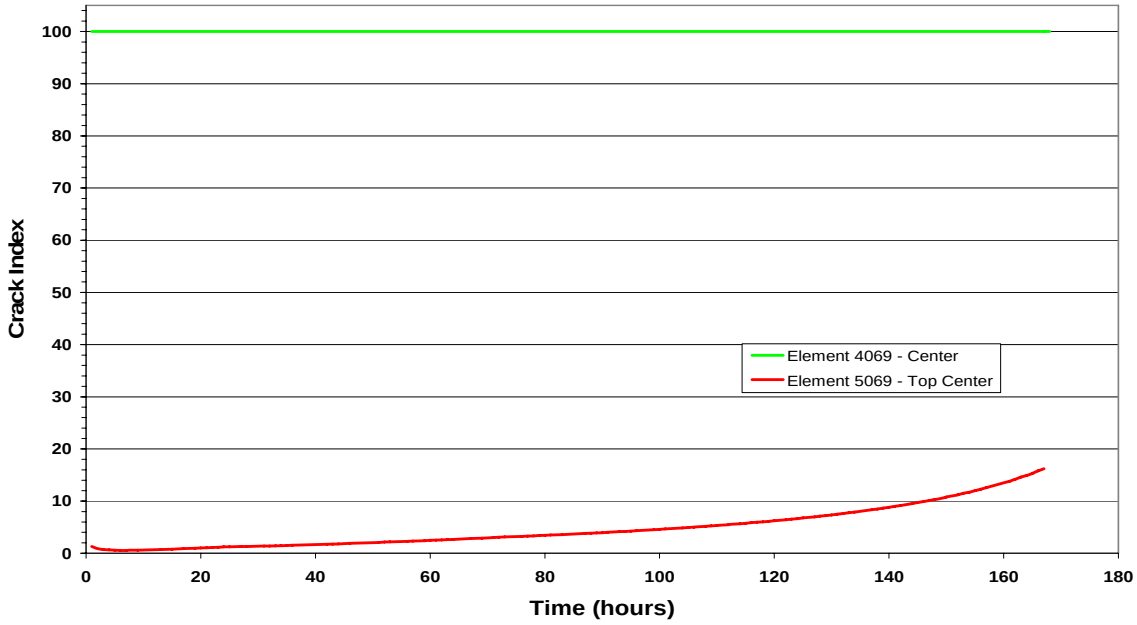

Figure 8-10. Crack index for elements along the center line of block with mixture 1

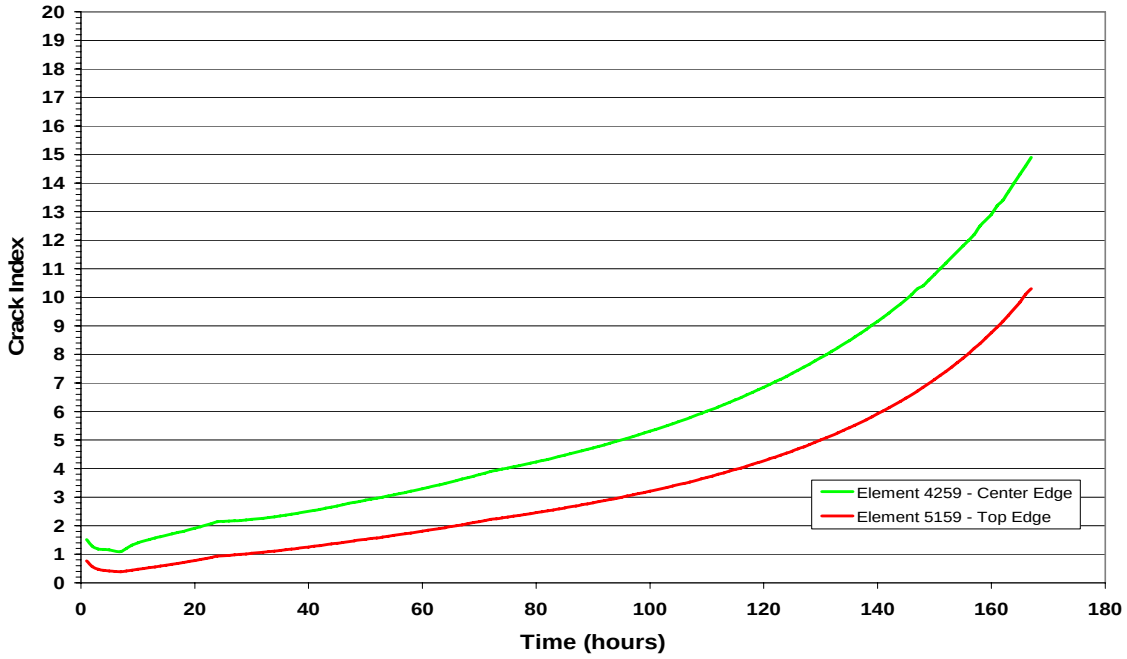

Figure 8-11. Crack index for elements along the edge of block with mixture 1

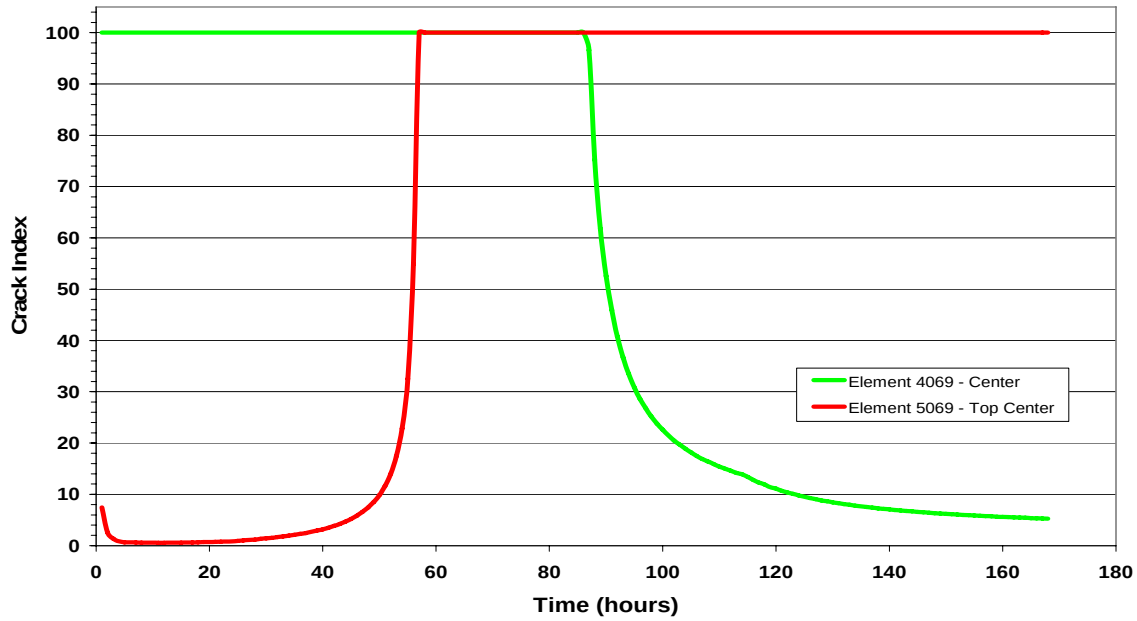

Figure 8-12. Crack index for elements along the center line of block with mixture 2

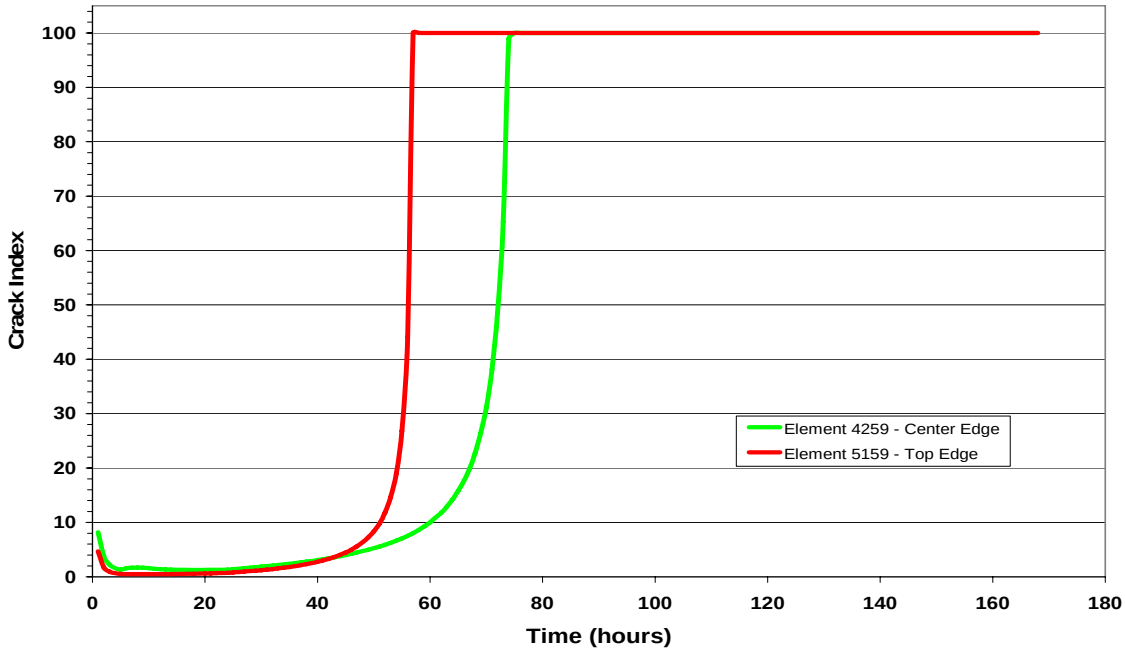

Figure 8-13. Crack index for elements along the edge of block with mixture 2

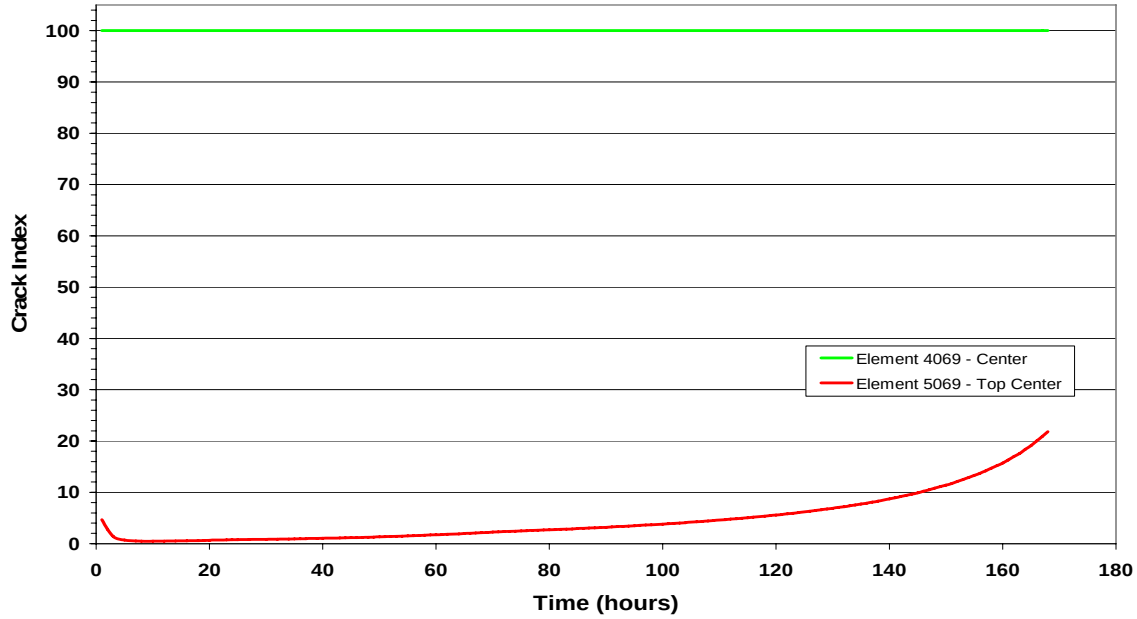

Figure 8-14. Crack index for elements along the center line of block with mixture 3

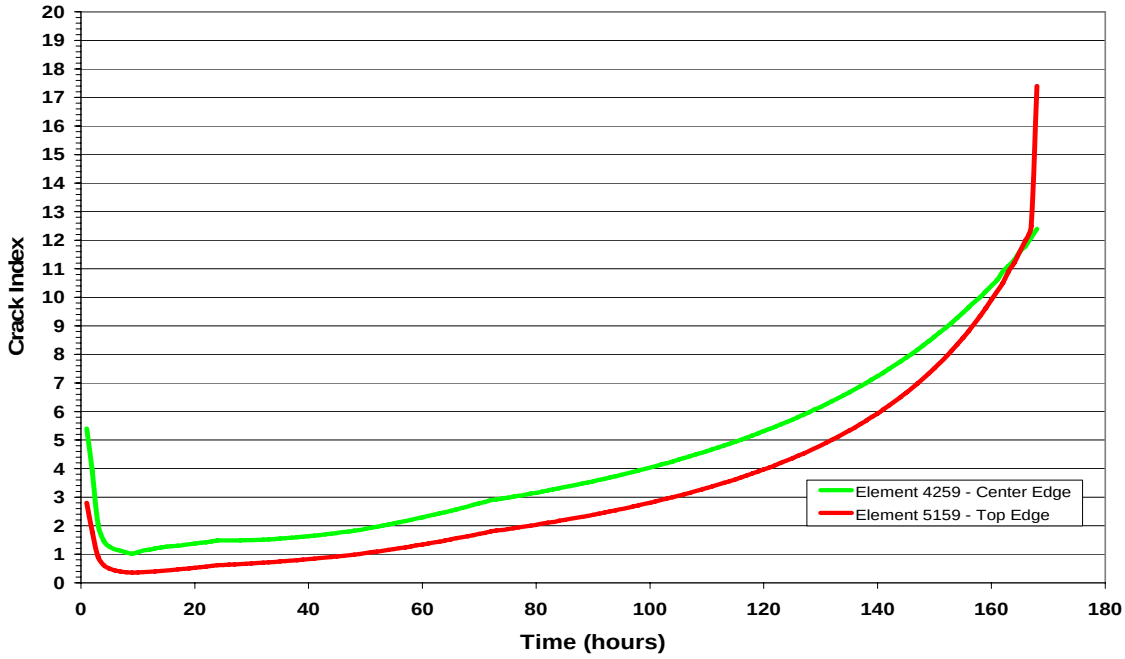

Figure 8-15. Crack index for elements along the edge of block with mixture 3

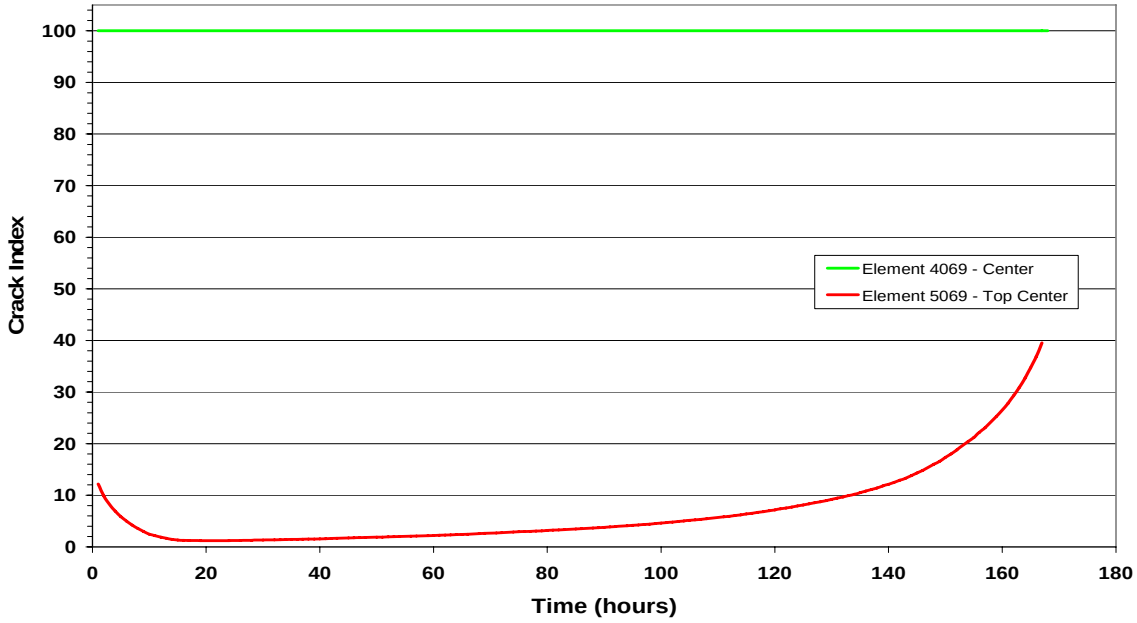

Figure 8-16. Crack index for elements along the center line of block with mixture 4

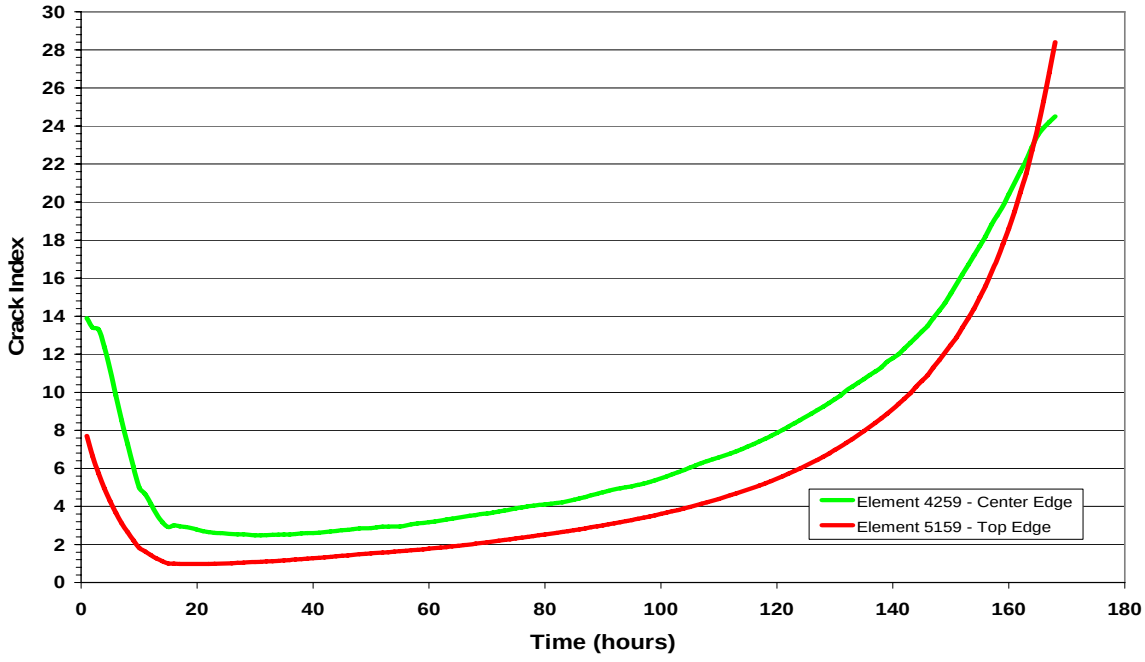

Figure 8-17. Crack index for elements along the edge of block with mixture 4

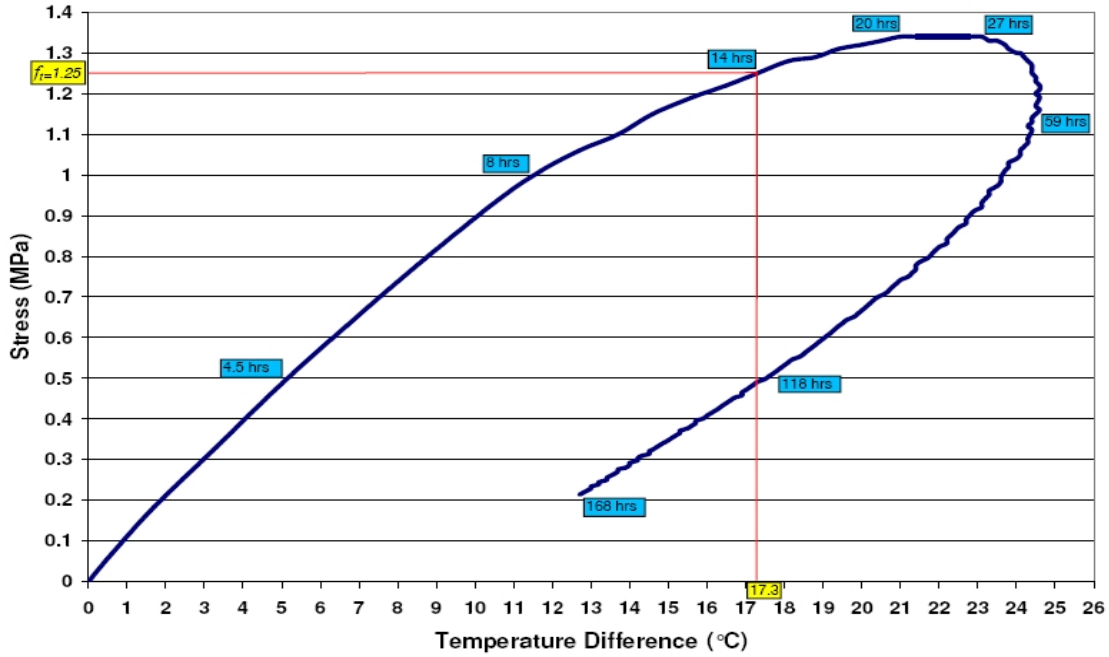

Figure 8-18. Induced stress with respect to temperature differential for mixture 1

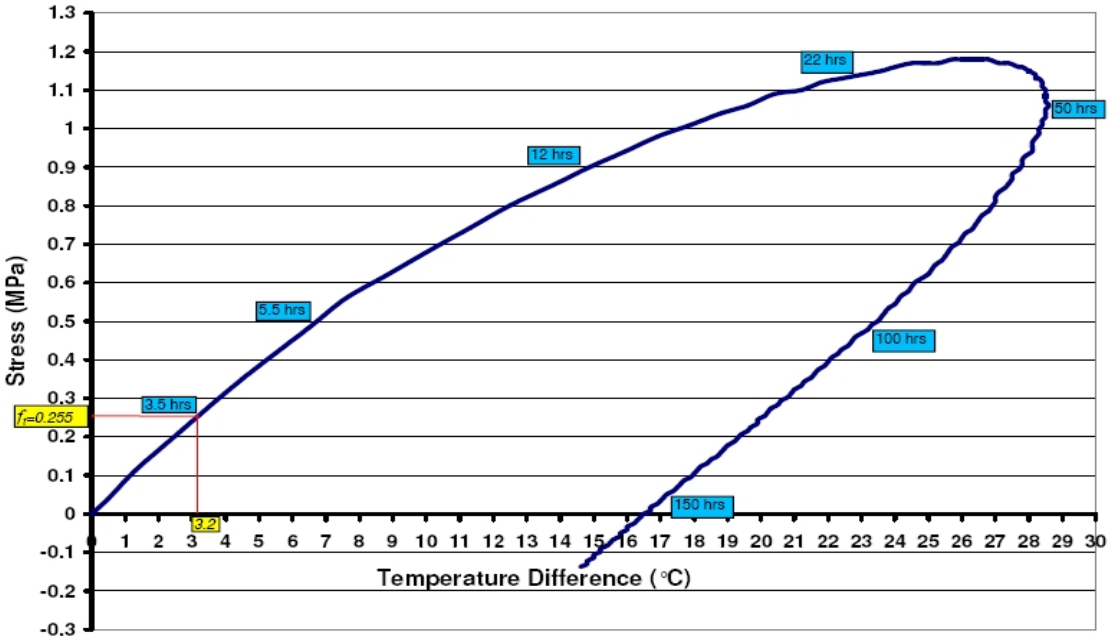

Figure 8-19. Induced stress with respect to temperature differential for mixture 2

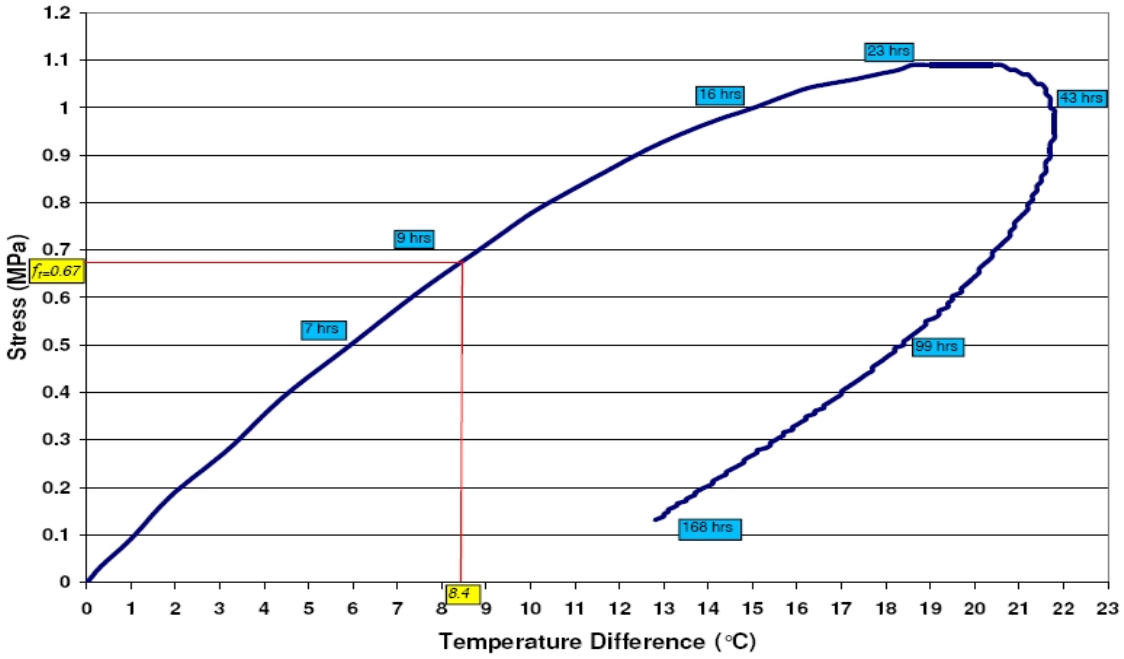

Figure 8-20. Induced stress with Respect to temperature differential for mixture 3

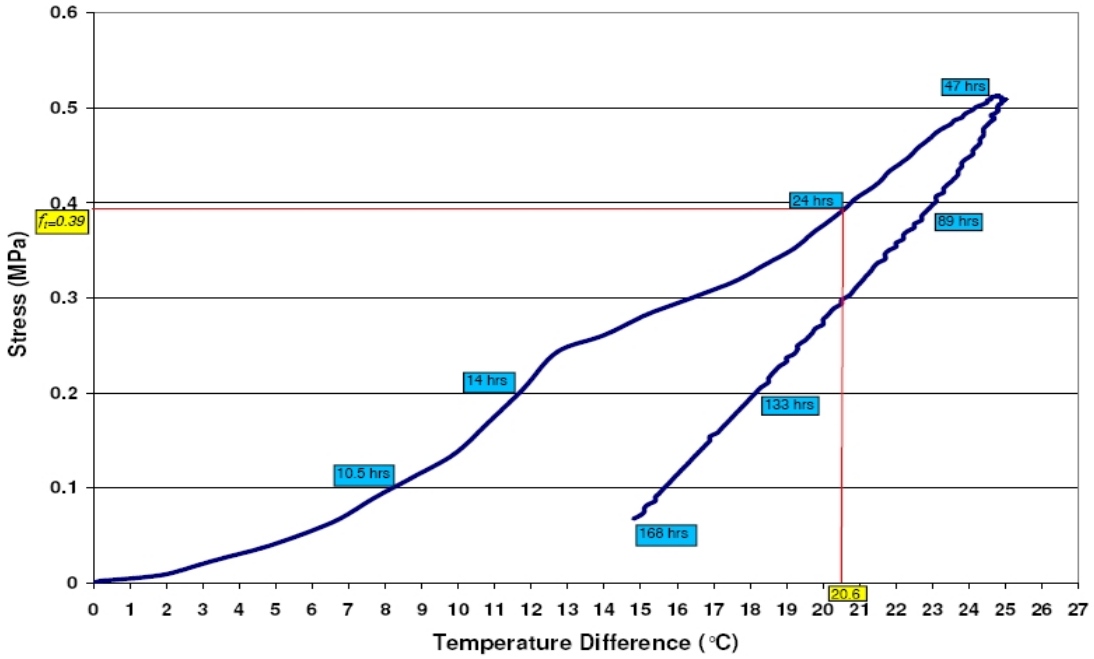

Figure 8-21. Induced stress with respect to temperature differential for mixture 4

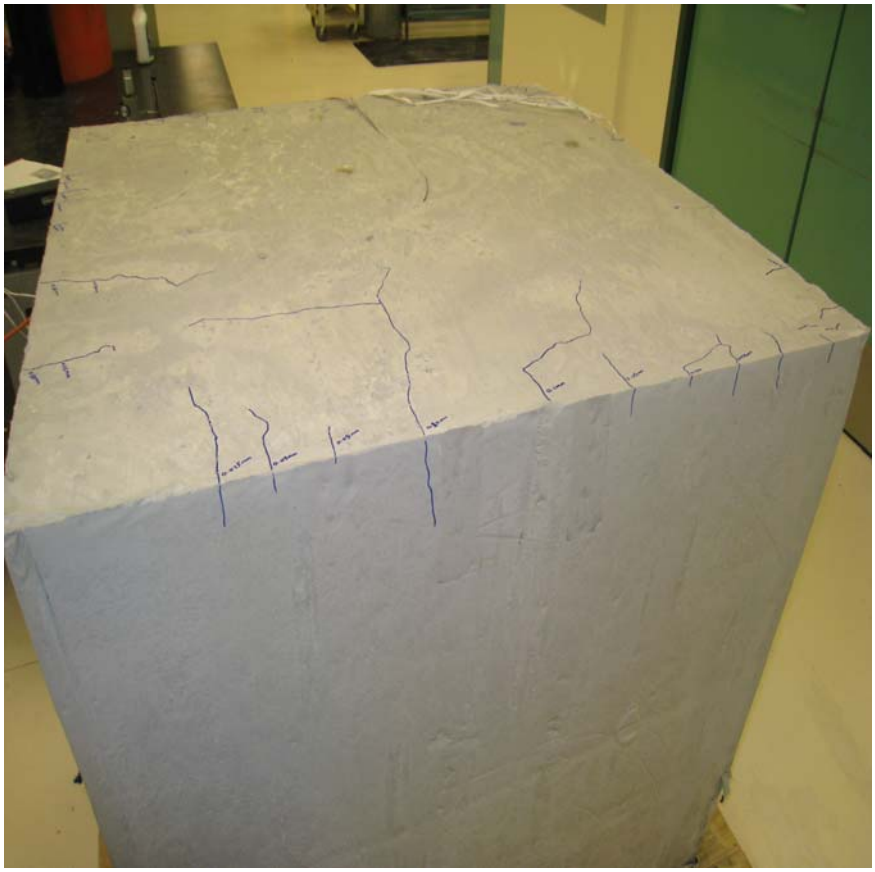

Figure 8-22. Top surface of experimental block containing mixture 1 showing numerous cracks along the edges

CHAPTER 9
PARAMETRIC STUDY

Introduction

This chapter discusses the results of a parametric study conducted with the aid of the DIANA finite element program. The parameters investigated are effects of the heat generation rate, size of the structure and the amount of insulation, on the peak temperature, temperature distribution and induced stresses in mass concrete structures.

Effect of Specimen Size

The standard specimen size used in this study was a block size of 1.07m x 1.07m x 1.07m. To study the effect of size on the behavior of concrete, three additional block sizes were modeled. The sizes chosen were a half sized block (0.5m x 0.5m x 0.5m), a block twice the size (2m x 2m x 2m), and a block four times the size (4m x 4m x 4m). A comparison of the temperature profiles at the center of blocks containing concrete using mix 1 is presented in Figure 9-1. Figure 9-2 shows the progression of the peak temperatures calculated in the block, as the size is increased. As expected, the peak temperature increased as the size of the block increased. A closer analysis of the effect of block size on the maximum temperature difference is presented in Figure 9-3, where it is shown that the maximum temperature differential between the center and top surface edge increases from 12.8 °C in the 0.5m block to 56.5 °C in the 4m block. Figures 9-4 and 9-5 are plots of the induced stress at the center of the top surface and the top surface edge respectively. In the 1m x 1m x 1m and 2m x 2m x2m blocks, the induced stress increases as we move from the center towards the edge of the blocks. However, in the 4m x 4m x 4m block we see that the stresses are the same at the top surface center and top surface edge suggesting that the stress is constant across the entire surface. The relationship between the maximum induced stress and the increasing maximum temperature differential caused by

increasing block size is presented in Figure 9-6, which shows that for a given concrete mixture, the maximum induced stress will increase with increasing maximum temperature differential. Figure 9-7 presents the maximum stress induced in each of the four types of concrete mixtures that were discussed in the previous chapters with respect to the maximum temperature difference for each size block. The maximum temperature difference and resulting stress in concrete elements larger than 1.07m x 1.07m x 1.07m is highly dependent on the type of concrete used.

Figure 9-8 shows the maximum induced stress with respect to maximum temperature gradient in each of the four types of concrete mixtures for each size block. The temperature gradients in the larger blocks tend to be lower for each type of concrete used in this study. A comparison of the results presented in Figure 9-7 with those presented in Figure 9-8 show that while maximum stress appears to be a function of temperature difference regardless of block size, it is not a function of temperature gradient alone. It appears that temperature difference, rather than temperature gradient is a better indicator of maximum stress in mass concrete.

Effect of Insulation Thickness

Two model blocks, one insulated 1.5 inch thick layer of polystyrene foam, and the other with a 6 inch thick layer polystyrene foam were created, analyzed and their results compared with the model analyzed in the previous chapters, to quantify the effect that the amount of insulation would have on the temperature distribution in a hydrating concrete element containing 100% Portland cement. Figure 9.9 and Figure 9.10 present the temperature profiles with respect to time of the concrete block insulated with 1.5 inch thick and 6 inch thick layers of polystyrene foam respectively. The block with the 1.5 inch thick layer of insulation had a maximum temperature difference between the center of the block and a point 2 inches below the exposed top surface of 14.9 °C, occurring 32 hours after casting, and was maintained for 7 hours before steadily decreasing to 3.6 °C. The maximum temperature difference between the center and a

point 2 inches below the exposed top surface calculated in the block with the 6 inch layer of insulation was 20 °C. This maximum difference was attained after 70 hours of hydration, slowly decreasing to 15.8 °C at the end of the analysis at 167 hours.

Figure 9-11 shows the comparison of the temperatures with respect to time 2 inches below the exposed top surface of the concrete blocks with varying insulation thickness. The peak temperature at this location was found to be the same and occurred at the same time in all three blocks. However the rate of temperature decrease was slowest in the model with the 6 inch insulation, and fastest in the model with the 1.5 inch insulation. The temperatures 4 inches below the top surface presented in Figure 9-12 were similar to those observed at 2 inches in terms of the three blocks attaining the same peak temperature at approximately the same time but having different rates of decline.

The comparison of the temperatures 21 inches below the top surface are shown in Figure 9-13. At this depth, the peak temperature and the time it is attained increase in accordance with the thickness of the polystyrene foam.

Although the top surface of the blocks modeled in this project were exposed to ambient conditions, the effectiveness of the insulation in reducing temperature differences within the concrete varied with respect to its thickness. This was determined by evaluating the temperature difference between the center of the block and a point at the same depth but on the side of the block. Figure 9-14 shows the temperature in the concrete block modeled with the 1.5 inch thick polystyrene insulation where a maximum temperature difference of 8.3 °C between the center and the side is observed. The temperatures in the block with the 3 inch thick polystyrene insulation are presented in Figure 9-15. Here, we see that the maximum temperature difference

between the two points decreases to 3.4 °C. Figure 9-16, shows that for the block insulated with a 6 inch thick layer of polystyrene the temperature difference was only 1.9 °C.

Having assessed the effects of the insulation thickness on the temperature distribution in the uncovered block, an investigation on the effect of the insulation thickness on the maximum temperature differential and maximum induced stress in a concrete block insulated on all faces was conducted. Figure 9-17 and Figure 9-18 show comparisons of the experimentally measured and numerically calculated temperature profiles 2 inches and 4 inches below the top surface of the fully insulated concrete block with mixture 1 for validation purposes.

Figure 9-18 presents the variation in maximum temperature differential within the concrete with respect to insulation thickness. Figure 9-19 also shows how the block size determines the effect increasing the insulation thickness will have on the maximum temperature differential within the concrete. As shown in Figure 9-19, increasing the insulation thickness from 1.5 inches up to 9 inches will reduce the temperature difference between the center and top surface of the block. In the 0.5m block, the maximum temperature difference moved from 5.6 °C with 1.5 inches of insulation, to 4.2 °C with 3 inches of insulation, to 3.2 °C with 6 inches of insulation, to 2.8 °C with 9 inches of insulation. The 1.07m block had values of 12.4 °C, 8.9 °C, 6.5 °C, and 5.4 °C with insulation thicknesses of 1.5 inches, 3 inches, 6 inches, and 9 inches respectively. The 2m block had a temperature difference of 22.8 °C at 1.5 inches, 16.7 °C at 3 inches, 11.6 °C at 6 inches, and 9.3°C at 9 inches. Finally, the 4m block saw the largest reduction in the magnitude of the maximum temperature difference with increasing insulation thickness. The maximum temperature difference in the block with 1.5 inches of insulation was calculated at 37.7 °C, with 3 inches of insulation, 27.2 °C, 6 inches of insulation, 18.1 °C and finally with 9 inches of insulation, 14 °C.

Figure 9-20 and Figure 9-21 show the effect of increasing the insulation thickness had the maximum induced stress in the concrete with respect to temperature difference. Figure 9-20 shows that the reduced magnitude of temperature difference caused by an increase in insulation thickness will result in lower induced stress within the concrete block. Figure 9-21 shows that by increasing the insulation thickness, significant reductions in stresses can be achieved in large concrete elements.

Time of Formwork Removal Effect

The effect model was modified so that the effect that the time of removal of the formwork had on the induced concrete stresses could be assessed. Knowledge of the optimal time to remove of the formwork and insulation around mass concrete is important in that the scheduling of construction time sequence is an essential aspect of project management. The times chosen for analysis were 12 hours, 1 day, 2 days, 3 days, 4 days and 6 days after pouring of the concrete.

Figure 9-22 through to Figure 9-27 show the induced stress with respect to time in a 1.07m x 1.07m x 1.07m concrete block concrete when the formwork and insulation is removed at times of 12 hours, 1 day, 2 days, 3 days, 4 days and 6 days.

A sharp sudden increase in tensile stress occurred along the surface immediately after formwork removal. The peak stress calculated for the removal times of 12 hours, 1 day, 2 days and 3 days were 0.964 MPa, 1.08 MPa, 1.31 MPa, 1.30 MPa respectively. These were 77% 86.4%, 79% and 67.4% of the attained concrete tensile strength respectively. While not exceeding the tensile strength of the concrete, these stress levels are high enough to cause micro-cracking. These micro-cracks do not pose an immediate threat to the structural integrity of the concrete however they will provide an entry point for invasive deleterious substances that can compromise the long term durability of the concrete. Figure 9-26 shows the state of stress in

concrete when the formwork is removed after 4 days of hydration. The stress also undergoes a sharp increase in magnitude the instant the formwork is removed, but is only slightly above 50% of the tensile strength at 4 days, therefore the risk of micro-cracking is small. Figure 9-27 shows the stresses for the concrete that had the formwork and insulation removed after 6 days of hydration. Here the peak stress of 1.08 MPa is 49% of the tensile strength of the concrete.

The results of the parametric study on the effect time of formwork and insulation removal suggests that the risk of micro-cracking is substantially reduced if the removal is done a minimum of 4 days after the concrete is poured.

Heat Generation Rate Effect

The effect the rate of internal heat generation has on the distribution of temperatures in a concrete element can be seen from the analysis of the block model with varying mixture designs described in Chapter 7. It was observed that concrete with 100% Portland cement generated heat at the fastest rate, followed by the concrete with the 35% replacement of fly ash, then by the substitution of 50% ground granulated blast-furnace slag, and the slowest rate of heat generation occurred in the mixture with 50% Portland cement, 30% Slag and 20% Fly Ash (ternary blend). Figure 9-28 shows the temperature profile with respect to time at the center of the concrete blocks containing each mix. It is seen that the concrete containing the highest rate of heat generation (100% Portland cement) had the sharpest rise in temperature and the highest peak temperature. The ternary blend concrete with the slowest rate of heat generation had the lowest temperature rise slope and also the lowest peak temperature.

Summary of Findings

The parametric study of the factors affecting the behavior of concrete resulted in the following:

- The peak temperature, internal temperature gradients and induced thermal stresses increase as the amount of concrete used in any one pour is increased.

- The thickness of the insulating layer around the block formwork has an indirect effect on the magnitude of the maximum temperature difference in the hydrating concrete. For a given Resistance value (R-Value) of an insulating material the temperature difference in concrete will decrease with increasing insulation thickness.

- Concrete with a fast rate of heat generation will have higher peak temperatures increasing the likelihood that thermal cracking will occur.

- The effectiveness of insulation thickness in the reduction of the maximum temperature differential in concrete is dependent on the size of the concrete block. An increase in insulation thickness from 1.5 inches to 9 inches reduced the maximum temperature differential by 50% in a 0.5m x 0.5m x 0.5m block while the reduction in a 4m x 4m x 4m block was 62.9%.

- Increasing the insulation thickness can achieve significant reductions in thermal stresses in large concrete elements.

- Although the tensile stresses that resulted from the removal of formwork and insulation 12 hours, 1 day, 2 days and 3 days after the pouring concrete were less than the tensile strength of the concrete as measured in the laboratory, the stresses were large enough to initiate micro-cracking. These micro-cracks can serve as an entry point for deleterious materials that can undermine the durability of the concrete.

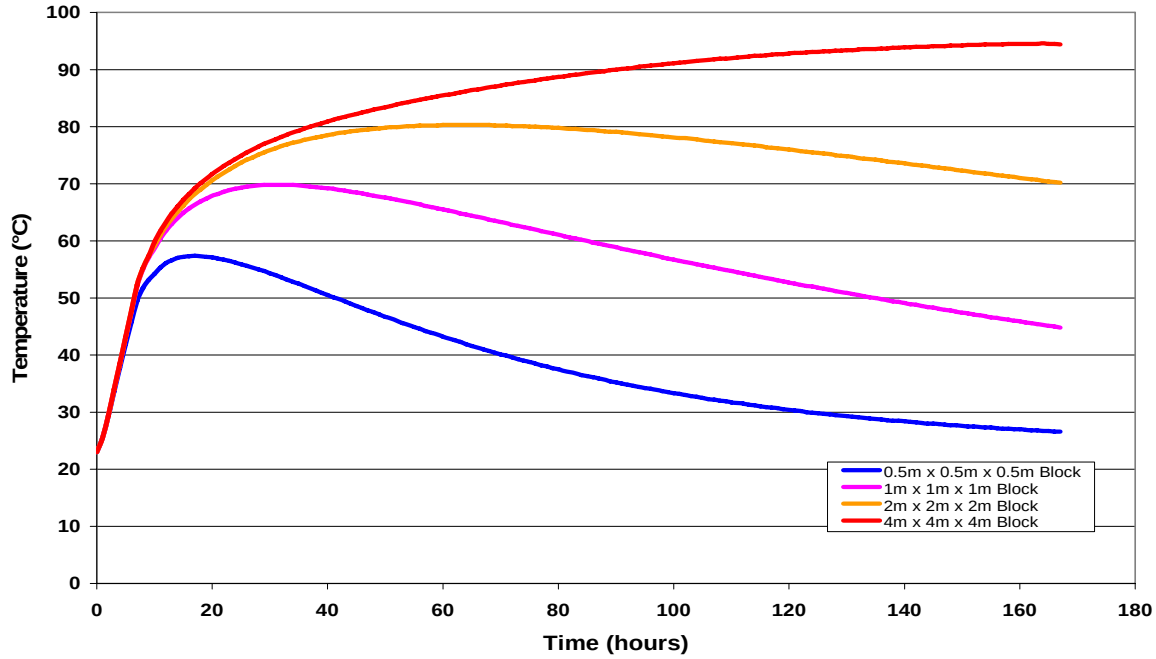

Figure 9-1. Comparison of temperature profiles calculated at the center of each block

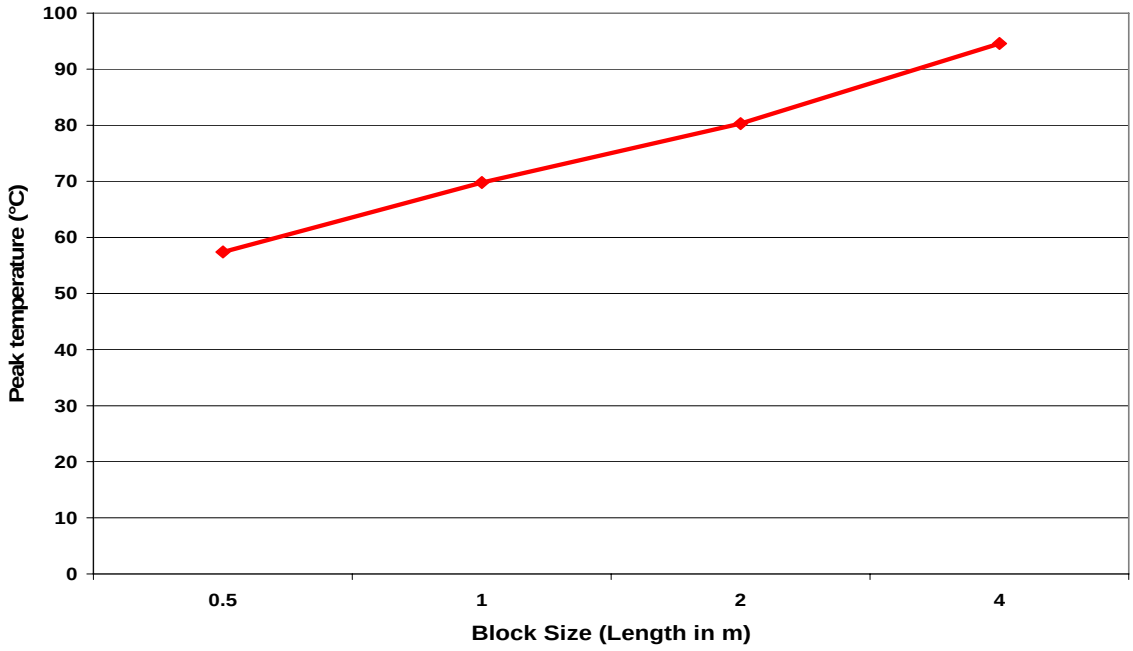

Figure 9-2. Calculated peak temperature values with respect to block size

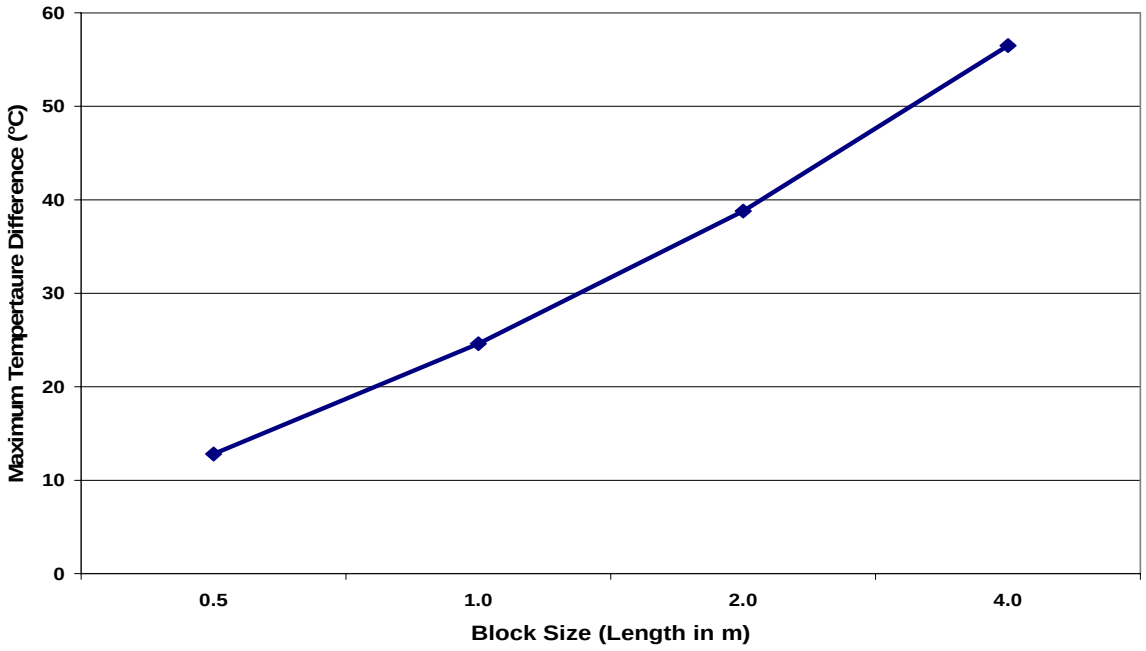

Figure 9-3. Effect of concrete block size on the maximum internal temperature difference

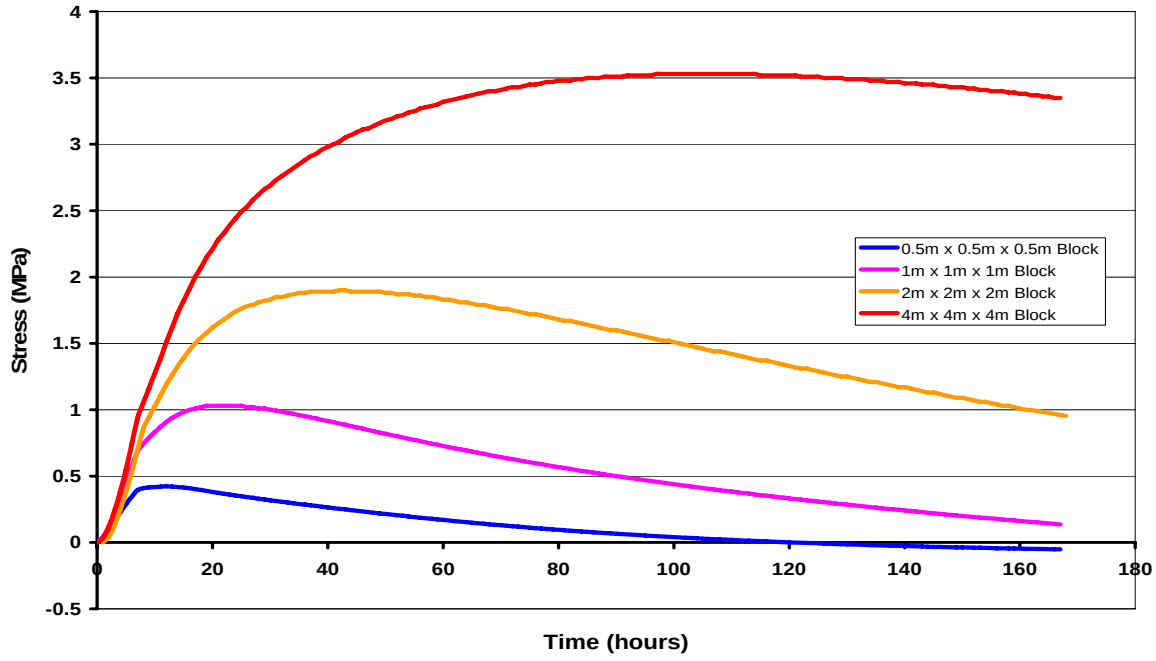

Figure 9-4. Comparison of stresses at the center of the top surface of each block

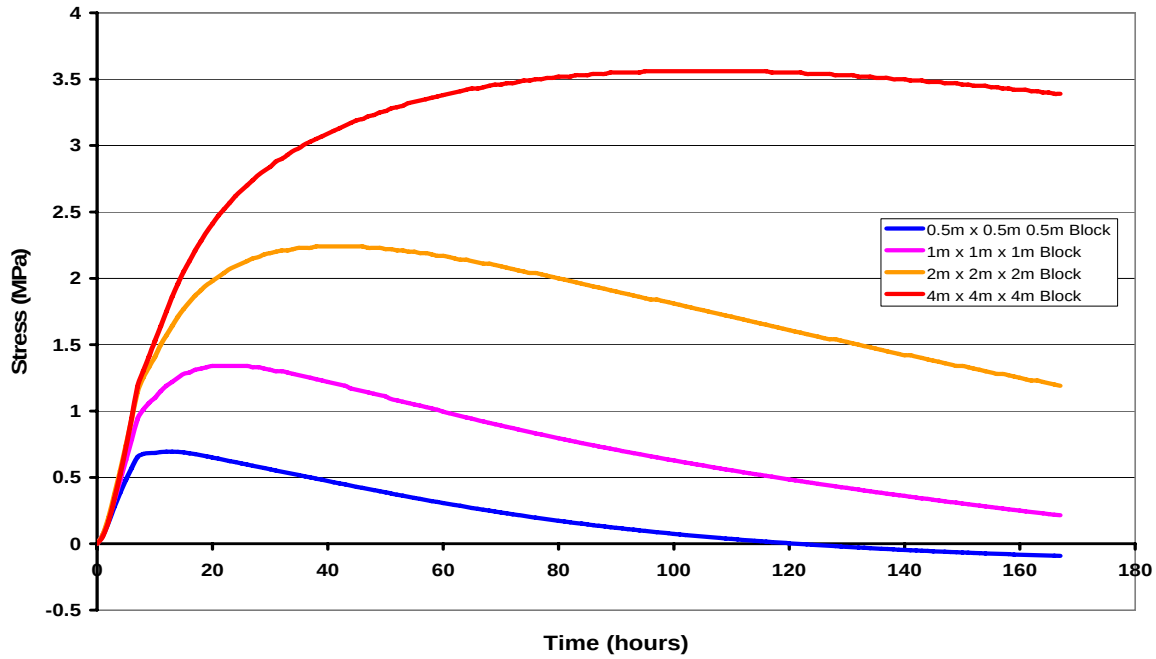

Figure 9-5. Comparison of stresses at the top surface edge of each block

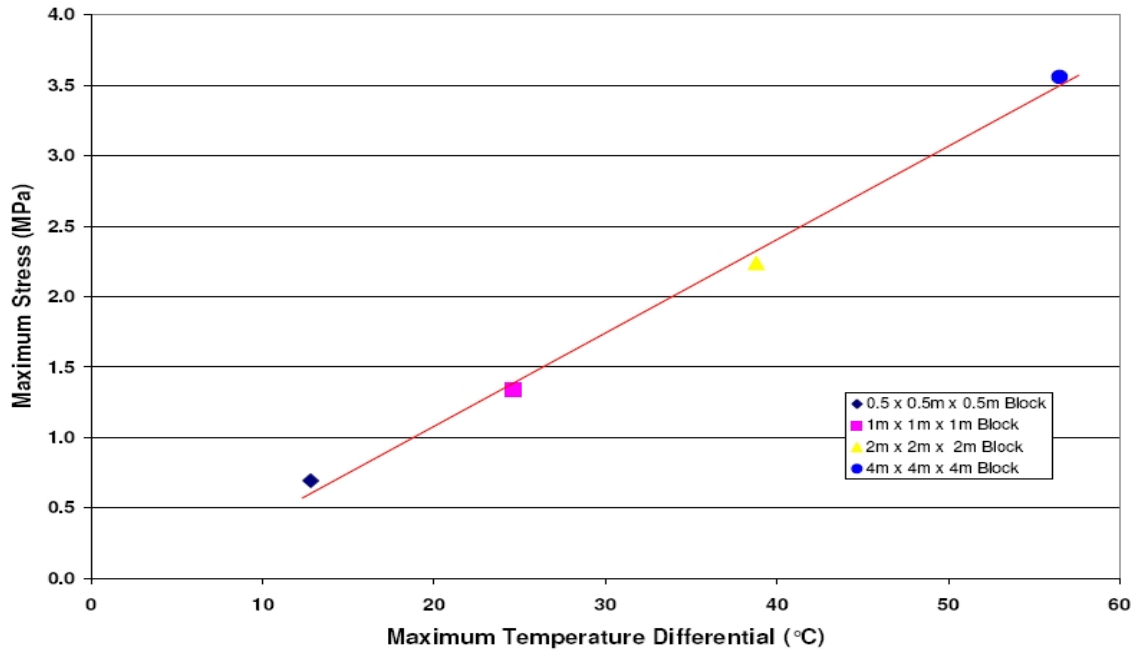

Figure 9-6. Maximum induced stress with respect to maximum temperature differential as a result of increasing block size

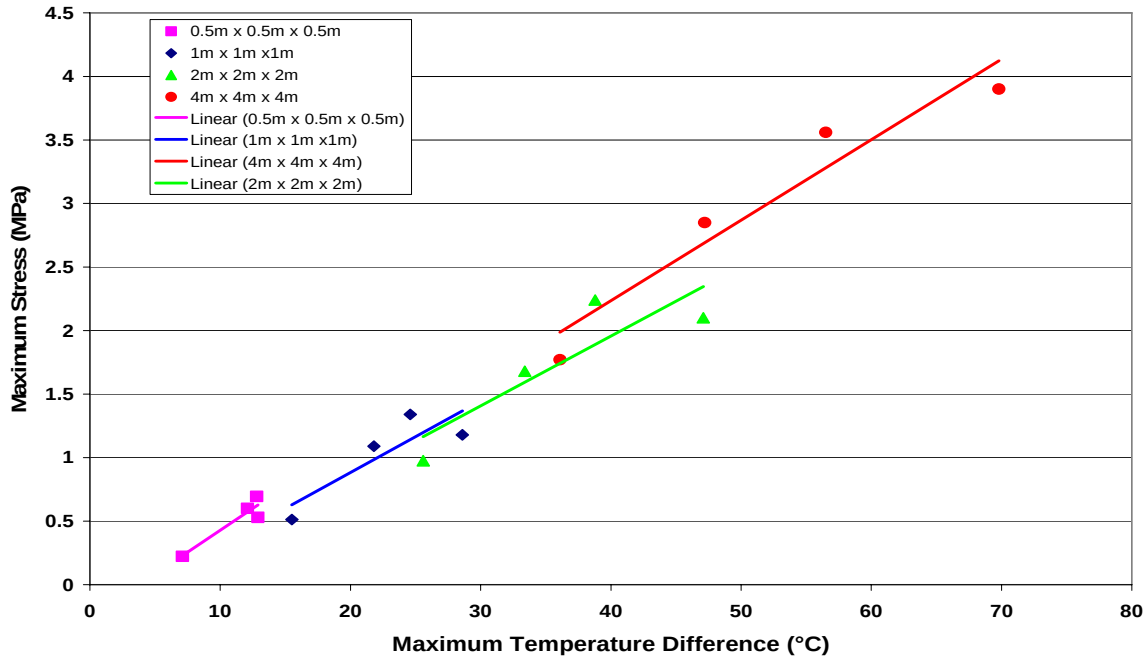

Figure 9-7. Plot of maximum stress versus maximum temperature difference with respect to block size and type of concrete used.

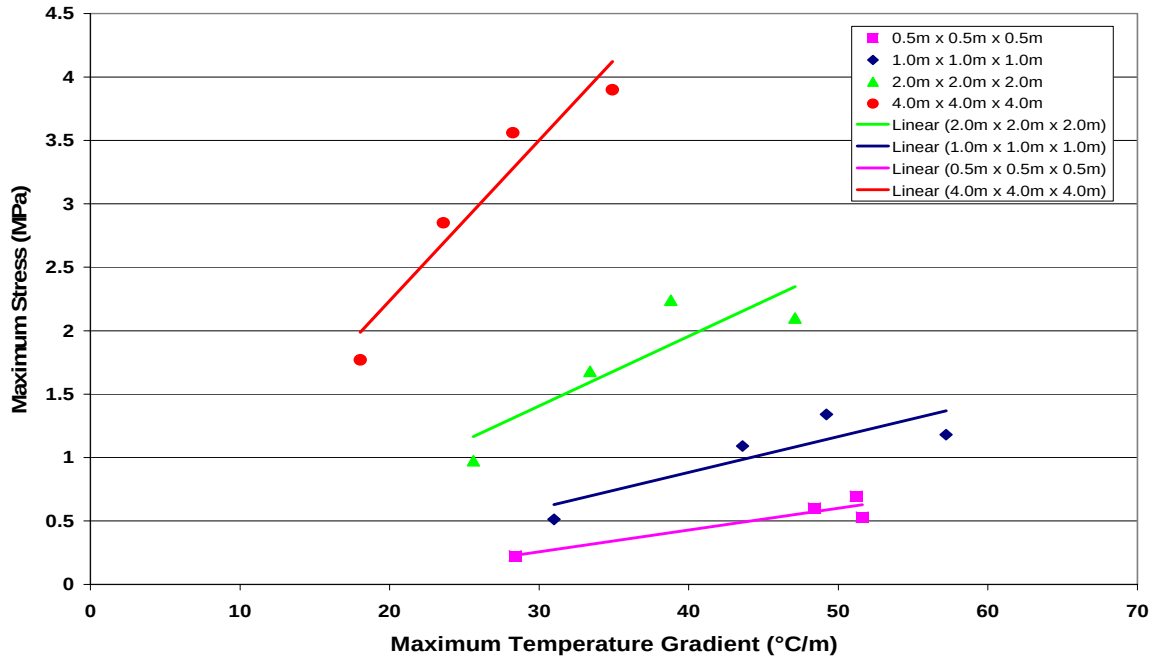

Figure 9-8. Plot of maximum stress versus maximum temperature gradient with respect to block size and type of concrete used.

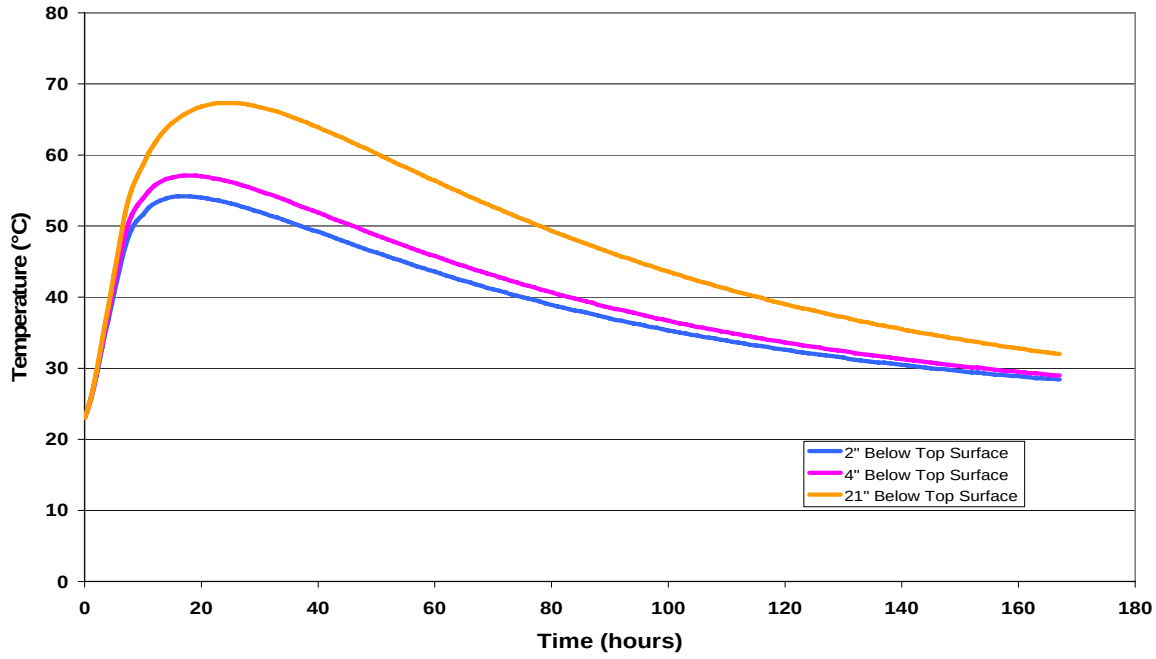

Figure 9-9. Temperature profiles with respect to time 2 inches, 4 inches and 21 inches below the top surface of the block insulated with a 1.5 inch thick layer of polystyrene foam

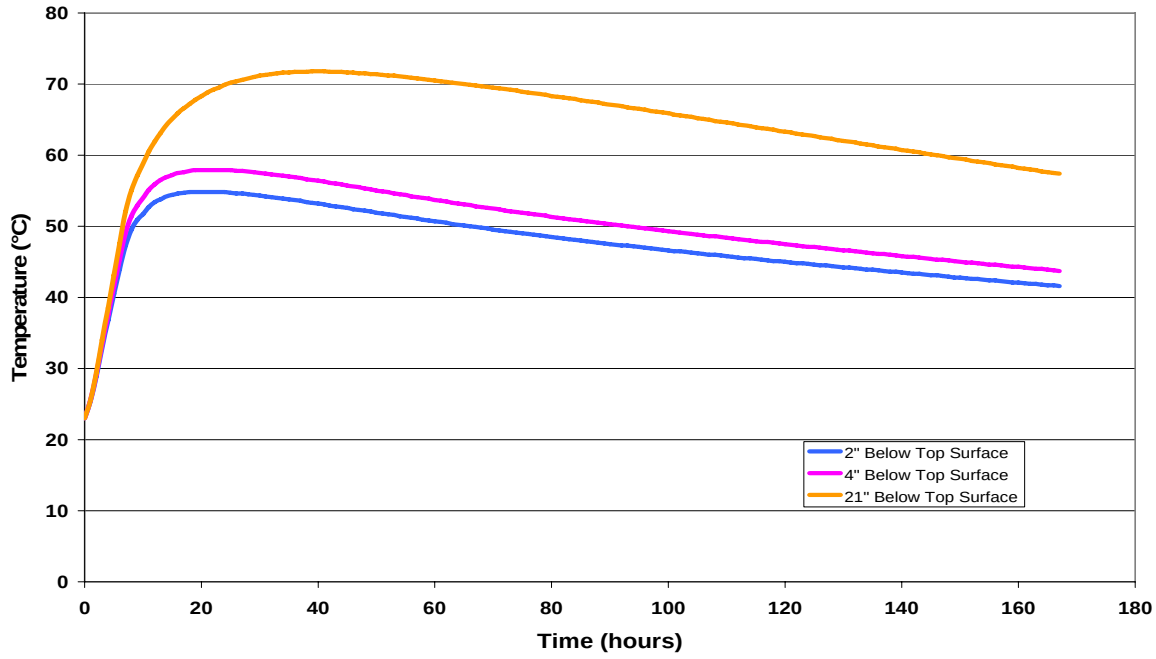

Figure 9-10. Temperature profiles with respect to time 2 inches, 4 inches and 21 inches below the top surface of the block insulated with a 6.0 inch thick layer of polystyrene foam

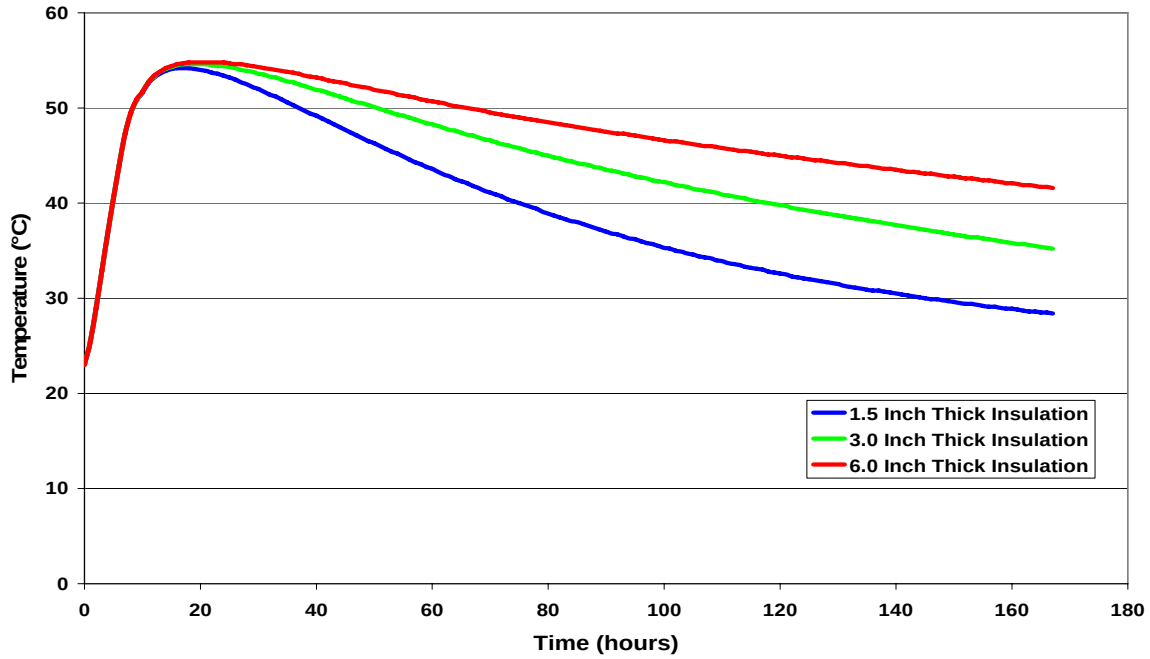

Figure 9-11. Comparison of temperature profiles with respect to time 2 inches below the top surface of the blocks with varying thicknesses of polystyrene foam insulation

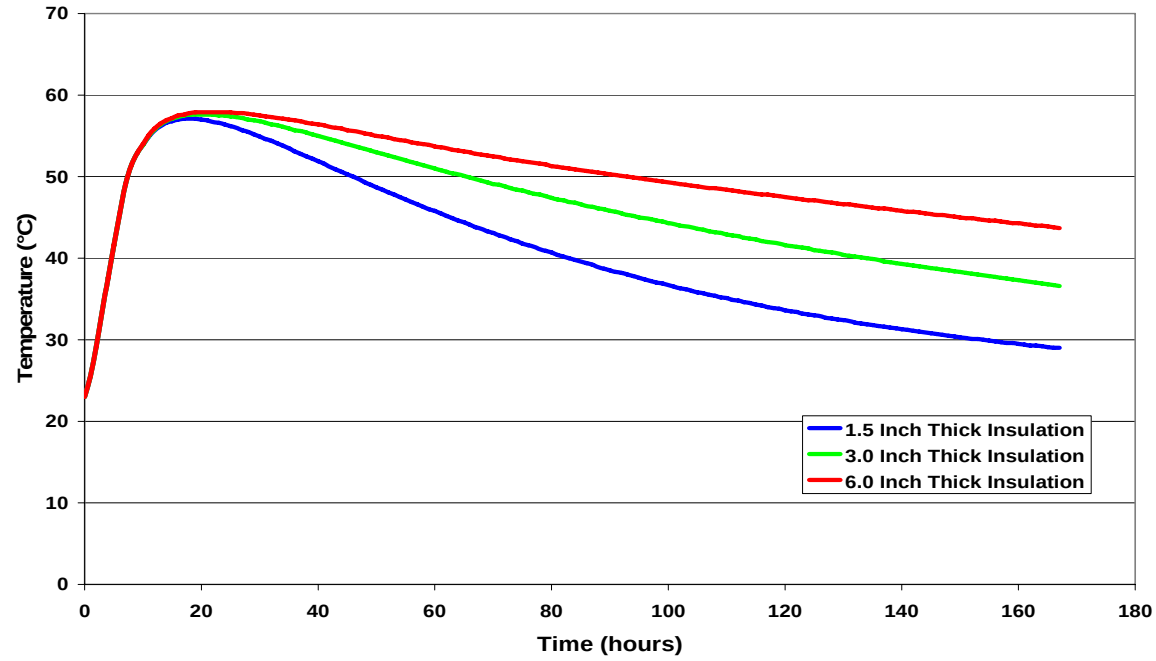

Figure 9-12. Comparison of temperature profiles with respect to time 4 inches below the top surface of the blocks with varying thicknesses of polystyrene foam insulation

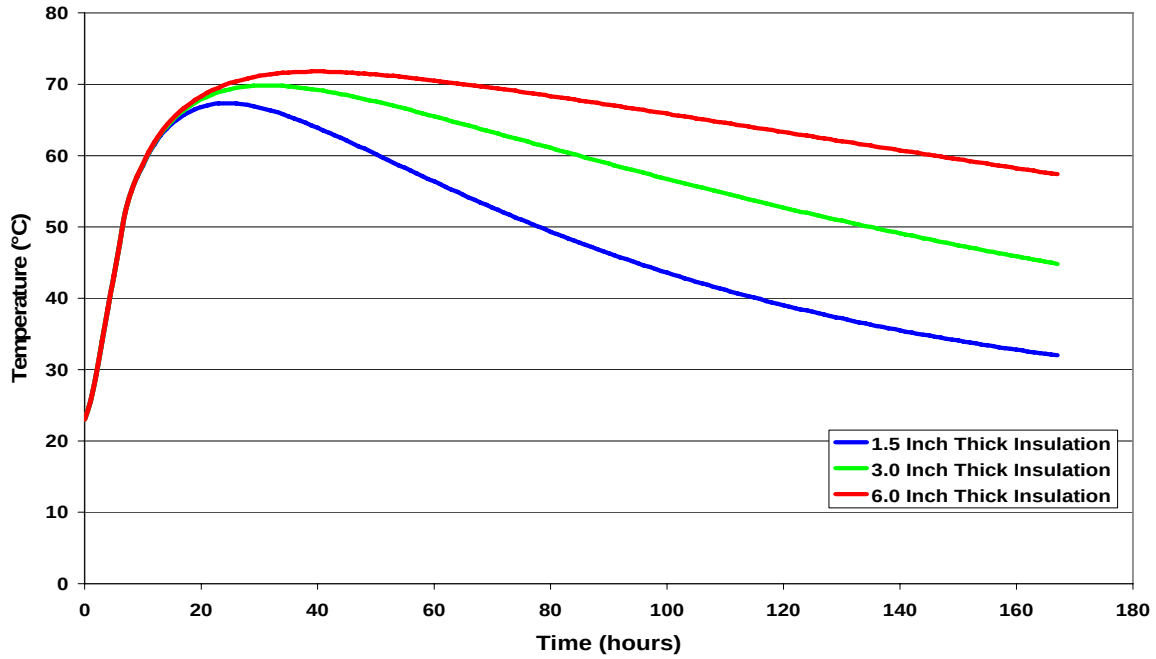

Figure 9-13. Comparison of temperature profiles with respect to time 21 inches below the top surface of the blocks with varying thicknesses of polystyrene foam insulation

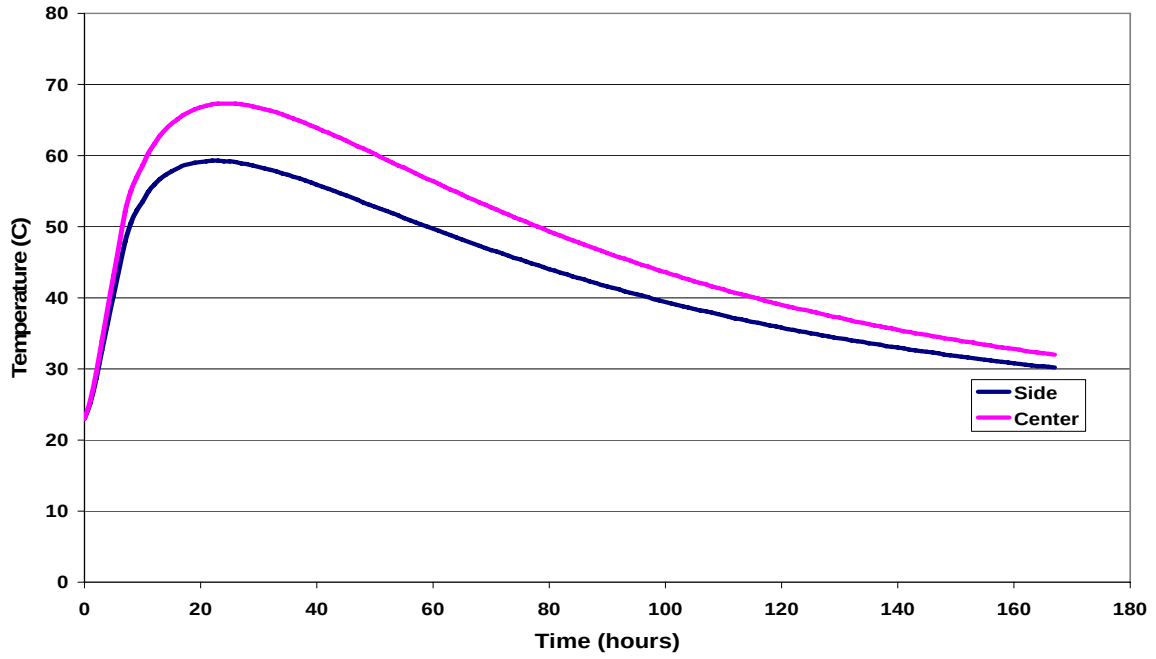

Figure 9-14. Temperatures calculated at the side and center of a concrete block with 1.5 inch thick insulation

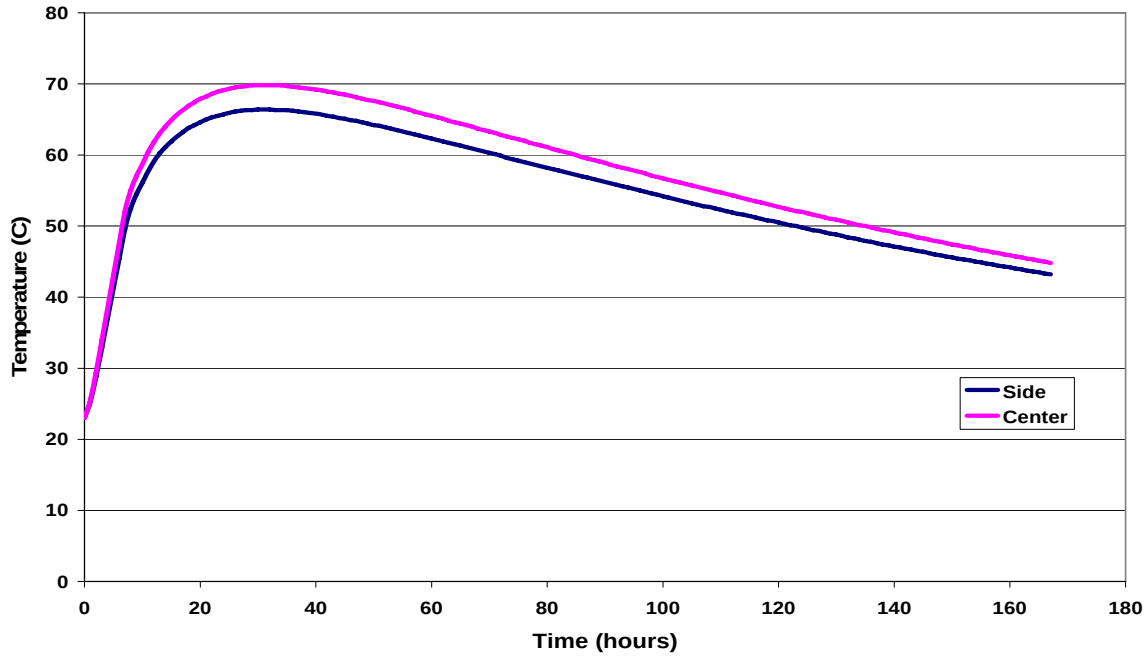

Figure 9-15. Temperatures calculated at the side and center of a concrete block with 3.0 inch thick insulation

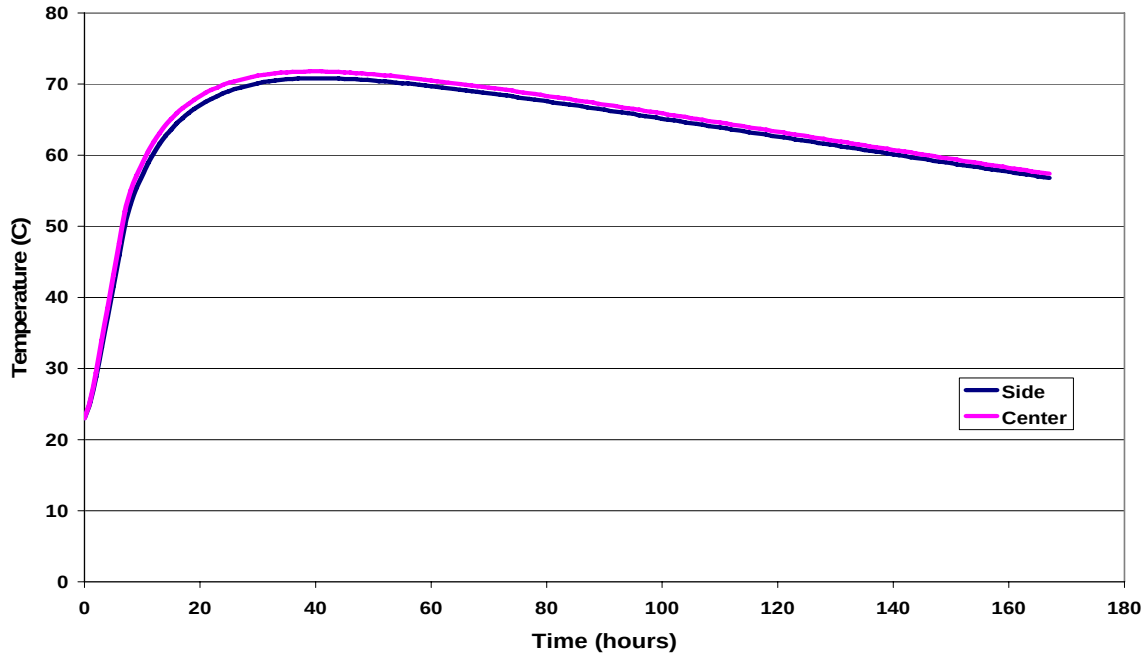

Figure 9-16. Temperatures calculated at the side and center of a concrete block with 6.0 inch thick insulation

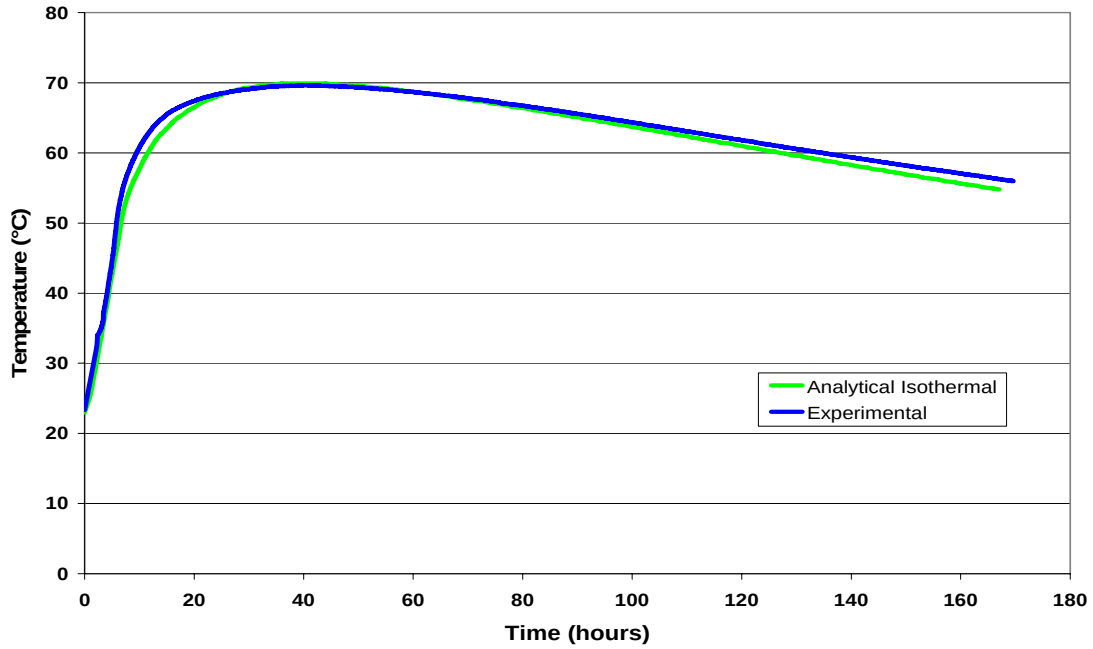

Figure 9-17. Comparison of experimentally measured and calculated temperature profiles 2 inches below the top surface at the centerline of concrete block with 3.0 inch thick insulation

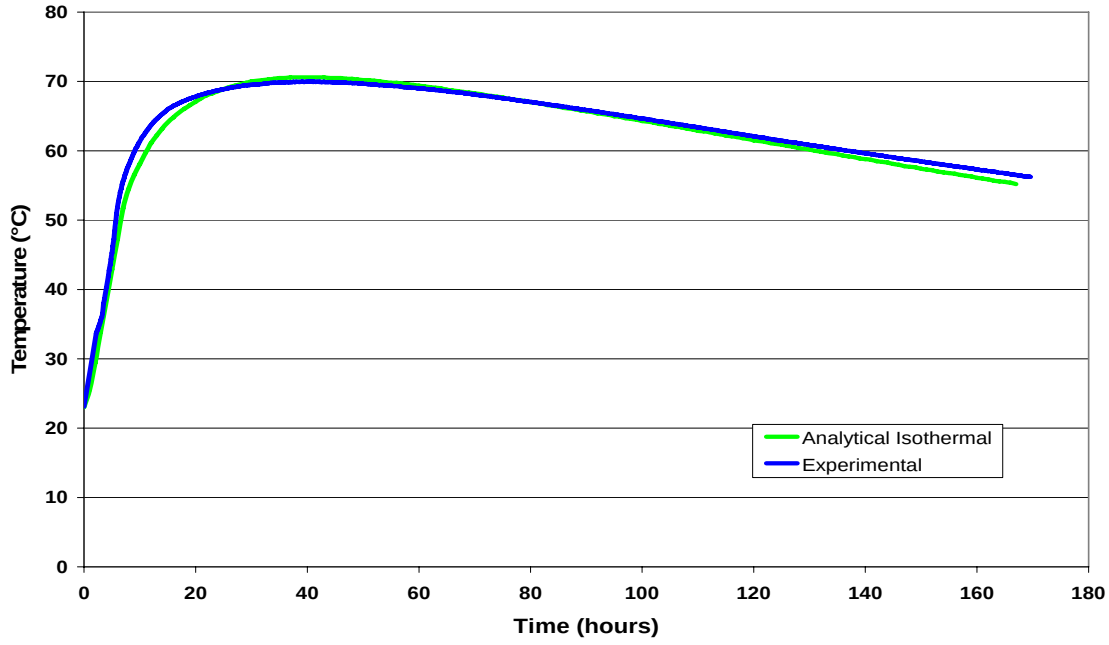

Figure 9-18. Comparison of experimentally measured and calculated temperature profiles 4 inches below the top surface at the centerline of concrete block with 3.0 inch thick insulation

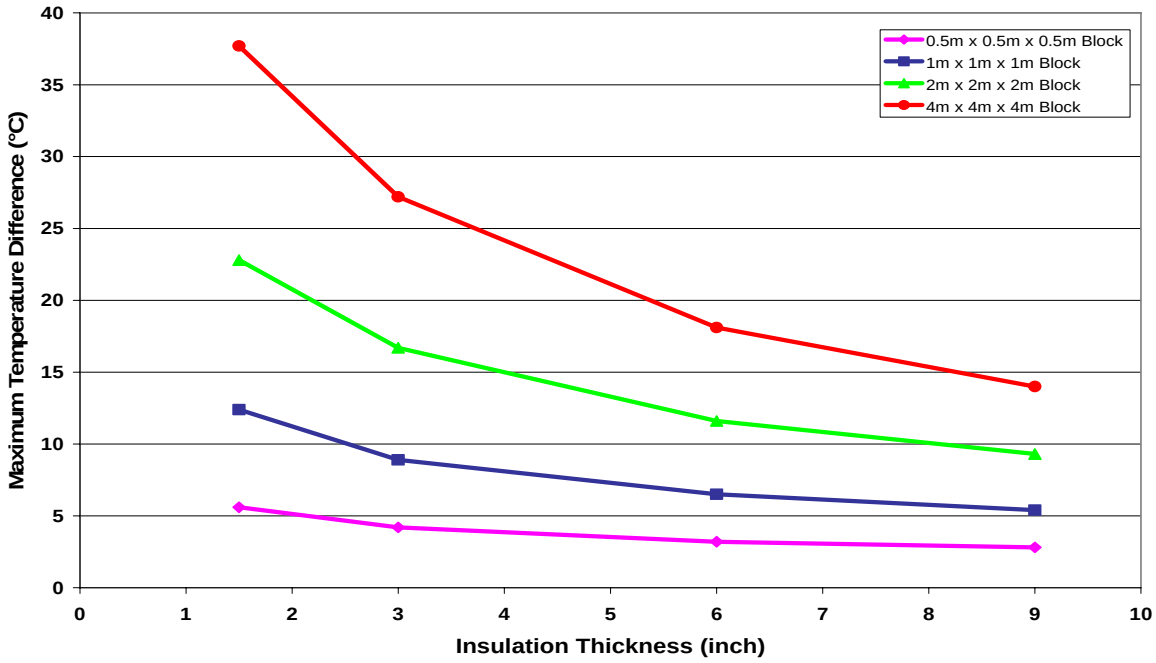

Figure 9-19. Variation in maximum temperature differential within the concrete with respect to insulation thickness for each block size

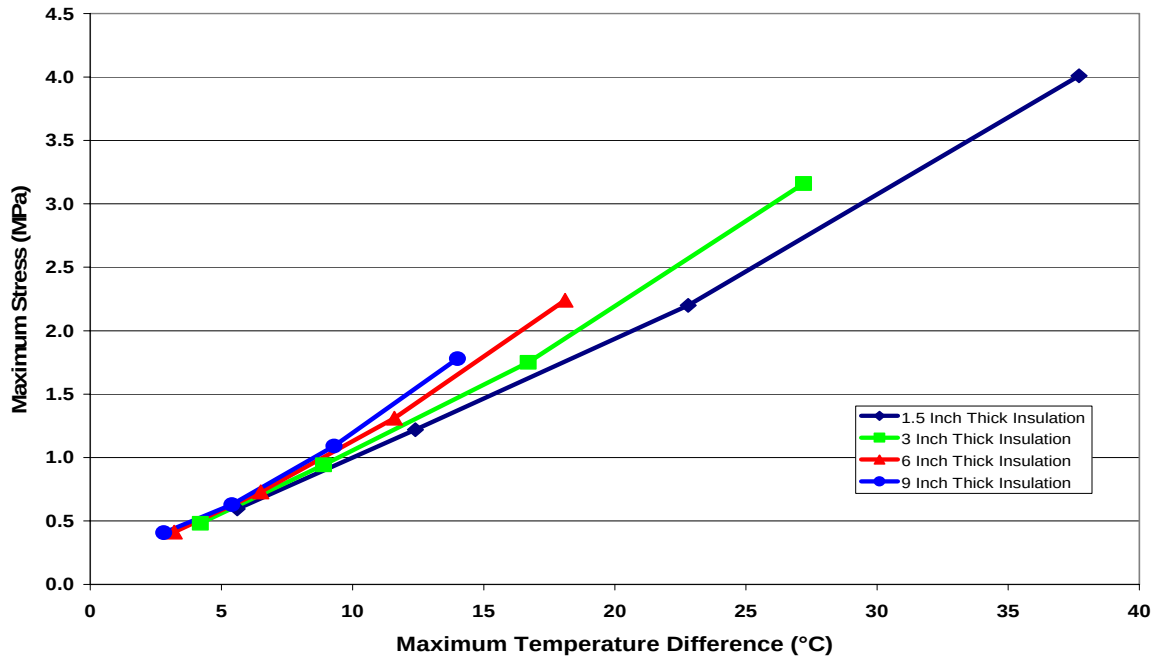

Figure 9-20. Effect of reduction of temperature differential caused by increasing insulation thickness on the maximum induced stress

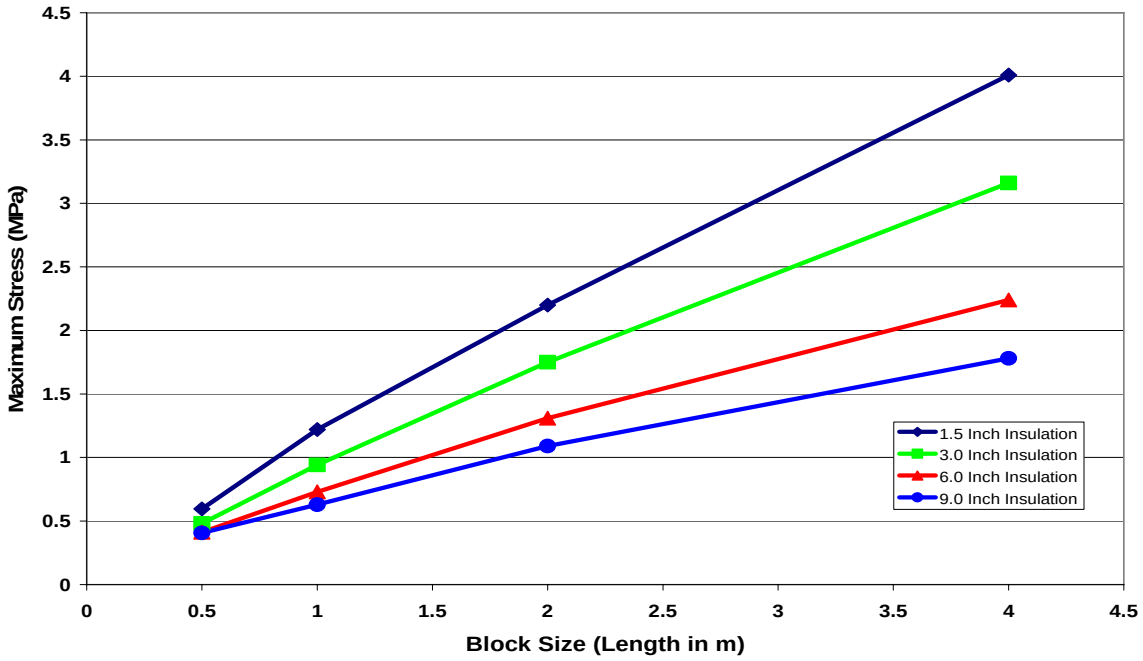

Figure 9-21. Effect of insulation thickness on the maximum induced stress in each block size

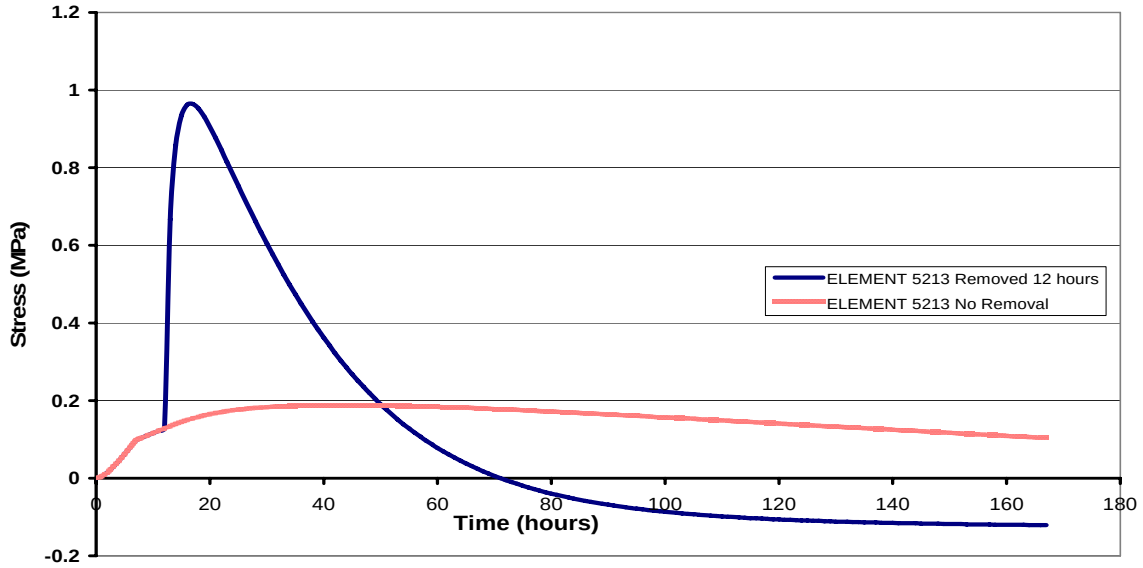

Figure 9-22. Plot of stress versus time at a point on the center of the surface of the concrete block when formwork is removed 12 hours after casting

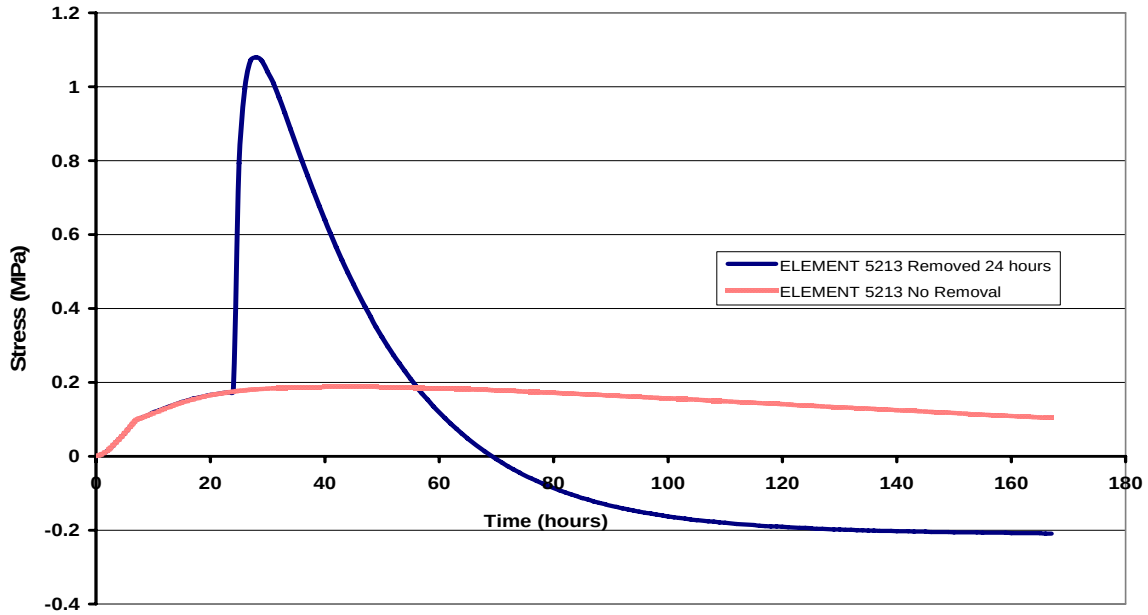

Figure 9-23. Plot of stress versus time at a point on the center of the surface of the concrete block when formwork is removed 1 day after casting

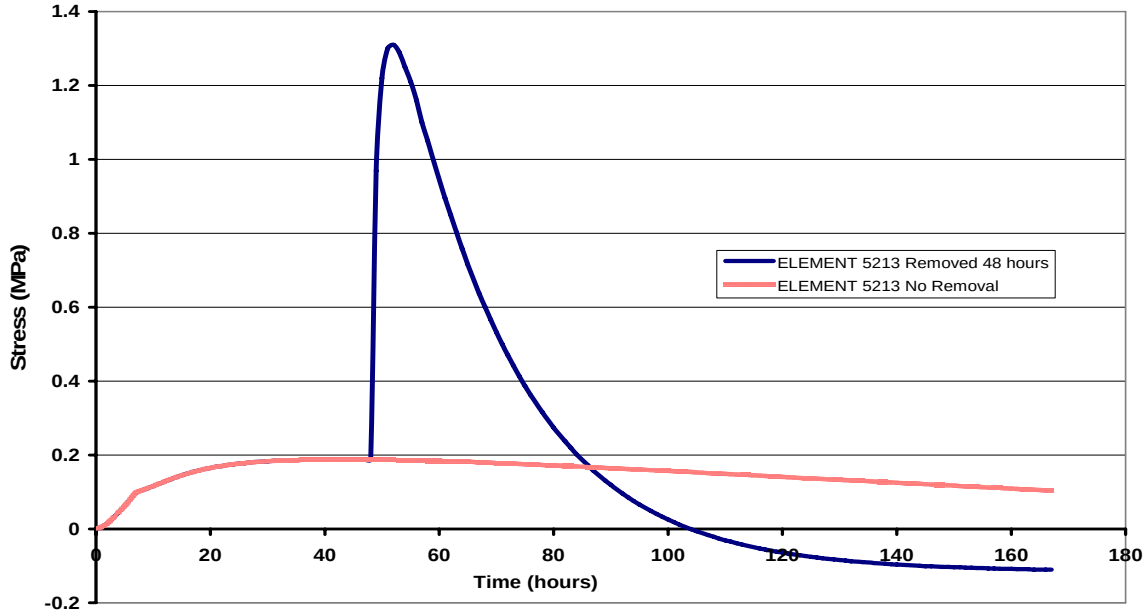

Figure 9-24. Plot of stress versus time at a point on the center of the surface of the concrete block when formwork is removed 2 days after casting

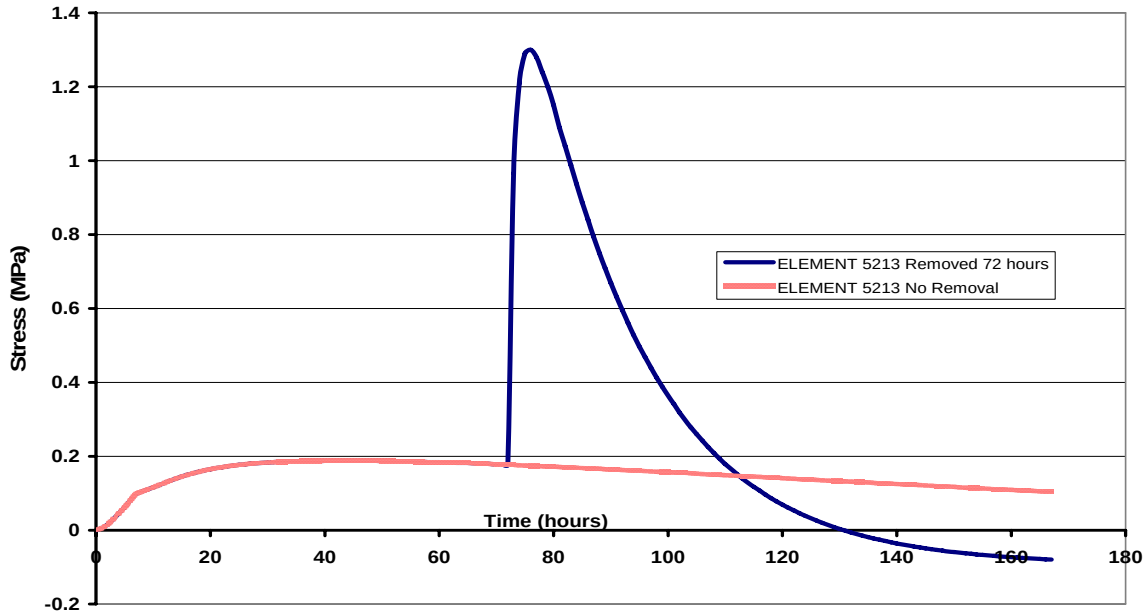

Figure 9-25. Plot of stress versus time at a point on the center of the surface of the concrete block when formwork is removed 3 days after casting

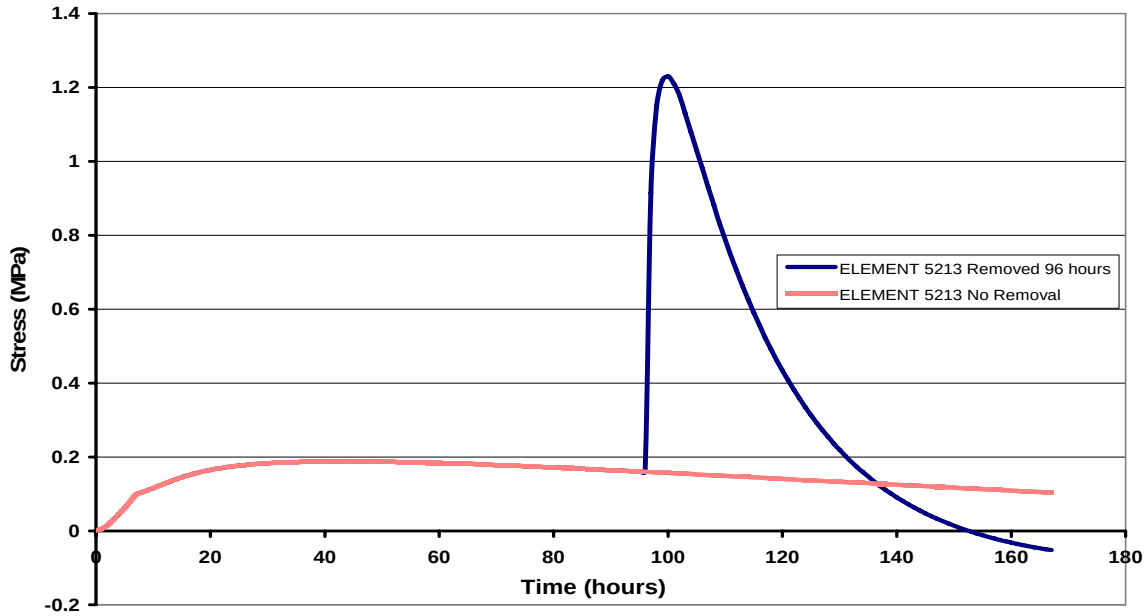

Figure 9-26. Plot of stress versus time at a point on the center of the surface of the concrete block when formwork is removed 4 days after casting

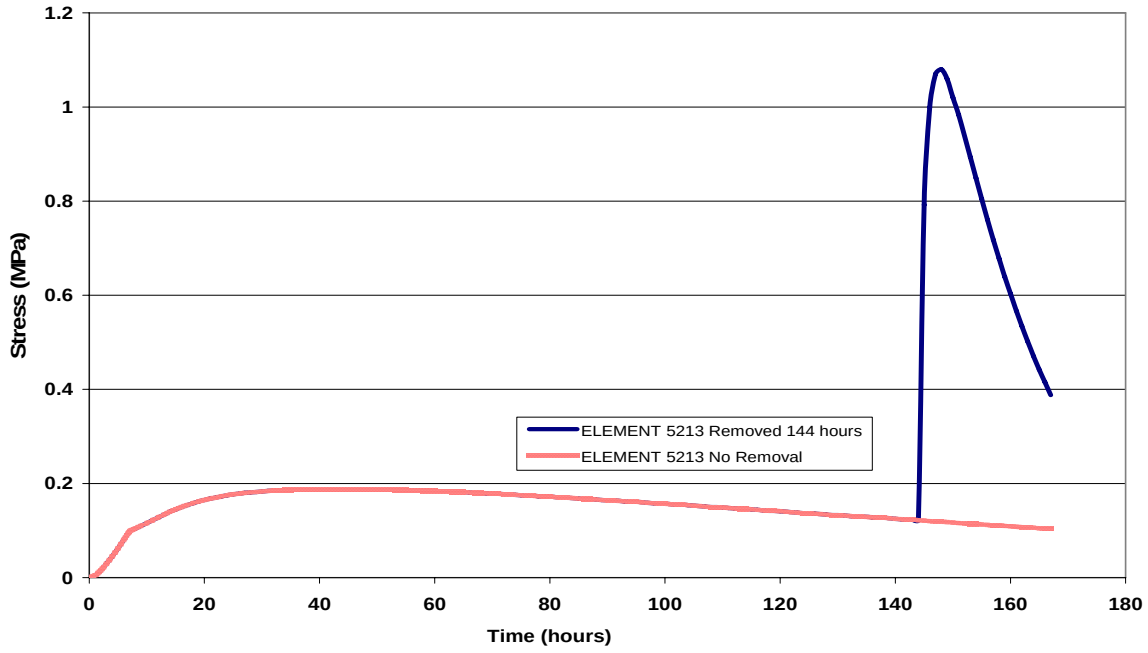

Figure 9-27. Plot of stress versus time at a point on the center of the surface of the concrete block when formwork is removed 6 days after casting

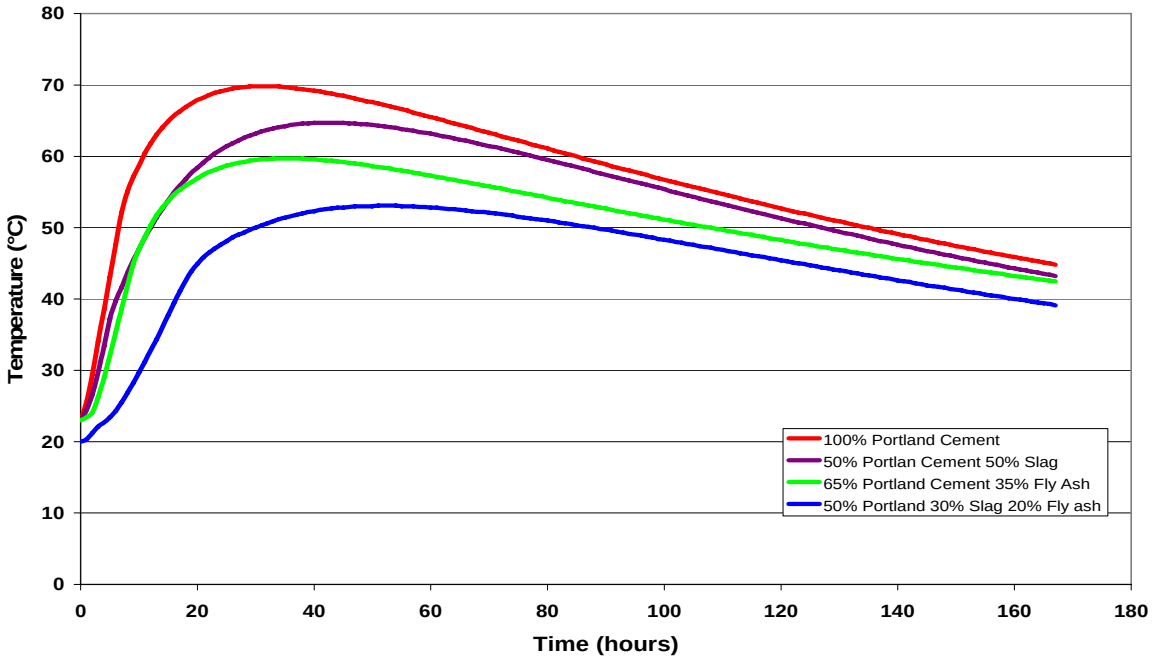

Figure 9-28. Temperature profiles with respect to time at the center of a concrete block with varying heat generation rates.

CHAPTER 10
CONCLUSIONS AND RECOMMENDATIONS

Findings

Results from analysis from a finite element model built to predict the early age behavior a hydrating concrete element in an effort to quantify the maximum allowable temperature difference to prevent cracking have been presented and discussed. To validate the accuracy of the model and hence verify the results obtained from the model, four different concrete mixtures were used in experimental blocks with dimensions 3.5ft x 3.5ft x 3.5ft and monitored for temperature distributions. The material and physical properties of the concretes used were obtained from laboratory testing and used in the finite element model. The two types of tests done on the concrete mixtures to determine the energy released during hydration were semi-adiabatic calorimetry and isothermal calorimetry. The calculated adiabatic energy rise obtained from each test was used in the model to determine which procedure would give the best results when compared with the temperatures measured in the experimental block.

Based on the results of the thermal analysis of the concrete block model the following findings were made:

- The semi-adiabatic calorimetry test consistently gave lower heat of hydration and lower predicted temperature of concrete as compared with the isothermal calorimetry test.
- The input of adiabatic energy captured in the isothermal calorimetry test provided temperature distributions that were very similar to those measured in the experimental blocks. At some locations the predicted temperatures were higher than the measured temperatures and so the isothermal test can be said to provide conservative predictions of the temperature distribution.

The induced stresses caused by the varying temperatures within the concrete element of each mixture were analyzed using the results from the model that utilized the energy from isothermal calorimetry test. The magnitude and type of the stresses were of particular interest so

as to determine the likelihood of thermal cracking. The results of this structural analysis for the concrete block study led to the following observations:

- The highest tensile stresses were located at the top edge of the surface exposed to ambient conditions.

- Concrete containing 100% Portland cement experienced tensile stresses high enough to cause cracking on all surfaces, even those insulated, when the temperature difference was 17.3 °C.

- In the case where 50% of the Portland cement was replaced with ground granulated blast-furnace slag the rate of hydration reaction and hence rate of temperature increase was significantly slower. The associated reduction in early age tensile strength resulted in the cracking risk not being reduced.

- In the case where 35% of the Portland cement was substituted with Fly Ash there was little effect on the early age rate of hydration and thus the time in which the maximum temperature was achieved was not affected significantly. However, the maximum temperature achieved was itself significantly less. Again the early age tensile strength was less than the 100% Portland cement case resulting in similar cracking on all surfaces as before even though the tensile stresses experienced were less.

- Concrete that had a blend of 50% Portland Cement, 30% Slag, and 20% Fly Ash performed the best in terms of reducing the induced thermal stresses relative to the tensile strength, and hence the cracking potential.

- The temperature differential that induced cracking in the concretes used in this project varied from mixture to mixture. This was due to the corresponding changes in the tensile strength.

The parametric study on factors affecting the temperature distribution in concrete produced very interesting results

- The thermal stresses in large mass concrete elements were effectively reduced with the use of thick layers of insulating polystyrene foam. This method is advantageous because the polystyrene foam if removed carefully can be reused often making it relatively inexpensive when compared to other single use methods such as cooling pipes and liquid nitrogen.

- Although the tensile stresses that resulted from the removal of formwork and insulation 12 hours, 1 day, 2 days and 3 days after the pouring concrete were less than the tensile strength of the concrete as measured in the laboratory, the stresses could be large enough to initiate micro-cracking. These micro-cracks can serve as an entry point for deleterious materials that can undermine the durability of the concrete. For insulation removed after

4 days, the tensile stresses were significantly less than the tensile strength, reducing the risk of microcracking.

Conclusions

Based on the results obtained in this study, the following conclusions are made:

- The heat of hydration energy data obtained from the isothermal calorimetry test should be used for the input for the heat generation function in the finite element modeling of concrete hydration.

- Reliance on a limiting maximum temperature differential to control cracking in massive concrete applications should be supplemented with a requirement for the presentation of a finite element analysis showing the calculated stress response to the predicted temperature distribution within the concrete, to ensure that the induced tensile stresses will not exceed the tensile strength of the concrete.

- Adequate insulation should be used in conjunction with the usual formwork material to reduce the temperature differentials during the early age hydration of massive concrete. However caution should be taken as the occurrence of delayed ettringite formation (DEF) and drying shrinkage due to high concrete temperatures was not studied.

- A safety factor should be applied to the tensile strength values for concrete obtained from the splitting tension and third-point flexural strength tests to guard against the initiation of micro-cracks which although by themselves will not cause structural failure, can act as an entry point for deleterious materials which can undermine the durability of the concrete.

- The current restrictions on maximum temperature imposed by state regulating bodies should take into consideration the type of cementitious materials that will be used in the concrete mix.

Recommendations for Future Research

The testing and analysis of additional blends of cementitious materials and on additional and larger blocks of mass concrete in order to assess the universal applicability of the hypotheses deduced and concluded from this study.

APPENDIX A
GRAPHICAL USER INTERFACE INPUT COMMANDS

Define Geometry Points for Base of Model

```
GEOMETRY POINT COORDINATE  0 0 0
GEOMETRY POINT COORDINATE  0.5334 0 0
GEOMETRY POINT COORDINATE  0.552445 0 0
GEOMETRY POINT COORDINATE  0.62865 0 0
GEOMETRY POINT COORDINATE  0 0.5334 0
GEOMETRY POINT COORDINATE  0.5334 0.5334 0
GEOMETRY POINT COORDINATE  0.552445 0.5334 0
GEOMETRY POINT COORDINATE  0.62865 0.5334 0
GEOMETRY POINT COORDINATE  0 0.55245 0
GEOMETRY POINT COORDINATE  0.5334 0.55245 0
GEOMETRY POINT COORDINATE  0.552445 0.55245 0
GEOMETRY POINT COORDINATE  0.62865 0.55245 0
GEOMETRY POINT COORDINATE  0 0.62865 0
GEOMETRY POINT COORDINATE  0.5334 0.62865 0
GEOMETRY POINT COORDINATE  0.552445 0.62865 0
GEOMETRY POINT COORDINATE  0.62865 0.62865 0
```

Connectivity

```
GEOMETRY SURFACE 4POINTS P1 P2 P6 P5
GEOMETRY SURFACE 4POINTS P2 P3 P7 P6
GEOMETRY SURFACE 4POINTS P3 P4 P8 P7
GEOMETRY SURFACE 4POINTS P5 P6 P10 P9
GEOMETRY SURFACE 4POINTS P6 P7 P11 P10
GEOMETRY SURFACE 4POINTS P7 P8 P12 P11
GEOMETRY SURFACE 4POINTS P9 P10 P14 P13
GEOMETRY SURFACE 4POINTS P10 P11 P15 P14
GEOMETRY SURFACE 4POINTS P11 P12 P16 P15
```

Merge Geometries

```
CONSTRUCT SET BOTFOAM APPEND ALL
VIEW GEOMETRY ALL BLUE
LABEL GEOMETRY LINES ALL RED
LABEL GEOMETRY SURFACE ALL BLUE
```

Group Lines with Equal Divisions into Sets

```
CONSTRUCT SET SELIN1 APPEND LINES L1 L2 L3 L4 L6 L9 L12 L19
CONSTRUCT SET SELIN2 APPEND LINES L5 L7 L8 L10 L11 L13 L14 L15 L16 L17
CONSTRUCT SET SELIN2 APPEND LINES L18 L20 L21 L22 L23 L24
```

Divide Lines

```
MESHING DIVISION LINE SELIN1 10
MESHING DIVISION LINE SELIN2 1
```

Create Volumes for 3D Model

```
GEOMETRY SWEEP BOTFOAM BOTPLY 1 TRANSLATE 0 0 0.762
GEOMETRY SWEEP BOTPLY BOTBLOCK 1 TRANSLATE 0 0 0.0381
GEOMETRY SWEEP BOTBLOC TOPBLOC 20 TRANSLATE 0 0 1.0668


CONSTRUCT SET MODEL APPEND ALL

LABEL GEOMETRY BODIES ALL BLUE
```

Group Geometries into Materials

```
CONSTRUCT SET CONCRETE APPEND BODIES B19
CONSTRUCT SET OPEN POLSTYRENE
CONSTRUCT SET APPEND BODIES B1 B2 B3 B4 B5 B6 B7 B8 B9 B12
CONSTRUCT SET APPEND BODIES B15 B16 B17 B18 B21 B24 B25 B26 B27
CONSTRUCT SET CLOSE
CONSTRUCT SET PLYWOOD APPEND BODIES B10 B11 B13 B14 B20 B22 B23
```

Generate Mesh for Entire Model

```
MESHING TYPES MODEL HE8 HX8HT
MESHING GENERATE
```

Turn of DIANA's Element Space Conflict Check

```
CONSTRUCT SPACE TOLERANCE OFF
GEOMETRY COPY CONCRETE CONC TRANSLATE 0 0 0
```

Specifiy Element Type For Concrete used in Flow-Stress Analysis

```
CONSTRUCT SET SELIN3 APPEND LINES L145 L146 L147 L148 L149 L150 L151
                                                    L152
CONSTRUCT SET SELIN4 APPEND LINES L153 L154 L155 L156
MESHING DIVISION LINE SELIN3 20
MESHING DIVISION LINE SELIN4 40
MESHING TYPES CONC HE20 CHX60
MESHING GENERATE
MESHING MERGE ALL 0.001          Merges all nodes within a distance of 0.001
```

Identify Surfaces that Experience Boundary Convection

CONSTRUCT SET OPEN BOUNDA
CONSTRUCT SET APPEND SURFACES S1 S2 S3 S4 S5 S6 S7 S8 S9 S27
CONSTRUCT SET APPEND SURFACES S34 S37 S40 S41 S42 S60 S67 S70 S73 S74
CONSTRUCT SET APPEND SURFACES S75 S77 S78 S79 S81 S82 S83 S84 S93 S100
CONSTRUCT SET APPEND SURFACES S103 S106 S107 S108 S110
CONSTRUCT SET CLOSE

CONSTRUCT SPACE TOLERANCE OFF
GEOMETRY COPY BOUNDA OUTER TRANSLATE 0 0 0
MESHING TYPES OUTER QU4 BQ4HT
MESHING GENERATE
MESHING MERGE ALL 0.001

Define Material Properties
Properties are Defined Using the Property Manager Dialog Box
View Property Manager
Materials Material Name: CONC
External External Data from File: concrete.dat

Material Name: MAPLY (Plywood)
Conductivity=540 J/m-hr-°C, Heat Capacity=8.54E5 J/m^3-°C
Material Name: MAINSUL (Polystyrene Insulation)
Conductivity=126 J/m-hr-°C, Heat Capacity=2.84E4 J/m^3-°C

Material Name: MAOUT (Boundary Elements)
Convection Coefficient=2.016E4 J/m^3-hr-°C

Assign Properties to Geometries and Elements

PROPERTY ATTACH CONC MACONC
PROPERTY ATTACH PLY MAPLY
PROPERTY ATTACH POLYSTRENE MAINSUL
PROPERTY ATTACH OUTER MAOUT

Boundary Conditions

PROPERTY LOADS EXTTEMP 1 OUTER 23
PROPERTY LOADS GRAVITY 2 CONC -0.981E-5 3 *Weight acting downwards*

Assign Variations of Loads and Boundary Conditions to Time

CONSTRUCT TCURVE TCDUM LIST 0 1. 168.1.
PROPERTY ATTACH LOADCASE 1 TCDUM

PROPERTY ATTACH LOADCASE 2 TCDUM

Boundary Constraints ie. Support Conditions and Symmetry Conditions

PROPERTY BOUNDARY CONSTRAINT S109 Z
PROPERTY BOUNDARY CONSTRAINT S111 Y
PROPERTY BOUNDARY CONSTRAINT S114 X

Set Initial Temperatures

PROPERTY INITIAL INITEMP ALL 23

UTILITY WRITE DIANA QUARTERBLOCKMODEL

APPENDIX B
BATCH FILE INPUT COMMANDS

```
FEMGEN MODEL      : QUARTERBLOCK1
ANALYSIS TYPE     : Heatflow-Stress Staggered 3D
'UNITS'
LENGTH   M
TIME     HOUR
TEMPER   CELSIU
FORCE    N
'COORDINATES'
    1     0.000000E+00     0.000000E+00     0.000000E+00
    2     5.334000E-02     0.000000E+00     0.000000E+00
    3     1.066800E-01     0.000000E+00     0.000000E+00
    4     1.600200E-01     0.000000E+00     0.000000E+00
    5     2.133600E-01     0.000000E+00     0.000000E+00
    6     2.667000E-01     0.000000E+00     0.000000E+00
    7     3.200400E-01     0.000000E+00     0.000000E+00
    8     3.733800E-01     0.000000E+00     0.000000E+00
    9     4.267200E-01     0.000000E+00     0.000000E+00
   10     4.800600E-01     0.000000E+00     0.000000E+00
                                                  Lines Skipped

12460     1.600200E-01     4.800600E-01     1.154430E+00
12461     2.133600E-01     4.800601E-01     1.154430E+00
12462     2.667000E-01     4.800601E-01     1.154430E+00
12463     3.200400E-01     4.800601E-01     1.154430E+00
12464     3.733800E-01     4.800601E-01     1.154430E+00
12465     4.267200E-01     4.800601E-01     1.154430E+00
12466     4.800600E-01     4.800601E-01     1.154430E+00
'ELEMENTS'
CONNECTIVITY
    1 HX8HT  1 2 13 12 122 123 134 133
    2 HX8HT  2 3 14 13 123 124 135 134
    3 HX8HT  3 4 15 14 124 125 136 135
    4 HX8HT  4 5 16 15 125 126 137 136
    5 HX8HT  5 6 17 16 126 127 138 137
    6 HX8HT  6 7 18 17 127 128 139 138
    7 HX8HT  7 8 19 18 128 129 140 139
    8 HX8HT  8 9 20 19 129 130 141 140
    9 HX8HT  9 10 21 20 130 131 142 141
   10 HX8HT  10 11 22 21 131 132 143 142
                                                  Lines Skipped

 3168 HX8HT  3589 3609 3869 3849 3588 3608 3868 3848
 3169 CHX60  339 3888 340 3899 351 3909 350 3898 4347 4386 5888 5868
          647 4366 666 6050 5969 6059 1388 5887
```

3170 CHX60 340 3889 341 3900 352 3910 351 3899 4386 4425 5889 5888
666 4405 685 6051 5970 6060 5969 6050
3171 CHX60 341 3890 342 3901 353 3911 352 3900 4425 4464 5890 5889
685 4444 704 6052 5971 6061 5970 6051
3172 CHX60 342 3891 343 3902 354 3912 353 3901 4464 4503 5891 5890
704 4483 723 6053 5972 6062 5971 6052
3173 CHX60 343 3892 344 3903 355 3913 354 3902 4503 4542 5892 5891
723 4522 742 6054 5973 6063 5972 6053
3174 CHX60 344 3893 345 3904 356 3914 355 3903 4542 4581 5893 5892
742 4561 761 6055 5974 6064 5973 6054
3175 CHX60 345 3894 346 3905 357 3915 356 3904 4581 4620 5894 5893
761 4600 780 6056 5975 6065 5974 6055
3176 CHX60 346 3895 347 3906 358 3916 357 3905 4620 4659 5895 5894
780 4639 799 6057 5976 6066 5975 6056
3177 CHX60 347 3896 348 3907 359 3917 358 3906 4659 4698 5896 5895
799 4678 818 6058 5977 6067 5976 6057
3178 CHX60 348 3897 349 3908 360 3918 359 3907 4698 4737 4776 5896
818 4717 837 4756 856 6068 5977 6058

Lines Skipped

5168 CHX60 12205 12376 990 5089 1009 5128 1028 12385 12466 5069 5108
5147 616 4306 617 4317 628 4327 627 4316
5169 BQ4HT 1 2 13 12
5170 BQ4HT 2 3 14 13
5171 BQ4HT 3 4 15 14
5172 BQ4HT 4 5 16 15
5173 BQ4HT 5 6 17 16
5174 BQ4HT 6 7 18 17
5175 BQ4HT 7 8 19 18
5176 BQ4HT 8 9 20 19
5177 BQ4HT 9 10 21 20
5178 BQ4HT 10 11 22 21
5179 BQ4HT 12 13 24 23

Lines Skipped

5982 BQ4HT 626 627 3377 3376
5983 BQ4HT 627 628 3378 3377

:Nodes Grouped to Materials
MATERIALS
/ 145-254 265-275 2289-2488 2689-2908 / 1
/ 5169-5983 / 2
/ 3169-5168 / 3
/ 1-144 255-264 276-288 2489-2688 2909-3168 / 4

'MATERIALS'

:Plywood Properties
1 CONDUC 5.400000E+02
CAPACI 8.543999E+05

:Boundary Properties
2 CONVEC 2.016000E+04

:Concrete Properties
3 CONDUC 7.920E+03
CAPACI 2.675596E+06
ADIAB 0.0 23
1.0 23.73796428
2.0 25.42189049
3.0 28.73104768
4.0 33.31326448
5.0 38.24138423
6.0 42.95409819
7.0 47.74431264
8.0 52.63938071
9.0 56.42322844
10.0 59.06166443
11.0 61.06186104
12.0 62.68025374
13.0 64.07070381
14.0 65.2901969
15.0 66.38432155
16.0 67.38157057
17.0 68.30473824
18.0 69.14242742
19.0 69.94022664
20.0 70.68673876
21.0 71.37626523
22.0 72.03160031
23.0 72.65274398
24.0 73.23969627
25.0 73.78675859
26.0 74.30532808
27.0 74.79540474
28.0 75.26838571
29.0 75.71287385
30.0 76.13456772
31.0 76.5391659
32.0 76.91527124
33.0 77.28567802

34.0	77.63329054
35.0	77.96950592
36.0	78.29432418
37.0	78.60204673
38.0	78.90407072
39.0	79.18899902
40.0	79.46822874
41.0	79.73606134
42.0	80.00389393
43.0	80.2603294
44.0	80.50536773
45.0	80.75040606
46.0	80.98404726
47.0	81.22338703
48.0	81.43993253
49.0	81.6621766
50.0	81.87302353
51.0	82.08956904
52.0	82.29471741
53.0	82.49986578
54.0	82.70501415
55.0	82.90446395
56.0	83.09251663
57.0	83.28626786
58.0	83.4800191
59.0	83.66237321
60.0	83.84472732
61.0	84.02708142
62.0	84.20373697
63.0	84.37469394
64.0	84.55704805
65.0	84.72230646
66.0	84.89326343
67.0	85.05852184
68.0	85.22947882
69.0	85.3833401
70.0	85.54859851
71.0	85.70815835
72.0	85.86201963
73.0	86.01588091
74.0	86.16974219
75.0	86.32930203
76.0	86.47746474
77.0	86.61992889
78.0	86.77379017
79.0	86.91625431

80.0	87.05871846
81.0	87.20688117
82.0	87.34364675
83.0	87.48041233
84.0	87.62287648
85.0	87.75964206
86.0	87.88501051
87.0	88.02177609
88.0	88.15854167
89.0	88.28960868
90.0	88.41497713
91.0	88.54604415
92.0	88.67711116
93.0	88.80817817
94.0	88.92784806
95.0	89.05321651
96.0	89.17288639
97.0	89.29825484
98.0	89.41792472
99.0	89.5375946
100.0	89.65156592
101.0	89.7712358
102.0	89.89090569
103.0	90.004877
104.0	90.11314976
105.0	90.22712107
106.0	90.34109239
107.0	90.44936514
108.0	90.55193933
109.0	90.66591064
110.0	90.77418339
111.0	90.87675758
112.0	90.9907289
113.0	91.08760452
114.0	91.1901787
115.0	91.29845145
116.0	91.39532707
117.0	91.49220269
118.0	91.60047544
119.0	91.6916525
120.0	91.79422668
121.0	91.87970517
122.0	91.98227935
123.0	92.07915497
124.0	92.17033203
125.0	92.26150908

126.0	92.35268613
127.0	92.44956175
128.0	92.53504024
129.0	92.63191586
130.0	92.71739435
131.0	92.8085714
132.0	92.89404989
133.0	92.97952838
134.0	93.06500687
135.0	93.15048535
136.0	93.24166241
137.0	93.3271409
138.0	93.40122225
139.0	93.49239931
140.0	93.57217923
141.0	93.65765772
142.0	93.7431362
143.0	93.82291612
144.0	93.90839461
145.0	93.98247597
146.0	94.06225589
147.0	94.14203581
148.0	94.23321287
149.0	94.30159566
150.0	94.38707414
151.0	94.45545693
152.0	94.53523686
153.0	94.61501678
154.0	94.68909813
155.0	94.76317949
156.0	94.84295941
157.0	94.92273933
158.0	94.99682069
159.0	95.07090205
160.0	95.1449834
161.0	95.21906476
162.0	95.28744755
163.0	95.3615289
164.0	95.4299117
165.0	95.50399305
166.0	95.57237584
167.0	95.6464572
ARRHEN	4117.75
EQUAGE	ARRTYP
TEMREF	23.0
YOUNG	2.523500E+04

```
    POISON    2.000000E-01
    DENSIT    2.2480000E+03
    THERMX    9.160000E-06
    FTTIME    0. 24.  48.  72.  167.
    FTVALU    0. 1.25 1.66 1.93 2.206
    MAXWEL    1
 ,1
    TIME      0. 24. 48. 72. 167.
    YOUNG     13445. 13445. 16892. 18064. 20202.

:Polystyrene Properties
  4 CONDUC    2.248500E+02
    CAPACI    2.082400E+04

:Geometry and Element Groupings
'GROUPS'
NODES
  1 BOTFOAM / 1-121 243-253 265-275 287-297 309 311 313-323 335
          337 /
  2 SELIN1 / 1-12 22 23 33 34 44 45 55 56 66 67 77 78 88 89 99 100
          110-121 243-253 265-275 287-297 313-323 /
  3 SELIN2 / 11 111 121 243 253 265 275 287 297 309 311 313 323
          335 337 /
  4 BOTPLY / 122-242 254-264 276-286 298-308 310 312 324-334 336
          338 /
  5 BOTBLOC / 339-507 /
  6 TOPBLOC / 508-628 2928-2938 3148-3158 3368-3378 3588 3608 3628-3638
          3848 3868 /
ELEMEN
  7 MODEL / 1-3168 /
NODES
  8 MODEL_N / 1-3887 /
ELEMEN
  9 CONCRE / 289-2288 /
NODES
 10 CONCRE_N / 339-459 508-2927 /
ELEMEN
 11 POLYSTY / 1-144 255-264 276-288 2489-2688 2909-3168 /
NODES
 12 POLYSTY_N / 1-338 460-507 2928-3887 /
ELEMEN
 13 PLY / 145-254 265-275 2289-2488 2689-2908 /
NODES
 14 PLY_N / 122-242 254-264 298-308 310 339-470 482-493 518 529
          540 551 562 573 584 595 606 617-628 819-1217 2928-3147
          3368-3607 /
```

```
ELEMEN
  15 CONC / 3169-5168 /
NODES
  16 CONC_N / 339-459 508-1388 3888-12466 /
  17 SELIN3 / 339-350 360 361 371 372 382 383 393 394 404 405 415 416
          426 427 437 438 448-459 508-519 529 530 540 541 551 552
          562 563 573 574 584 585 595 596 606 607 617-628 3888-3898
          3908 3919 3929 3940 3950 3961 3971 3982 3992 4003
          4013 4024 4034 4045 4055 4066 4076 4087 4097-4118
          4128 4139 4149 4160 4170 4181 4191 4202 4212 4223
          4233 4244 4254 4265 4275 4286 4296 4307 4317-4327 /
  18 SELIN4 / 339 349 449 459 508 518 618 628-647 819-837 1009-1027
          1199-1217 4328-4347 4718-4737 5108-5127 5498-5517 /
  19 BOUNDA / 1-121 243-253 265-297 309 311-338 471-481 494-628
          2928-2938 3148-3378 3588 3608-3887 4108-4327 /
ELEMEN
  20 OUTER / 5169-6283 /
NODES
  21 OUTER_N / 1-121 243-253 265-297 309 311-338 471-481 494-628
           2928-2938 3148-3378 3588 3608-3887 4108-4327 /
'SUPPORTS'                                          (Boundary Constraints)
 / 339 350 361 372 383 394 405 416 427 438 449 508 519 530 541 552
   563 574 585 596 607 618 629-647 1199-1388 3898 3919 3940 3961
   3982 4003 4024 4045 4066 4087 4118 4139 4160 4181 4202 4223 4244
   4265 4286 4307 4328-4347 5498-5887 /   TR     1
 / 339-349 508-518 629-837 3888-3897 4108-4117 4328-4737 /   TR     2
 / 339-459 3888-4107 /   TR     3

:Ambient Temperature
'BOUNDA'
CASE 1
ELEMEN
5169  EXTEMP    0.230000E+02
5170  EXTEMP    0.230000E+02
                                                          Lines Skipped

5982  EXTEMP    0.230000E+02
5983  EXTEMP    0.230000E+02

:Ambient Temperature Variation with Time
'TIMEBO'
BOUNDA 1
TIMES  0.000000E+00   0.167000E+03   /
FACTOR 0.100000E+01   0.100000E+01   /
```

```
:Selfweight/Gravity Load
'LOADS'
CASE 2
WEIGHT
 3    -0.981000E-05

:Variation of Load  with Time
'TIMELO'
LOAD   2
TIMES  0.000000E+00   0.167000E+03   /
FACTOR 0.100000E+01   0.100000E+01   /

:Initial Temperatures
'INIVAR'
TEMPER 1
   1     0.230000E+02
   2     0.230000E+02
                                                          Lines Skipped
12466     0.230000E+02
'DIRECTIONS'
   1   1.000000E+00   0.000000E+00   0.000000E+00
   2   0.000000E+00   1.000000E+00   0.000000E+00
   3   0.000000E+00   0.000000E+00   1.000000E+00
'END'
```

APPENDIX C
STAGGERED ANALYSIS COMMANDS

In this appendix, the analysis commands for the standard staggered analysis are presented. The standard staggered analysis is one in which the thermal flow analysis is coupled with the structural analysis. The temperatures calculated in the thermal analysis are automatically converted to input for the structural analysis.

```
*FILOS
INITIA                                          Initiate Analysis
*INPUT
*HEATTR                                         Analysis Type Thermal
BEGIN INITIA
 BEGIN NONLIN
  EQUAGE                                        Calculate Equivalent Age
  HYDRAT DGRINI=0.01
 END NONLIN
 TEMPER INPUT FIELD=1
END INITIA
BEGIN EXECUT
 BEGIN NONLIN
  HYDRAT ITERAT
  BEGIN ITERAT
   CONVER TEMPER TOLCON=0.01
   MAXITE=30                                    Maximum No. of Iterations
  END ITERAT
 END NONLIN
 SIZES 1.0(167)                                 Magnitude & No. Time Steps
END EXECUT
BEGIN OUTPUT FEMVIE FILE="FLOW"                 File to print to output
 EQUAGE TOTAL INTPNT
 TEMPER
 REACTI TOTAL INTPNT
END OUTPUT
*NONLIN
BEGIN TYPE
 BEGIN PHYSIC                                   Analysis Type Structural
  TEMPER                                        Read Temperatures as Input
  VISCOE                                        Viscoelastic Behaviour
 END PHYSIC
END TYPE
BEGIN EXECUTE
 TIME STEPS EXPLIC SIZES 1.0(167)
 BEGIN ITERAT
  BEGIN CONVER
   SIMULT
   FORCE TOLCON=1.0E-2
   DISPLA TOLCON=1.0E-2
  END CONVER
 END ITERAT
END EXECUT
BEGIN OUTPUT FEMVIE FILE="STRUC"
 DISPLA
 STATUS
```

```
 STATUS CRACK
 STRAIN TEMPER
 STRAIN
 STRAIN CRACK GREEN
 STRESS
 STRESS TOTAL CAUCHY PRINCI
 STRESS TOTAL CAUCHY CRKIND
 TEMPER
END OUTPUT
*END
```

APPENDIX D
PHASED ANALYSIS COMMANDS

In this appendix, the analysis commands for the phased analysis in which the formwork is removed sometime during the hydration process is presented. The example presented here is for the removal of the formwork 96 hours (4 days) after the hydration reaction commences.

```
*FILOS
INITIA
*INPUT
*PHASE                                                    Start Phase 1
ACTIVE ELEMEN CONC PLY POLYSTY OUTER                      Elements active in Phase 1
*HEATTR
BEGIN INITIA
 BEGIN NONLIN
  EQUAGE
  HYDRAT DGRINI=0.01
 END NONLIN
 TEMPER INPUT
END INITIA
EXECUT SIZES 1.0(96)
BEGIN OUTPUT FEMVIE FILE="FLOW_1m4Days"
 EQUAGE
 TEMPER
 REACTI
END OUTPUT
*NONLIN
BEGIN TYPE
 BEGIN PHYSIC
  TEMPER
  VISCOE
 END PHYSIC
END TYPE
BEGIN EXECUTE
 TIME STEPS EXPLIC SIZES 1.0(96)
 BEGIN ITERAT
  BEGIN CONVER
   SIMULT
   FORCE TOLCON=1.0E-2
   DISPLA TOLCON=1.0E-2
  END CONVER
 END ITERAT
END EXECUT
BEGIN OUTPUT FEMVIE FILE="STRUC_1m4Days"
 DISPLA
 STRAIN TEMPER
 STRAIN
 STRESS
 STRESS TOTAL CAUCHY PRINCI
 STRESS TOTAL CAUCHY CRKIND
 TEMPER
```

```
END OUTPUT
*END


*PHASE                                                  Start Phase 2
BEGIN ACTIVE
 ELEMEN CONC OUTER2                                    Elements active in Phase 2
END ACTIVE
*HEATTR                                                 Analysis Type Thermal
BEGIN INITIA
 BEGIN NONLIN
  EQUAGE
  HYDRAT DGRINI=0.01
 END NONLIN
 TIME=96.                                              Phase 2 Start time
 TEMPER INPUT
END INITIA
EXECUT SIZES 1.0(71)
BEGIN OUTPUT FEMVIE FILE="FLOW_1m4Days2"
 EQUAGE TOTAL INTPNT
 TEMPER
 REACTI TOTAL INTPNT
END OUTPUT
*NONLIN
BEGIN TYPE
 BEGIN PHYSIC                                          Analysis Type Structural
  TEMPER
  VISCOE
 END PHYSIC
END TYPE
BEGIN EXECUTE
 BEGIN START
  TIME=96.0                                            Phase 2 Start time
  INITIA STRESS PHASE
  LOAD LOADNR=3                                        Activate Load No. 3
  STEPS
 END START
 BEGIN ITERAT
  BEGIN CONVER
   SIMULT
   FORCE TOLCON=1.0E-2
   DISPLA TOLCON=1.0E-2
  END CONVER
 END ITERAT
END EXECUT
BEGIN EXECUTE
```

```
 TIME STEPS EXPLIC SIZES 1.0(71)
 BEGIN ITERAT
  BEGIN CONVER
   SIMULT
   FORCE TOLCON=1.0E-2
   DISPLA TOLCON=1.0E-2
  END CONVER
 END ITERAT
END EXECUTE
BEGIN OUTPUT FEMVIE FILE="STRUC_1m4Days2"
 DISPLA
 STRAIN TEMPER
 STRAIN
 STRESS
 STRESS TOTAL CAUCHY PRINCI
 STRESS TOTAL CAUCHY CRKIND
 TEMPER
END OUTPUT
*END
```

LIST OF REFERENCES

ACI Committee 207 (2005), 207.1R-05: Guide to Mass Concrete, Farmington Hill, MI USA.

ACI Committee 207 (2005), 207.2R-07: Report on Thermal and Volume Change Effects on Cracking of Mass Concrete, Farmington Hills, MI USA.

Ayotte, E., Massicotte, B. Houde, J., Gocevski, V. (1997) Modeling of Thermal Stresses at Early Ages in a Concrete Monolith, ACI Materials Journal, 94,.6, Figure 1, 577-587

Bamforth, P.B., (1984). Mass Concrete. Concrete Society Digest. Concrete and Cement Association.

Ballim, Y.A. (2003). A Numerical Model and Associated Calorimeter for Predicting Temperature Profiles in Mass Concrete. Cem. Concr. Compos., 26(6), 695-703

Branco, F., Mendes, P.E., Mirambell, E. (1992). Heat of Hydration Effects in Concrete Structures. ACI Materials Journal, 89, 2, 139-145.

Bentz, d. (1997). Three-Dimensional Computer Simulation of Portland Cement Hydration and Microstructure Development. J. Am Ceram. Soc., 80, 1.

Burg, R.G., and Fiorato, A.E. (1999). High-Strength Concrete in Massive Foundation Elements. Research and Development Bulletin RD117, Portland Cement Association, Skokie, Illinois, U.S.A.

De Schutter, G. (2002). Finite Element Simulation of Thermal Cracking in Massive Hardening Concrete Elements Using Degree of Hydration Based Material Laws. Comput. Struct., 80, 2035-2042.

De Schutter, G., and Taerwe, L. (1995). General Hydration Model for Portland Cement and Blast Furnace Slag Cement. Cem. Concr. Res., 25(3), 593-604.

De Schutter, G., and Taerwe, L. (1995). Specific Heat and Thermal Diffusivity of Hardening Concrete. Mag. Concr. Res., 47(172), 203-208.

Escalante-Garcia, J.I., and Sharp, J.H. (2001). The Microstructure and Mechanical Properties of Blended Cements Hydrated at Various Temperatures. Cem. Concr. Res, 31(5) 675-702.

Evju, C., (2003). Initial Hydration of Cementitious Systems Using a Simple Isothermal Calorimeter and Dynamic Correction. Journal of Thermal Analysis and Calorimetry 71, 829-840.

Faria, R., Azenha, M., and Figueiras, J. (2006). Modeling of concrete at early ages: Application to an externally restrained slab. Cem. Concr. Compos., 28, 572-585.

Florida Department of Transportation, Standard Specifications for Road and Bridge Construction, Florida Department of Transportation, Tallahassee 2007.

Gajda, J., (2007). Mass Concrete for Buildings and Bridges, Portland Cement Association Skokie, Illinois.

Khan, A., Cook, W., and Mitchell, D. (1998). Thermal Properties and Transient Analysis of Structural Members During Hydration. ACI Materials Journal." 95(28) 293-300.

Klein, A., Pirtz, D., and Adams, R.F., (1963). Thermal Properties of Mass Concrete During Adiabatic Curing. Symposium on Mass Concrete, ACI SP-6, 199-218.

Machida, N., and Uehara, K., (1987). Nonlinear Thermal Stress Analysis of a Massive Concrete Structure. Comput. Struct., 26, 287-296.

Majorana, C.E., Zavarise, G., Borsetto, M., and Giuseppetti (1990). Nonlinear Analysis of Thermal Stresses in Mass Concrete Castings. Cem. Concr. Res., 20, 559-578.

Morabito, P., (1998). Methods to Determine Heat of Hydration of Concrete, Prevention of Thermal Cracking in Concrete at Early Ages., RILEM Report 15, Edited by R. Springenschmid, E&FN Spon, London.

Nasser, K.W., Lothia, R.P. (1971). Mass Concrete Properties at High Temperatures. J. Am. Concr. Inst., 68(3), 180-186.

Neville, A., (1995). Properties of Concrete 4th Edition., Essex, England Pearson Education Limited.

Radovanovic, S., (1998). Thermal and Structural Finite Element Analysis of Early Age Mass Concrete Structures. University of Manitoba, Winnipeg, Manitoba, Canada.

Ulm, F., and Coussy, O. (2001). "What is a Massive Concrete Structure at Early Ages? Some Dimensional Arguments. J. Eng. Mech., 127(5), 512-522.

U.S. Army Corps of Engineers. (1997). Appendix A: Techniques for Performing Concrete Thermal Studies. Manual ETL 1110-2-542, Washington, D.C.

U.S. Army Corps of Engineers. (1997). Appendix A: Techniques for Performing Concrete Thermal Studies. Manual ETL 1110-2-542, Washington, D.C.

BIOGRAPHICAL SKETCH

The author began his undergraduate education in 1996 at Howard University in Washington, D.C. On graduating with a Bachelor of Science degree in civil engineering in May 1999, he returned to his home country Jamaica to work at the civil engineering consulting firm Jentech Consultants Limited. In August 2000, the author returned to the United States to study at the University of Miami, Coral Gables, Florida obtaining a Master of Science degree in civil engineering, with emphasis in structural engineering, in December 2002. Once again the author returned to Jamaica to work at Jentech until August 2005 when he enrolled at the University of Florida to pursue a Doctor of Philosophy degree in civil engineering, with a concentration in materials engineering. The author anticipates obtaining this degree in December 2009.